CRANFIELD UNIVERSITY

Jessica Taylor

Assessment of Crack Arrest Behaviour in Modern Structural Steels

School of Water, Energy and Environment
Renewable Energy Marine Structures Centre for Doctoral Training
(REMS CDT)

EngD Thesis
Academic Year: 2020 - 2021

Supervisor: Ali Mehmanparast
Associate Supervisor: Hossein Farrahi
March 2021

CRANFIELD UNIVERSITY

School of Water, Energy and Environment
Renewable Energy Marine Structures Centre for Doctoral Training
(REMS CDT)

EngD Thesis

Academic Year 2020 - 2021

Jessica Taylor

Assessment of Crack Arrest Behaviour in Modern Structural Steels

Supervisor: Ali Mehmanparast
Associate Supervisor: Hossein Farrahi
March 2021

This thesis is submitted in partial fulfilment of the requirements for the degree of REMS EngD
(NB. This section can be removed if the award of the degree is based solely on examination of the thesis)

ABSTRACT

It is vital to prevent brittle cracks in large structures. This is particularly important for a number of industry sectors including offshore wind, Oil & Gas, and shipbuilding where structural failure risks loss of human life and loss of expensive assets. Wide-plate test methods allow for direct measurement of the crack arrest toughness but this kind of testing is incredibly expensive. Therefore, there is a need for cheaper and simpler test methods which are able to measure a material's brittle crack arrest toughness. Some modern steels exhibit high Charpy energy – i.e. high initiation fracture toughness, but poor resistance to crack propagation – i.e. low crack arrest toughness. The correlation between initiation and arrest toughness measured through small-scale testing is investigated in five different steels, which include S355 structural steel (with two different thicknesses), X65 pipeline steel, two high strength reactor pressure vessel steels and EH47 shipbuilding steel. In this work, Compact Crack Arrest (CCA) testing, which is standardised in ASTM E1221, has been successfully used to measure the crack arrest toughness of thick sections of EH47 shipbuilding steel. A wide range of supplementary tests were carried out, including instrumented Charpy, drop weight Pellini, fracture toughness, tensile testing, and microscopy. Small scale mechanical tests were used to characterise the materials' properties and the results were compared to the materials' microstructures. The results presented in this study have been discussed in terms of the effectiveness of the CCA test method and small-scale test methods for measurement of brittle crack arrest toughness and integrity assessment of large-scale structures.

Keywords:

brittle crack arrest, ferritic steel, small-scale testing, CCA, compact crack arrest testing

ACKNOWLEDGEMENTS

This work was supported by Industrial CASE grant EP/P510464/1 (reference 2002942) and grant EP/L016303/1 for Cranfield, Oxford and Strathclyde Universities, Centre for Doctoral Training in Renewable Energy Marine Structures - REMS (http://www.rems-cdt.ac.uk/), from the UK Engineering and Physical Sciences Research Council (EPSRC). This work was made possible by sponsorship and support of Lloyds' Register Foundation. The Foundation helps to protect life and property by supporting engineering-related education, public engagement and the application of research. The work was enabled through, and undertaken at, the National Structural Integrity Research Centre (NSIRC), a postgraduate engineering facility for industry-led research into structural integrity established and managed by TWI through a network of international Universities.

I would like to thank my supervisors Dr. Ali Mehmanparast, Dr. Philippa Moore, Dr. Rob Kulka and Prof. Hossein Farrahi for their continued support, encouragement, and patience over the last four and a half years. I am extremely grateful to Lloyds Register Foundation and those at Lloyds Register who have lent their expertise and support, in particular Weihong He and Dr. Li Xu who helped me with material acquisition.

Special thanks to the invaluable support from TWI Ltd. in carrying out my experimental work, especially the lab technicians, technical experts, and friends I made during my time there. I would like to thank all members of the REMS Centre for Doctoral Training and my colleagues at Cranfield University for their help and support throughout the course of my doctoral studies. Thank you to Rutherford Appleton Laboratory, who carried out the neutron diffraction measurements for this work, particularly Dr. Winfried Kockelmann.

Most of all I'm grateful to my friends and family who have supported me and kept me sane, especially my doctoral friends who have struggled alongside me and shared their valuable advice. Thank you to my parents who raised me to aim high and always supported my education. Pierrick, Matt, Anna, Daisy, Jess: thank you from the bottom of my heart. Completing a doctorate during a global pandemic was a challenge I never could have succeeded at without your support. Piepie: thank you for your encouragement and support, thank you for listening and being my sounding board, thank you for making me pasta and getting pizza when I'm stressed out, thank you for everything you do for me.

TABLE OF CONTENTS

LIST OF FIGURES

LIST OF TABLES

LIST OF EQUATIONS

1 Introduction

Brittle fracture can happen suddenly and unexpectedly, and in most circumstances causes complete catastrophic failure of a structure. Therefore, structures are designed so that they would eventually fail by fatigue cracking after their design life is complete since the fatigue lifetime can be predicted. Some structures such as reactor pressure vessels, pipelines, and container ships are at particular risk of accidental brittle fracture due to an unexpected event such as impact, explosion, or environmental loading. In these cases, total structural failure may result in loss of life and expensive assets, along with potential for serious environmental damage. Materials used for these applications often take into account the concept of crack arrest. Although a crack may initiate in a region of high stress concentration or local embrittlement, the material is designed to resist crack propagation and once the crack leaves this region it will stop growing i.e. arrest. This prevents total structural failure due to unexpected brittle fracture. Crack arrest toughness is typically measured using large-scale wide-plate testing which has recently been published in an ISO standard. Because wide-plate testing is very expensive, crack arrest toughness can been approximated using small-scale testing such as Charpy testing or drop-weight Pellini testing. It has been observed that some modern steels show high Charpy impact toughness, but poor resistance to a propagating crack. Previously, it was thought that high Charpy toughness would equate to high crack arrest toughness, but this is evidently not the case. This raises some concerns over the legitimacy of the use of small-scale testing as a measure of crack arrestibility.

1.1 Aims and Objectives

The aim of this work is to determine which small-scale test methods accurately predict the large-scale brittle crack arrest properties of steel. The focus will be on EH47 shipbuilding steel as this is of greatest interest to the sponsor, Lloyd's Register Foundation, and large scale wide-plate testing has been carried out extensively on this material. Four other structural steels will be analysed to determine if trends can be found between various material properties which are known to affect crack initiation and propagation.

The main objectives of this work are:

- Carry out comprehensive material characterisation using a wide range of experimental methods to fully characterise various steels' mechanical and microstructural properties.
- Investigate the relationship between a material's microstructure and its fracture properties in terms of initiation toughness and brittle crack arrest toughness.
- Investigate the relationship between Charpy energy and resistance to fracture propagation and why some materials with high Charpy energy show low crack arrest toughness.
- Determine which parameters that can be measured through small-scale testing are able to determine a steel's fracture properties in terms of initiation toughness and brittle crack arrest toughness.
- Carry out quantitative large-scale testing on EH47 shipbuilding steel to validate the predictions made from small-scale testing.
- Verify previously proposed empirical relationships to determine if they are relevant for modern structural steels, and identify which are most appropriate for future use.

1.2 Structure of thesis

This thesis is presented in "paper" format. Each of the following papers is a self-contained piece of work which comes together to form this piece of EngD research:

Chapter 2: Literature review. This covers the theory of the brittle crack arrest methodology in the context of popular modern and historical test methods. This paper discusses the challenges faced by the shipbuilding industry and classification societies and therefore the areas which need further research.

Chapter 3: Microstructural analysis. This comprises a characterisation of five different structural steels though optical and electron microscopy, and neutron diffraction. Microstructural characteristics including grain size, elongation and texture of the material are determined. This feeds heavily into the following chapter where the influence of microstructure on material properties is discussed.

Chapter 4: Small-scale testing. This chapter includes results from a wide range of experiments including tensile, drop weight Pellini, instrumented Charpy, and SEN(B) fracture toughness testing. The key microstructural parameters are included from the previous chapter to determine how the microstructure influences a material's fracture properties. The relationship between initiation and arrest properties of steels is investigated and compared to empirical predictions which are discussed in the literature review. The key results from this chapter are published in a journal paper, along with some of the microstructural results. Preliminary results were presented at conferences and two conference papers were produced in total.

Chapter 5: Large-scale testing. These are the key results from this EngD research. Ambitious CCA testing was carried out on EH47 shipbuilding steel to verify the predictions from small-scale testing in the previous chapter. The advantages of CCA testing are discussed alongside the challenges associated with large-scale crack arrest testing. This paper is currently under review for publication in a journal.

1.3 Publications

1.3.1 Conference Papers

- Taylor, J., Mehmanparast, A., Kulka, R. and Moore, P., 2019. Correlation between steel initiation toughness and arrest toughness determined from small-scale mechanical testing. *Procedia Structural Integrity*, *17*, pp.472-478.
    - This contains some of the preliminary results given in chapters 3 and 4.
- Taylor, J., Moore, P., Mehmanparast, A. and Kulka, R., 2019, June. Correlation Between Steel Microstructural Characteristics and the Initiation and Arrest Toughness Determined From Small-Scale Mechanical Testing. In *ASME 2019 38th International Conference on Ocean, Offshore and Arctic Engineering*. American Society of Mechanical Engineers Digital Collection.

- This contains some of the preliminary results given in chapters 3 and 4, analysed from a different perspective to the previous conference paper.

1.3.2 Journal Papers

- Taylor, J., Mehmanparast, A., Kulka, R., Moore, P., Xu, L. and Farrahi, G.H., 2020. Experimental study of the relationship between fracture initiation toughness and brittle crack arrest toughness predicted from small-scale testing. *Theoretical and Applied Fracture Mechanics, 110*, p.102799.
    - This contains the final results for all materials from chapter 4 and the optical microscopy from chapter 3.
- Taylor, J., Mehmanparast, A., Kulka, R., Moore, P., Xu, L. and Farrahi, G.H., (2021). Compact Crack Arrest Testing and Analysis of EH47 Shipbuilding Steel. *Theoretical and Applied Fracture Mechanics*, p.103004.
    - This covers the CCA testing from chapter 5.

1.3.2.1 Wider Research Activities

- Mehmanparast, A., Taylor, J., Brennan, F. and Tavares, I., 2018. Experimental investigation of mechanical and fracture properties of offshore wind monopile weldments: SLIC interlaboratory test results. *Fatigue & Fracture of Engineering Materials & Structures*, *41*(12), pp.2485-2501.
    - I contributed to this joint industry project between a consortium of major wind farm operators as part of my wider research into offshore wind support structures and structural steels. This project involved a wide range of experimental testing of a number of plates of steel and their weldments. Through analysis of round-robin testing, the variation in material properties of nominally identical steels was determined, including variation between steel plates from the same batch. My contribution to this project was analysis of the experimental data and being involved in writing the paper.
- Moghaddam, B.T., Hamedany, A.M., Taylor, J., Mehmanparast, A., Brennan, F., Davies, C.M. and Nikbin, K., 2020. Structural integrity assessment of floating offshore wind turbine support structures. *Ocean Engineering*, *208*, p.107487.

- I contributed to this joint project between Cranfield University, Strathclyde University, and Imperial College London as part of my wider research into offshore wind support structures. The aim of this SUPERGEN Wind Hub-sponsored project was to predict the fatigue life and ultimate capacity of a spar-type floating offshore wind turbine foundation with a focus on corrosion pitting at the mooring chain connection. My contribution to this project was carrying out engineering criticality assessments under a range of conditions determined from finite element modelling, along with being involved in writing and editing of the paper.

1.3.3 Presentations

- Taylor, J., Mehmanparast, A., Eren E., He, W., Farrahi, H. (2017, June 18-23). *Review of Crack Arrest Theory, Techniques and Applications* [Conference presentation]. International Conference on Fracture (ICF14). Rhodes, Greece.
- Taylor, J., Mehmanparast, A., Moore, P., Kulka, R. (2017, September 18-19). *Assessment of crack arrest behaviour in modern structural steels* [Conference presentation]. 3rd REMS Annual Conference. Cranfield, UK.
- Taylor, J. (2018, May 9-10). *Brittle Crack Arrest for Container Ships - "three-minute thesis"* [Presentation]. Lloyd's Register Foundation International Conference 2018 Student Competition. London, UK.
- Taylor, J., Kulka, R., Mehmanparast, A. (2018, July 3-4). *Review of Crack Arrest Theory, Techniques, and Applications* [Conference presentation] National Structural Integrity Research Centre (NSIRC) 2018 Annual Conference. Cambridge, UK.
- Taylor, J. (2019, March 13). *Using Small Scale Mechanical Tests to Predict the Crack Arrest Properties of Modern Structural Steels* [Poster Presentation]. STEM for Britain Poster Competition 2019. Houses of Parliament, London, UK.
- Taylor, J., Mehmanparast, A., Kulka, R., Moore, P. (2019, May 24). *Assessment of crack arrest behaviour in modern structural steels* [Conference presentation]. 4th REMS Annual Conference. Glasgow, Scotland, UK.

- Taylor, J., Moore, P., Mehmanparast, A., Kulka, R. (2019, June 9-14). *Correlation between steel microstructural characteristics and the initiation and arrest toughness determined from small-scale mechanical testing* [Paper presentation]. 38th International Conference on Ocean, Offshore & Arctic Engineering (ASME OMAE 2019). Glasgow, Scotland, UK.
- Taylor, J., Kulka, R. (2019, July 2-3). *What is the correlation between fracture initiation and brittle crack arrest behaviour? Results from small-scale mechanical testing and microstructural analysis* [Conference presentation] National Structural Integrity Research Centre (NSIRC) 2019 Annual Conference. Cambridge, UK.
- Taylor, J., Moore, P., Mehmanparast, A., Kulka, R. (2019, September 2-5). *Correlation between steel microstructural characteristics and the initiation and arrest toughness determined from small-scale mechanical testing* [Paper presentation]. International Conference on Structural Integrity (ICSI 2019). Funchal, Madeira, Portugal.
- Taylor, J., Kulka, R., Mehmanparast, A. (2020, July 23). *Compact Crack Arrest testing of EH47 Shipbuilding Steel* [Conference presentation] National Structural Integrity Research Centre 2020 Annual Conference (NSIRC 2020 Live). Online.
- Taylor, J., Mehmanparast, A., Kulka, R., Moore, P. (2020, August 13). *Can you predict brittle crack arrest behaviour of modern structural steels from Charpy testing?* [Webinar]. TWI The Welding Institute Global Webinar. Online
- Taylor, J. (2020, September 23). *Small scale brittle crack arrest testing of EH47 shipbuilding steel* [Technical forum presentation]. IACS Expert Group (for Materials, Welding, and NDT) Technical Forum, Online.

2 Literature Review

Abstract

It is vital to prevent brittle fracture which can result in total catastrophic failure of a structure. This is particularly important in the shipbuilding and energy industries where structural failure can result in loss of life and expensive assets. A brittle crack can be arrested under certain circumstances which depend on the material and operating conditions. The arrestibility can be characterised through parameters measured from large scale testing such as: the crack arrest toughness, K_{Ia}, and the crack arrest temperature, CAT. These parameters can be related empirically to parameters measured from small-scale testing. However, since modern steel plates have increased toughness and thickness, these relationships begin to break down and the crack arrest behaviour may not be fully understood. This review summarises current knowledge and findings and highlights the most promising methods to predict crack arrest toughness from small-scale testing.

Keywords: brittle crack arrest, literature review, fracture mechanics, shipbuilding

Nomenclature

a	Crack length
a_0	Initial crack length
a_a	Crack length at arrest
B	Specimen thickness
B_N	Specimen net thickness between side-grooves
d	Change in CMOD over one cycle
δ	Crack mouth opening displacement
E	Elastic Young's modulus
F	Applied Load
H	Length of sample to centre, $2H = L$
K	Stress concentration factor
K_0	Fracture initiation toughness

K_a	Crack arrest toughness
K_{ca}	Crack arrest toughness: critical stress intensity factor for crack arrest under mode I fracture mechanics loading condition
K_{Ia}	Crack arrest toughness: measured via ASTM E1221
K_{Ic}	Critical stress intensity factor for mode I fracture initiation, also fracture initiation toughness
L	Length of sample from edge to edge
L_p	Distance between loading pins
mmt	Thickness in millimetres
N	Slot width
n	Number of cycles to arrest
P	Applied Load
σ_{Yd}	Dynamic yield strength
σ_{Ys}	Static yield strength
T	Temperature
t	Thickness
W	Specimen width
x_a	Distance in x direction to the crack arrest point
x_{br}	Distance in x direction to a branched crack's arrest point
y_a	Distance in y direction to the crack arrest point
CAT	Crack arrest temperature
CCA	Compact crack arrest test method or specimen
CMOD	Crack mouth opening displacement
COD	Crack opening displacement
DTT	Double tension test
DWT	Drop weight test
DWTT	Drop weight tear test
FATT	Fracture appearance transition temperature
LEFM	Linear elastic fracture mechanics
NDTT	Nil ductility transition temperature
SIF	Stress intensity factor

2.1 Introduction

Structures in offshore environments are exposed to very harsh loading conditions, with both wind and wave loading in addition to the operating loads i.e. its own mass and moving components[1,2]. To withstand these conditions, the materials used must be very strong and tough. Nonetheless, there is a risk of accidental damage resulting in brittle fracture which is usually catastrophic. In such structures a crack will usually initiate around a welded region, which is the part of a structure most susceptible to cracking due to: material mismatch; heat input which changes material properties; locked-in residual stresses; and increased chance of impurity inclusions during the welding process[3]. It is essential to ensure that accidental damage does not cause total structural failure of an asset which can result in loss of life and great expense.

2.1.1 Motivation: issues facing shipbuilding industry

Brittle fracture is an issue which has caused many catastrophic failures of large welded structures in history. Some of the earliest high-profile major structural failures due to brittle fracture are those of the Liberty ships during WWII[4]. Other major catastrophes which fuelled research into brittle fracture have included those of storage vessels such as the Fawley crude oil storage tank in 1952 and the John Thompson pressure vessel in 1965[5]. Research conducted on the topic of brittle fracture discovered that (ferritic) structural steels exhibit a transition from ductile to brittle behaviour as the temperature decreases and that welds are hotspots for brittle crack initiation[6]. The ductile-brittle transition behaviour was initially characterised through Charpy V notch impact testing and later Pellini drop weight testing was also used[5,6].

Advancements have been made in the shipbuilding industry since the 1940s including designing ships to have fewer sharp corners to act as stress concentrators and reinforcing the hulls to prevent brittle fracture[7,8]. In modern days, the requirements for shipbuilding steels are set by the International Association of Classification Societies (IACS), which includes assurance organisations worldwide. This EngD project is sponsored by IACS member Lloyd's Register. There is a drive to reduce carbon emissions of the shipping industry by using larger ships which can carry more cargo per journey[9]. These ships require stronger and thicker plates of steel for their hulls, and this carries with it an

increased risk of brittle fracture, particularly in the case of bad weather or accidental damage[1,2]. A brittle crack can be prevented from causing catastrophic failure of the structure by ensuring that the materials used have a sufficient resistance to a propagating fracture i.e. high brittle crack arrest toughness[10]. Regardless, the shipping industry still faces structural integrity challenges which are caused by the up-sizing of container ships[7,11]. In recent years, this has resulted in break-in-two failure of two major container ships, the MSC Napoli in 2007 and the MOL Comfort in 2013, which has accelerated research into the brittle fracture properties of ship hull steels[12–14].

2.1.2 Fracture mechanics theory

Chance of crack initiation in large steel structures can be reduced by employing the best possible welding practice to reduce the chance of impurity inclusion and minimise heat input along with using well-matched weld metal. Smaller components can be heat-treated after welding, to reduce the damaging effects of welding residual stresses and reinforce the materials microstructure and larger structures can receive local heat treatment or compressive treatments such as peening[3]. However, this is simply not commercially viable for very large components such as ships, wind turbine support structures, or long welded pipelines.

The most common kind of cracking is fatigue cracking, where a crack slowly grows over many loading cycles[15]. Fatigue cracks can be monitored through inspection, although this may not feasible or effective for a large complex structure such as a ship which may have a double hull for strength and many inaccessible areas. By monitoring the growth of a crack, appropriate maintenance can be carried out when necessary – for example grinding out a crack before it reaches a critical size. A load cannot be transferred through a crack, so once it grows too large the whole structure will fail. In contrast to fatigue cracks, which grow slowly, a brittle crack cannot be monitored as failure happens almost instantaneously. The fracture initiation prevention approach uses multiple techniques to minimise the chance of a crack initiating, for example: the number of welds is minimised to reduce the number of weak spots, and sharp corners are avoided as these can cause a concentration of stress which leads to cracking.

An alternative approach to initiation prevention is the crack arrest approach. Using this concept, it can be considered that fracture may occur in a local region of high stress, embrittlement or under accidental damage. However, the material's properties are carefully controlled so it has a sufficient toughness to inhibit fracture propagation in the bulk metal[16]. When the crack arrests before growing too long, catastrophic failure can be prevented. This is vital for a structure with welds, which can be a hotspot for defects or embrittled zones which promote fracture initiation. Moreover, the crack arrest approach can be more reliable than the initiation approach at preventing catastrophic fracture as it accounts for accidental damage and is effective even once a crack is growing[17]. At a temperature, *T*, above the nil ductility transition temperature[10] (*NDTT*), i.e. $T > NDTT$, and small crack lengths up to 10mm, the arrest approach is a more reliable approach, and becomes more reliable at temperatures well above *NDTT* [17].

Crack growth behaviour is predicted using the principles of fracture mechanics, which use the theories of elasticity and plasticity to determine the macroscopic material behaviour. Brittle fracture can be characterised using linear elastic fracture mechanics (LEFM), in which plastic deformation is negligible or limited to a small region ahead of the crack tip[10]. This is an energy based approach, where the strain energy release rate as the crack grows can be used to find the stress intensity at the crack tip under loading. The stress intensity factor, *K*, predicts the stress state near the crack tip and it depends on the size and location of the crack along with the loading conditions and material behaviour[10]. There are 3 orthogonal loading configurations analysed by LEFM, shown in Figure 2-1: mode I is pure tensile loading perpendicular to the crack plane; mode II is pure shear loading in plane with the crack; and mode III is pure shear loading out of plane with the crack. In reality, loading can be a very complex combination of these modes which is termed 'mixed mode' loading.

K is also used as the material's toughness i.e. above what stress intensity factor will a crack begin to grow in this material. For further fracture mechanics theory, see Anderson's Fracture Mechanics[10].

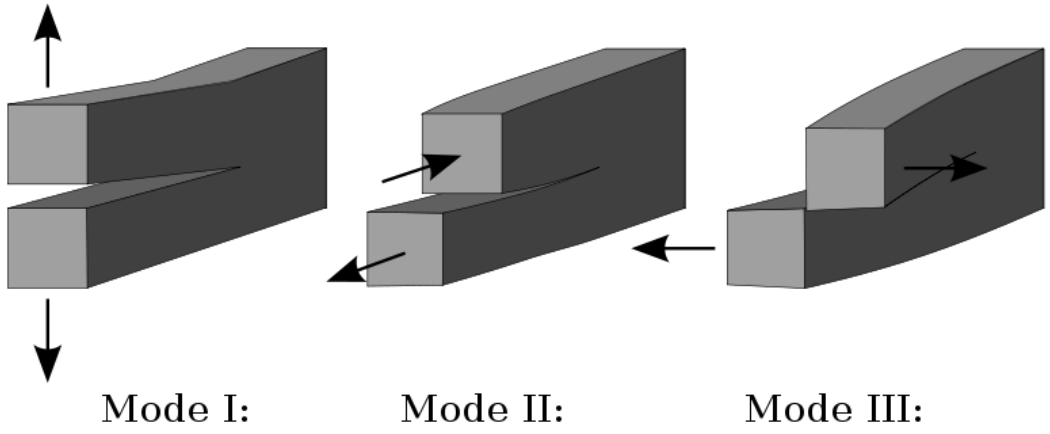

Figure 2-1: The three distinct fracture mechanics modes. For each mode, different equations are needed to be used to characterise the material's behaviour. Image by Twisp, public domain.

A material's resistance to crack initiation can be described by the critical linear-elastic toughness for mode I fracture, K_{IC}, or the elastic-plastic fracture toughness J_{IC}. It is practically simpler to measure K_{IC}, but materials more realistically show both elastic and plastic behaviour and so J_{IC} is a better measure of toughness. J_{IC} is measured using the J-integral, which measures the energy release rate as the crack grows. A related method measures the critical crack tip opening displacement (CTOD) required for a crack to initiate in a particular material. K_{IC}, J_{IC} and CTOD are defined as material properties, but they depend on specimen geometry, loading conditions, and temperature.

Crack arrest properties are typically measured by one of the following two parameters: crack arrest toughness (K_a); crack arrest temperature (CAT). The crack arrest toughness, K_{ca}, can be defined as the critical stress intensity factor under mode I fracture mechanics loading above which a fast-running crack is arrested. Alternatively, a lower bound approximation of crack arrest toughness, K_{Ia}, can be used, although this may give a conservative estimate[18–20]. The CAT is the lowest temperature that a fast-running brittle crack will arrest in a certain material under specified conditions. K_{Ia} and K_{ca} can be determined through standardised methods such as those described in ASTM E1221 and ISO 20064[21–24]. The CAT can be determined by initiating a brittle crack in a material at a range of temperatures and finding the lowest temperature where a brittle running crack arrests[16]. In such experiments, fracture is typically initiated by impacting a region with a notched brittle weld bead.

2.2 Comparison of BCA evaluation methods

The CAT approach often employs simple pass/fail crack propagation tests such as drop weight tests which are carried out at different temperatures in order to find the minimum temperature at which a crack initiates and arrests. Additionally, the fracture surface can be examined to find the fracture surface ductility, and the crack length at arrest a_a, which can be empirically related to large-scale test results[25,26]. However, these empirical relations are typically only valid for particular materials, thicknesses, and sample sizes, and new relations need to be found for each material developed. If the operating conditions are known, then the CAT gives confidence that the material is fit for service at the operating temperature range.

As technology progresses, the structural steels which are available are getting stronger and tougher. For a brittle crack to initiate in a very high toughness material, it needs to overcome a huge energy barrier. This means that the initial driving force of the crack is very high and it can propagate very quickly and jump further before being arrested. This can result in catastrophic failure or severe structural damage before the crack is arrested. Although crack arrest toughness, K_a, is thought of as a material property, it is strongly dependent on the plate thickness, test temperature, applied stress[27–30]. Furthermore, brittle crack arrest toughness shows a dependence on specimen width as well as manufacturing processes[31–34]. The increasing tonnage of container ships leads to a necessity in using thicker hulls of higher strength steels, which has an adverse effect on both their fracture toughness and crack arrestibility. A study looking at 35mm and 70mm thick shipbuilding steel found that even with added stiffeners, the crack could not be arrested in the thicker plate of steel under identical conditions[35]. An example of the effect of thickness on crack arrest behaviour can be seen in Figure 2-2. As seen in this figure, a thicker plate gives a lower toughness at a certain temperature[29]. As the thickness of the steel increases, some historic small scale tests are no longer considered valid to model the behaviour due to the difference in constraint levels[29] and a number of expensive large scale tests will need to be carried out to characterise the plate's behaviour. This makes it complex to predict the crack arrest properties of large structures from subsize specimens, thus introducing a need for a sufficiently conservative approach.

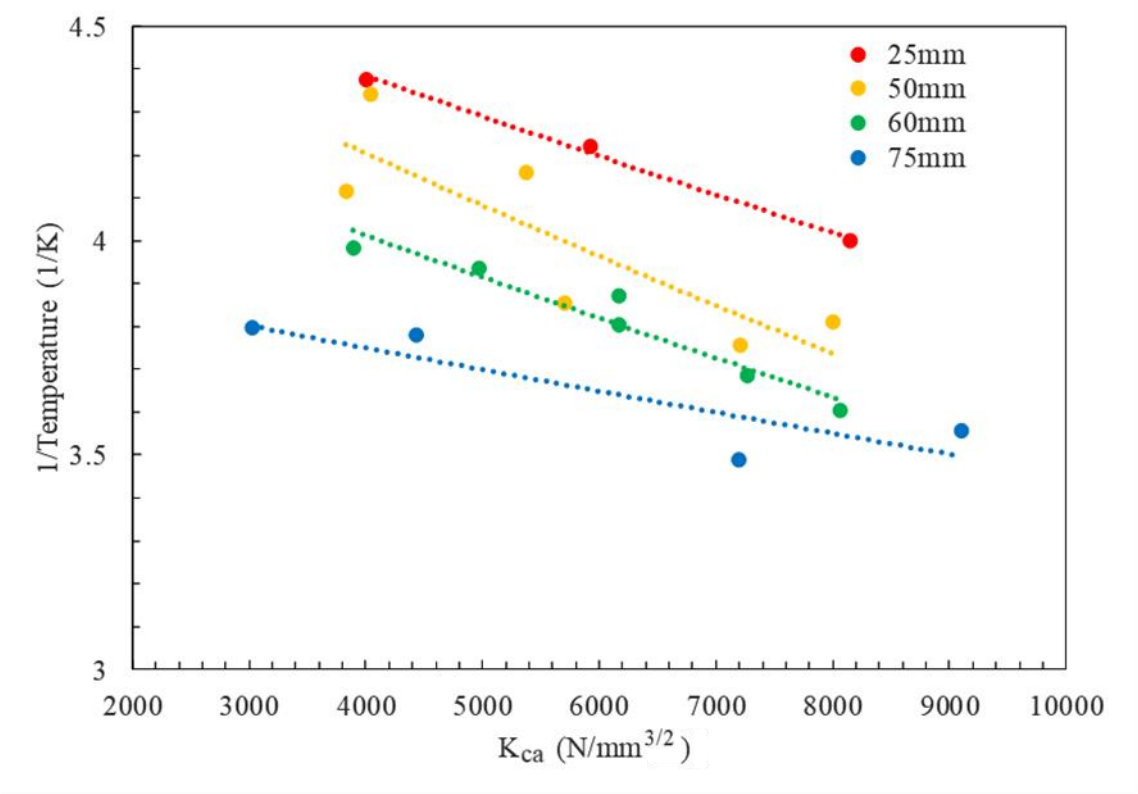

Figure 2-2: Arrhenius plot to show the effect of plate thickness on its crack arrest toughness[29].

Whilst the empirical relationships between small- and large-scale tests were valid for previous material specifications, they need to be verified for modern steels. Current test procedures need to be optimized in order for appropriate certification of thicker, and tougher materials to be possible. This would enable futureproof certification of shipping vessels, to ensure that catastrophic failure does not occur.

2.3 Standard Test Methods for Brittle Crack Arrest Testing and Analysis

The most reliable tests to measure brittle crack arrest are component-scale tests under operating conditions. Large-scale and small-scale tests can be used to approximate this, and find empirical relations from which K_{Ia}, K_{ca} or CAT can be calculated. Large scale wide-plate tests are favoured by the shipbuilding industry as these are the only test methods certified by classification societies (IACS[36]). However, large scale testing is incredibly expensive so there is a need for reliable small-scale testing which is representative of material properties.

This review will focus on the two main standards for brittle crack arrest toughness K_a testing, which are most practical and frequently used: ASTM E1221:2012[21] and ISO 20064:2019[24], which has been recently adopted and is based on JWES 2815:2014[32].

2.3.1 ASTM E1221:2012 Standard Test Method for Determining Plane-Strain Crack-Arrest Fracture Toughness, K_{Ia}, of Ferritic Steels

This approach employs side grooved crack-line-wedge-loaded compact crack arrest (CCA) specimens as shown in Figure 2-3, which gives a rapid run-arrest of a flat-tensile specimen with a nearly straight crack front. Equation 2-1 to Equation 2-5 are used to calculate K shortly after arrest, which is equivalent to K_{Ia} when particular size requirements are met as described by Equation 2-6 to Equation 2-10.

According to the guidelines provided in ASTM E1221 standard[21], the specimen thickness, B, must be large enough to satisfy plane strain conditions, or full plate thickness. The width, W, should be within the range $2B \leq W \leq 8B$, and the height, H, is $0.6W$. A wedge is loaded cyclically into the specimen loading hole (diameter D) with increasing peak load, and the crack mouth opening displacement (CMOD) is used to find K once an arrest event has occurred. According to the ASTM standard, the stress intensity factor can be calculated using Equation 2-1 to Equation 2-5:

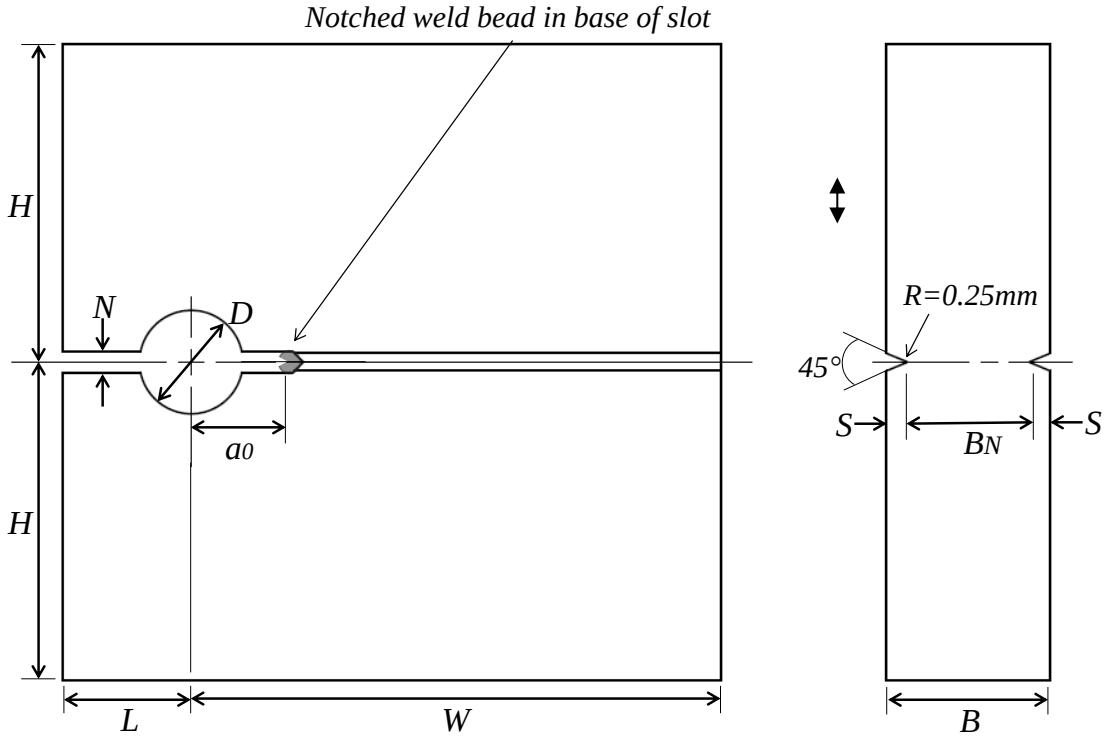

Figure 2-3: Schematic illustration of the CCA specimen design.

$$K = E\delta Y\sqrt{\frac{B}{B_N W}} \qquad \text{Equation 2-1}$$

$$Y = (1-x)^{\frac{1}{2}}(0.748 - 2.176x + 3.56x^2 - 2.55x^3 + 0.62x^4) \qquad \text{Equation 2-2}$$

$$x = \frac{a}{W} \qquad \text{Equation 2-3}$$

where E is the elastic Young's modulus in MPa, B is the specimen thickness in mm, B_N is the net thickness between the side grooves in mm, W is the specimen width in mm, δ is calculated from the CMOD using Equation 2-4 or Equation 2-5, and a is the crack length in mm (i.e. a_0 is the initial crack length and a_a is the arrested crack length). In order to calculate K_0, which is the stress intensity factor at initiation point (known as crack initiation toughness), the crack length is taken as $a = a_0$, and $\delta = d_0$. Similarly, K_a which is known as the crack arrest toughness is calculated using $a = a_a$ and $\delta = d_a$.

δ, used in Equation 2-1, is calculated from the equations below using Figure 2-4 as a reference to show how the parameters are calculated from the load-displacement curve over multiple cycles.

$$d_0 = \delta_0 - (\delta_p)_{n-1} \qquad \text{Equation 2-4}$$

$$d_a = \delta_0 - (\delta_p)_1 - 0.5\left[(\delta_p)_{n-1} - (\delta_p)_1\right] + 0.5[\delta_a - \delta_0] = 0.5\left[\delta_0 + \delta_a - (\delta_p)_1 - (\delta_p)_{n-1}\right] \qquad \text{Equation 2-5}$$

where n is the number of load cycles to the run-arrest event, δ_0 is the CMOD at the crack initiation point, $\delta_{p(n-1)}$ is the CMOD at the start of the nth loading cycle when the load has been reset to 0, and δ_a is the CMOD after the crack has arrested. It can be seen in Figure 2-4 that as the crack propagates, the crack mouth widens before it arrests.

According to ASTM E1221: when the following criteria are met K_a can be taken as K_{Ia} which is the critical stress intensity factor for crack arrest under the mode I fracture mechanics loading condition.

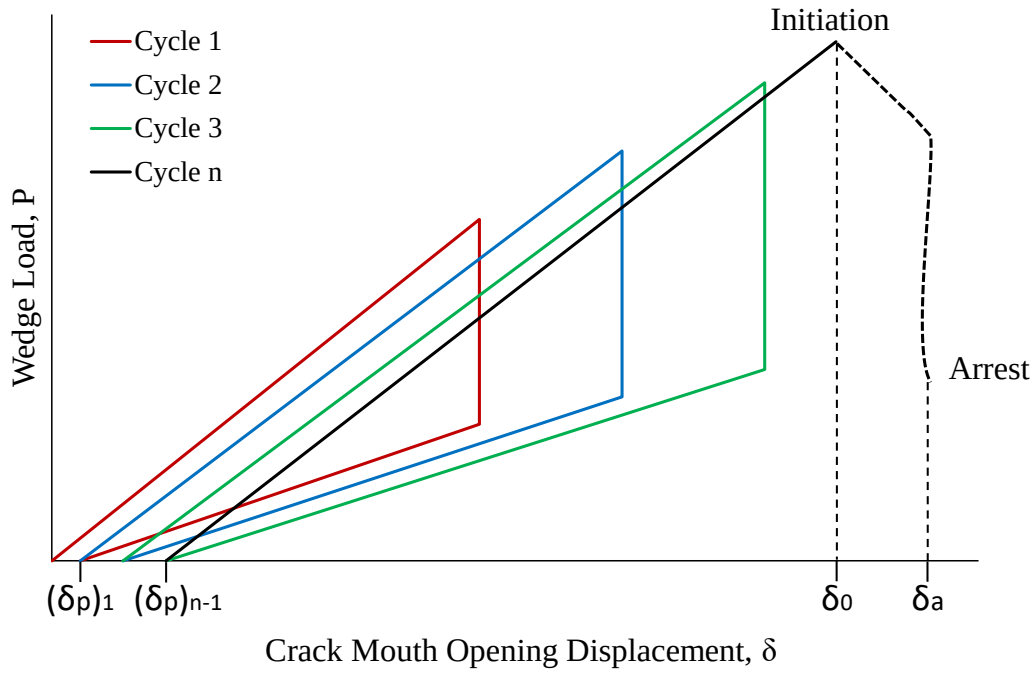

Figure 2-4: Wedge force vs. CMOD using cyclic loading technique. Each loading cycle is shown in a different colour until the final "cycle n" where the crack propagates and arrests.

$$W - a_a \geq 0.15W \quad \text{Equation 2-6}$$

$$W - a_a \geq 1.25(\frac{K_a}{\sigma_{Yd}})^2 \quad \text{Equation 2-7}$$

$$B \geq 1.0\ (\frac{K_a}{\sigma_{Yd}})^2 \quad \text{Equation 2-8}$$

$$a_a - a_0 \geq 2N \quad \text{Equation 2-9}$$

$$a_a - a_0 \geq \left(\frac{K_0}{\sigma_{Ys}}\right)^2 /2\pi \quad \text{Equation 2-10}$$

where N is the machined slot width, W-a is the uncracked ligament, σ_{Yd} is the dynamic yield stress and σ_{Ys} is the static yield stress. These criteria ensure that the specimen is of a sufficiently large size to satisfy plane strain conditions, and that the assumption of static behaviour during the crack jump event is appropriate i.e. dynamic effects are not present.

2.3.2 ISO 20064:2019 Metallic materials - Steel - Method of test for the determination of brittle crack arrest toughness, K_{ca}

The test procedure given in this approach[24,32] typically uses an impact to initiate the crack in a crack starter region which is embrittled either by cooling or by electron weld embrittlement. A temperature gradient is applied on the specimen, with a cooled region at the initiation point and increasing temperature along the crack path. The specimen is held under tension of up to ⅓ of the yield strength (σ_{ys}). This approach utilises "wide-plate" testing with very large specimen sizes. The standard test specimen recommended by this method is shown in Figure 2-5, although variations and adjustments to the procedure for double tension test (without impact) and duplex test (with extended crack starter region) methods are included in the appendices depending on what test configuration is available at the test centre. Following this standard, K_{ca} is measured from the maximum crack length after a run-arrest event. This method has multiple annexes to allow for flexibility with the test method, but the standard recommended method is shown here.

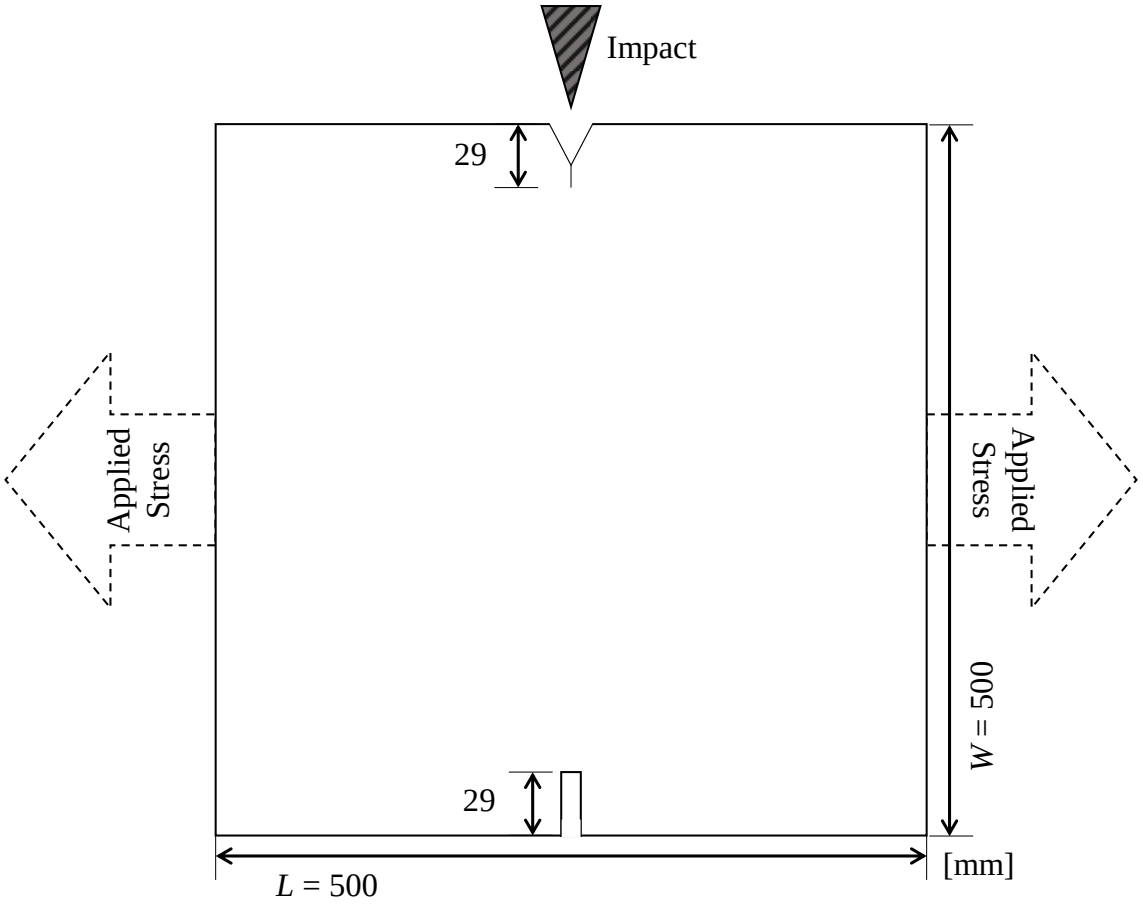

Test specimen thickness, t	$6\text{mm} \leq t \leq 200\text{mm}$
Test specimen width, W	$350\text{mm} \leq W \leq 1000\text{mm}$ (Standard width W=500mm)
Test specimen width/test specimen thickness, $\frac{W}{t}$	$\frac{W}{t} \geq 5$

Figure 2-5: Recommended test specimen employed in ISO 20064 and WES:2815 along with standard dimensions[24,32].

In this approach the specimen of maximum thickness 200mm is held under an applied stress between $\frac{1}{6}\sigma_{ys}$ and $\frac{1}{3}\sigma_{ys}$, and the notch is subjected to an impact from a falling tup in order to initiate a crack, which propagates a distance before arrest.

Once the test has finished, the specimen is broken open using a ductile fracture method and images of the fracture surfaces are recorded. The longest length to the first arrested crack tip, a_a, is measured, and the temperature can be interpolated by reading off a

temperature distribution curve of thermocouples along the surface. From this crack length, K_{ca} is found using Equation 2-11 and Equation 2-12:

$$K_{ca} = \sigma\sqrt{\pi a_a}\left[\frac{2W}{\pi a_a}\tan\left(\frac{\pi a_a}{2W}\right)\right]^{\frac{1}{2}} \quad \text{Equation 2-11}$$

$$\sigma = \frac{10^6 F}{Wt} \quad \text{Equation 2-12}$$

where F is the stress applied in MPa. This gives a valid value of K_{ca} when the following criteria in Equation 2-13 to Equation 2-19 are met:

$$y_a \leq 50\text{mm} \quad \text{Equation 2-13}$$

$$\frac{x_{br}}{x_a} \leq 0.6 \quad \text{Equation 2-14}$$

$$\frac{a}{L_p} \leq 0.15 \quad \text{Equation 2-15}$$

$$a_a = 0.5W \quad \text{Equation 2-16}$$

$$L_p \geq 3.4W \quad \text{Equation 2-17}$$

$$0.3 \leq \frac{a}{W} \leq 0.7 \quad \text{Equation 2-18}$$

$$\frac{a}{t} \leq 1.5 \quad \text{Equation 2-19}$$

where L_p is the distance to the loading pins from the crack tip in mm, y_a is the maximum crack extension in the y direction in mm, x_a is the maximum crack extension in the x direction in mm, x_{br} is the maximum extension in the x direction of any secondary crack branch in mm. This ensures that the crack is straight (Equation 2-13), with minimal crack branching (Equation 2-14), the dynamic effects of reflected stress waves from initiation are minimised (Equation 2-15 to Equation 2-17), and an adequate crack length is achieved to be considered a complete run-arrest event (Equation 2-18 and Equation 2-19). The calculated K_{ca} can be considered to be a reference value if the conditions above are not all met. A schematic illustration of the validity criteria given in equations Equation 2-13 to Equation 2-19 is shown in Figure 2-6.

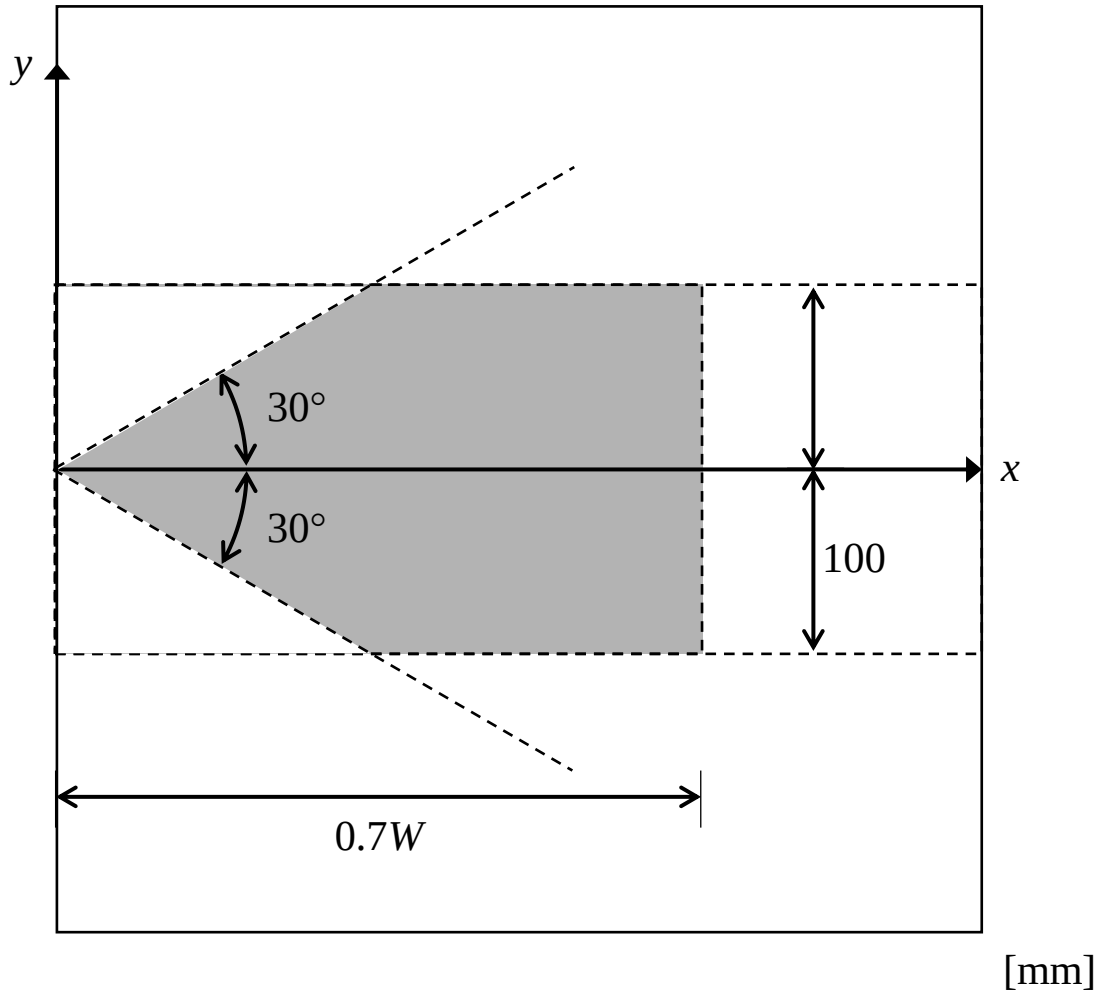

Figure 2-6: Allowable crack path and size for K_{ca} calculation. Allowable region in grey.

2.3.3 Comparison between ASTM1221 and WES2815

The ASTM standard uses a static approach to calculate a lower-bound K_{Ia}. The static approach assumes that the initiation, run, and arrest event is instantaneous. It is valid for small crack jump lengths, and where the initiation toughness and arrest toughness are similar, otherwise this analysis is too conservative. CCA test results agree well with large scale tests, but may underestimate the toughness[37–39].

The ISO standard additionally includes a document which explains the assumptions and validity criteria of the main standard, which are based on the results of experimental work. Further annexes in the standard include methods for finding results from tests with other conditions: dynamic measurement of results; isothermal tests; double tension loading configurations; duplex starter sections for use in high strength steels; and tests which

result in an overly curved crack. This means that this standard is valid for a wider range of test conditions than the ASTM test, and includes corrections to test technique which are not considered by ASTM, for example using a duplex sample to allow for easier crack initiation in a very tough material. However, the flexibility of using different methods increases the complication of the ISO standard compared to the simpler ASTM standard. It is important to consider that each test gives a different estimate crack arrest toughness, and can be used to complement each other and verify results.

Due to the large size requirements of the ISO standard "wide-plate" specimens and the need for the specimen to be under high levels of tension during the test (typically over 150 MPa), this kind of testing is expensive and complicated to carry out. CCA testing may give a lower estimate of brittle crack arrest toughness, but the tests are a lot cheaper and easier to carry out. CCA testing is a promising alternative to wide-plate testing which would make quantitative measurement of brittle crack arrest toughness cheaper and more accessible.

2.4 Wide-plate Tests

Large scale test specimens are typically in the size range of metres. These can be structurally representative, which are the most reliable tests but also the most expensive. Robertson tests, shown in Figure 2-7, cool the sample to a certain temperature, apply the maximum design stress, and impact the notch[40]. The minimum temperature at which a no-go result is observed is deemed to be the CAT. These are no longer commonly used because of the prohibitive cost of large scale isothermal testing. ESSO tests are a modified Robertson test with an increased test section length, which can be used to find K_a[41]. These are often the same as those in ISO 20064, but may have different dimensions or not meet the criteria in Equation 2-13 to Equation 2-19. ESSO tests are more commonly used in industry, both following the standard and other designs, and are described by Equation 2-20[42].

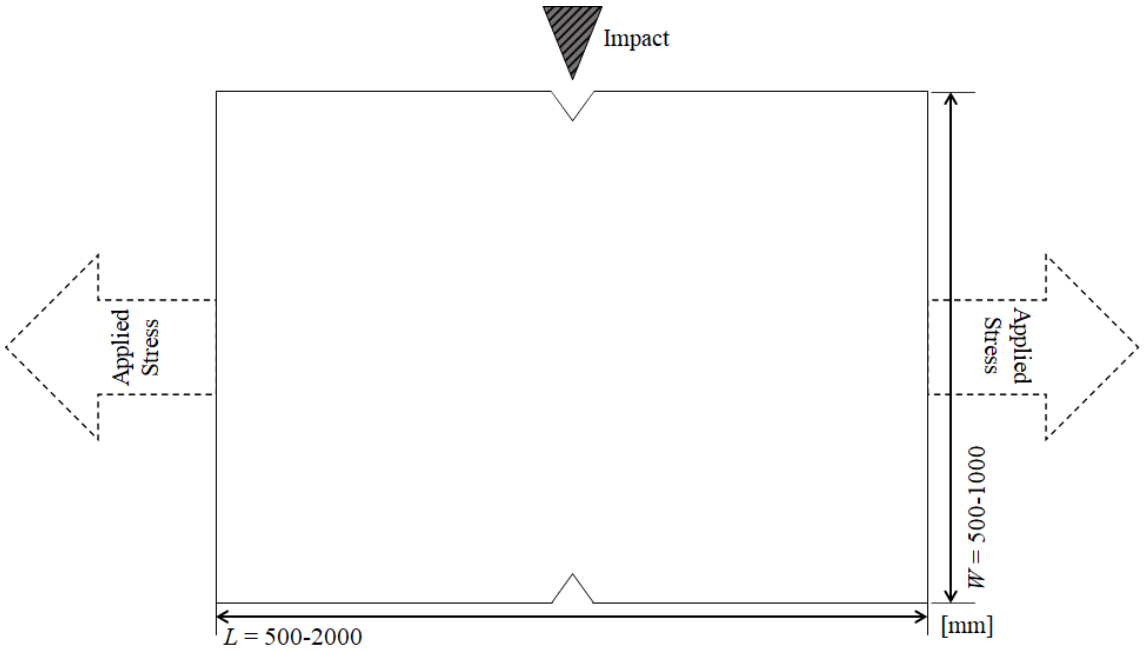

Figure 2-7: The basic set up for a Robertson test – a simple impact style test.

$$K_{ca} = \sigma\sqrt{\pi a_a}Y \qquad \text{Equation 2-20}$$

where Y is a geometry-dependent shape factor.

Double tension tests (DTT, Figure 2-8) have no impact loading, and instead use loading tabs to increase the stress concentration around the notch and introduce a high enough stress intensity factor to initiate brittle fracture, often using an embrittled starter section[43]. The subsidiary loading on the tabs contributes to the stress intensity factor at the crack tip and hence adds a term into the toughness calculation shown in Equation 2-21.

Large scale tests are extremely expensive and challenging to carry out. Of the wide plate tests, the DTT is recommended because: it can be used both isothermally and with a temperature gradient; the applied stress can be controlled through starter length and applied stress; and the initiation does not require an impact which may affect propagation. The same concerns mentioned in section 2.3.3 apply to the wide-plate testing discussed in this section which further demonstrates the need for reliable and affordable brittle crack arrest testing.

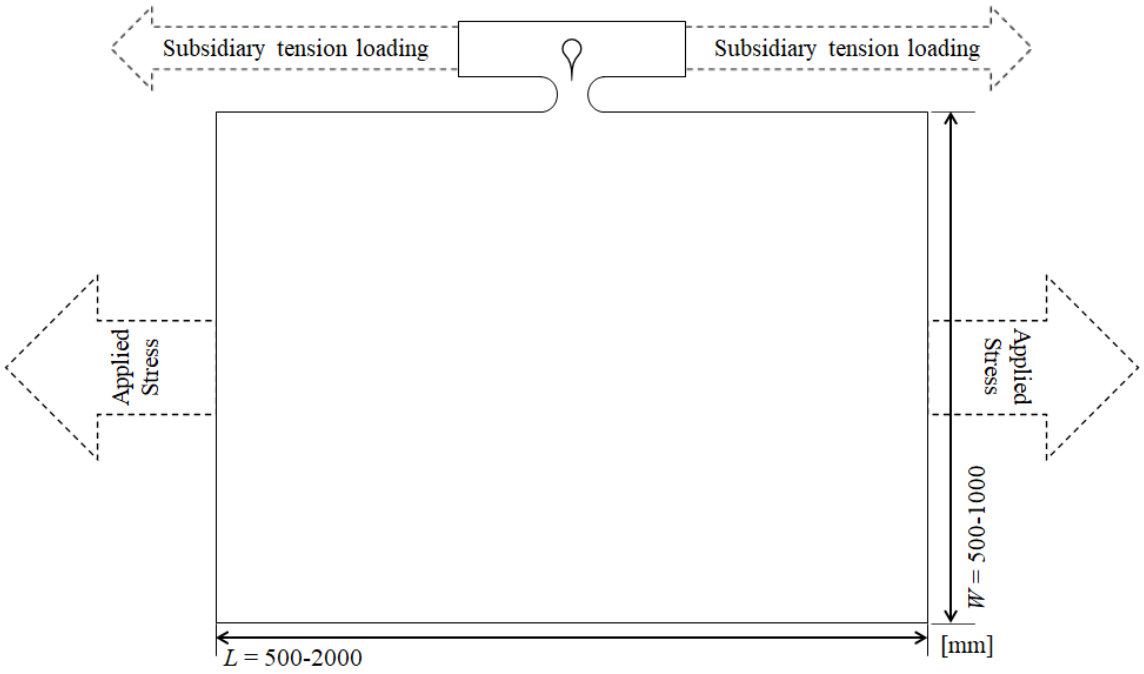

Figure 2-8: The basic set up for a DTT test – a simple non-impact style test.

$$K_{ca} = \sigma\sqrt{\pi a_a}Y + K_{tab} = \sigma\sqrt{\pi a_a}Y + \frac{P_{tab}Y_{tab}}{B\sqrt{\pi a}} \qquad \text{Equation 2-21}$$

where K_{tab} is the additional stress intensity factor due to the force applied to the tab, P_{tab}, and Y_{tab} is a geometry-dependent shape factor.

2.5 Small Scale Tests

Small scale tests are cheap and easy to carry out, and can be used to find empirical equations which relate them to larger scale test methods. However, the empirical equations are validated for certain specimen dimensions of a given material at a specified thickness, under a certain loading rate. This means that they cannot necessarily be applied to represent a large structure which would almost certainly not meet the strict validity criteria. Since crack arrest toughness depends on temperature, the ductile to brittle transition of the material must be understood and this can be done effectively through small-scale testing. Reference temperatures determined from the ductile-brittle transition of the material can be used to approximate the CAT.

There are a number of small-scale test methods which determine material properties that have been adopted for use in brittle crack arrest. Charpy impact tests measure the energy

absorbed during fracture of a material at different temperatures, and can be instrumented to measure: the impact force, the load point displacement, and CMOD[44]. Additionally, post mortem analysis can be carried out on the fracture surface to determine the % shear and crystalline fracture, and lateral expansion in line of impact. The ductile-brittle transition curve of the material can be characterised by Charpy impact tests over a wide temperature range. Drop weight tests include the Pellini test, which is impacted under 3 point bend and finds the NDTT, which is the maximum temperature at which a brittle crack initiates but does not arrest[22]. Using the empirical relations, this gives the best agreement of the simple small scale tests[43]. A second drop weight test is the drop weight tear test (DWTT), which is used at upper shelf temperatures and to calculate the CAT for ductile tearing and is popular in the pipeline industry[45–47]. Single edge notched bend (SEN(B)) fracture toughness tests can be used to find the K at arrest from the CMOD at arrest, which gives a conservative estimate of K_a compared to CCA wedge loading[48].

Small scale tests have a lower reliability than large scale tests, especially since empirical relations are limited to particular thickness, temperature, and stress ranges. However, they are cheap and easy to carry out reliably and under particular configurations can be rather accurate. Because they employ small test specimens, reflection of stress waves may be prominent and so care must be taken in choice of test method.

2.6 Historical Review of small-scale testing

2.6.1 1960s-1990s – Empirical relationships

Many equations have been proposed for relating crack arrest parameters to each other in order to utilise small-scale testing rather than expensive wide-plate testing. Many of these relations were developed in the 1990s or earlier and are not in common use nor verified for modern materials. Some relations to approximate the CAT in an isothermal Robertson test (CAT_{iso}) were derived in the 1980-90s in the UK[49,50]:

$$\mathrm{CAT}_{iso} = \mathrm{CAT}_{grad} + 20\ (\pm 20)°C \qquad \text{Equation 2-22}$$

$$\mathrm{CAT}_{iso} = 0.84\,\mathrm{T}_{27J} + 3\ (\pm 24)°C \qquad \text{Equation 2-23}$$

$$\mathrm{CAT}_{iso} = \mathrm{NDTT} + 10\ (\pm 15)\ °C \qquad \text{Equation 2-24}$$

This enables the CAT_{iso} to be determined from: the *CAT* from gradient tests (CAT_{grad}); the temperature at which the Charpy impact energy is 27J (T_{27J}); and the NDTT from Pellini testing. These relations were determined for plates of 50mm and all temperatures are measured in $°C$. Equation 2-25 allows for prediction of the CAT_{iso} from a combination of NDTT, applied stress (σ) and plate thickness (t)[51–53].

$$\mathrm{CAT}_{iso} = \mathrm{NDTT} + 10 + 1.3(\sigma - 12.6) + 5.3(\mathrm{t} - 12)^{\frac{1}{2}} °C \quad \text{Equation 2-25}$$

These can be compared to relations developed around the same time in Japan, where the CAT was compared between different test methods. With an applied stress of half of the yield stress and a plate thickness from 20-50mm, Equation 2-26 describes the general relationship between the results from isothermal and gradient testing which is quantified in Equation 2-27[54].

$$\mathrm{CAT}_{grad} > \mathrm{CAT}_{iso} \quad \text{Equation 2-26}$$

$$\mathrm{CAT}_{iso} = \mathrm{CAT}_{grad} - 16\ (\pm 10)°C \quad \text{Equation 2-27}$$

Equation 2-22 is in complete disagreement with Equation 2-27, which led to a drive to better understand brittle crack arrest and develop more reliable test methods. The following relations are the culmination of multiple studies of Charpy V-notch (CVN) and Pellini impact testing to relate the amount of energy absorbed during impact to the NDTT[22,40,43,45,55–59]. Similar relationships are available to relate the Charpy transition curve to the DWTT transition curve.

$$NDTT = T_{120J} + 50°C \quad \text{Equation 2-28}$$

$$NDTT = T_{40J} + 60°C \quad \text{Equation 2-29}$$

$$NDTT = T_{27J} + 60°C \quad \text{Equation 2-30}$$

$$NDTT = 50\%\ CVN\ FATT + 50°C \quad \text{Equation 2-31}$$

where T_{xJ} is the temperature at which xJ of energy is absorbed and is read from the best fit to the Charpy transition curve. The $50\%\ CVN\ FATT$ is the temperature at which the fracture surface of the Charpy specimens shows 50% ductile and 50% brittle fracture texture. The scatter in results is considerable, however it is well appreciated that Charpy

tests measure both fracture initiation and fracture propagation mechanisms and a good amount of plasticity is introduced during the fracture, which absorbs much of the energy[60]. In contrast, Pellini testing measures purely brittle behaviour with very little plasticity. In addition, the small size of the Charpy specimen causes difference in constraint as compared with the thicker Pellini test. Therefore, only very approximate relations exist between Charpy energy and crack arrest test results.

From early empirical relationships to evaluate brittle crack arrest from scale-scale testing, one relationship stood out through round robin testing as giving good agreement and conservative estimates of CAT[16]:

$$CAT = NDTT + 40°C \qquad \text{Equation 2-32}$$

This good correlation between NDTT and CAT for different materials and welds is not surprising since the drop weight test is a measure of the resistance against continuous fracture propagation. Resistance to continuous fracture propagation is equivalent to crack arrestibility, characterised by the CAT.

2.6.2 Semi-Empirical Relations with Corrections for Thickness and Applied Stress

From the simple relations given above, a range of tests were carried out to make corrections for a variation in applied stress and thickness[48]. This relationship uses the reference conditions of the CAT for 124 MPa applied stress (σ) on a 25 mm thick (B) plate and adds corrections for other stresses and thicknesses. Equation 2-33 and Equation 2-34 developed by Smedley cover the thickness range from 12-50mm[61].

$$\mathrm{CAT} = (\mathrm{NDTT} + 10) + (1.3\sigma - 16) + (5.3\sqrt{[\mathrm{B} - 12]} - 19)°C \qquad \text{Equation 2-33}$$

$$\mathrm{CAT} = (\mathrm{NDTT} + 10) + \left(\frac{\ln[\sigma]}{0.046} - 105\right) + (5.3\sqrt{[\mathrm{B} - 12]} - 19) + (100 \ln [f\left(\frac{a_a}{W}\right)]°C \qquad \text{Equation 2-34}$$

$$\text{where } f\left(\frac{a_a}{W}\right) = \sqrt{\left(\frac{2B}{\pi a_a}\tan\frac{\pi a_a}{2B}\right)} \qquad \text{Equation 2-35}$$

where $f\left(\frac{a_a}{W}\right)$ is the finite width correction for centre cracked plates which was theoretically derived and verified through experiment for each different test geometry.

Equation 2-36 developed by Wiesner is valid for 5-250mm thickness[16].

$$CAT = [NDTT + 10] + [\frac{\ln[\sigma]}{0.046} - 105] + [153(B-5)^{\frac{1}{13}} - 190]\,°C \qquad \text{Equation 2-36}$$

This in turn has led to the formula commonly used today, in the R6 defect tolerance assessment procedure for the UK nuclear industry[62,63]:

$$CAT = NDTT + 21.7\ln\sigma + 173.2(200B - 1)^{\frac{1}{13}} - 285\,°C \qquad \text{Equation 2-37}$$

Figure 2-9 shows the agreement with the experimental data, which is very good at the lower thicknesses but there is a distinct lack of data at higher thicknesses which gives a lack of confidence above 50mm thickness.

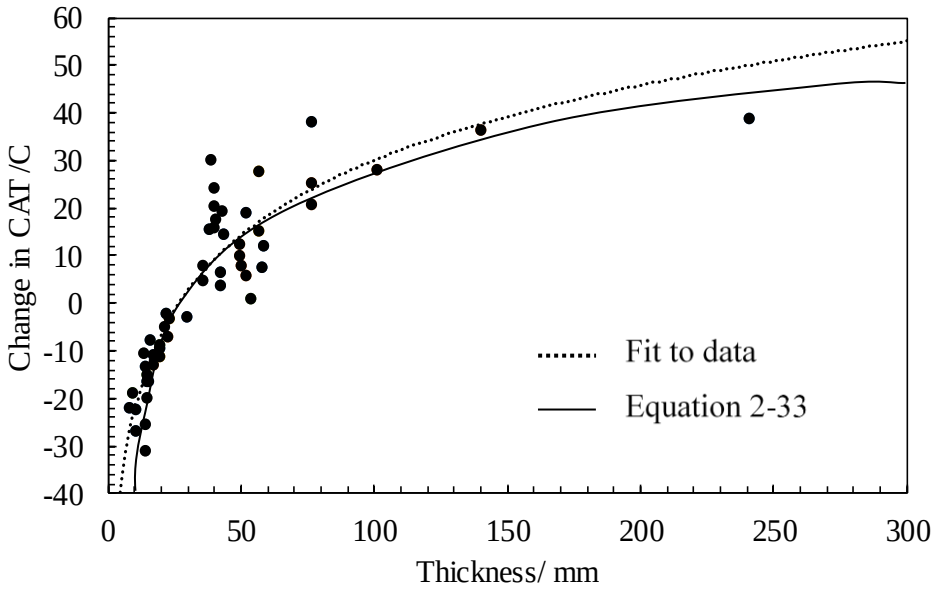

Figure 2-9: Change in CAT compared to that of a plate with 25mm thickness. From Wiesner[16], who collected the data from a range of previous studies. The fit to this data comes from Equation 2-33.

2.6.3 Reference Curves

Reference curves are used extensively in the pressure vessel industry to give a lower bound crack initiation toughness for all the grades of pressure vessel steel at temperatures

within the transition region[33]. Originally, the American Society of Mechanical Engineers (ASME) reference curve was used in industry[64], which gives an estimate based on extensive experimental results. The master curve approach is an alternative statistical approximation which may give a higher degree of accuracy[65,66]. These approaches use a reference temperature (for example T_0, the temperature corresponding to a mean initiation fracture toughness of 100 MPa√m) for the material to calculate its toughness at a given temperature[33]. The median fracture toughness, K_{JC}, is predicted using the following equation[33]:

$$K_{JC(median)} = 30 + 70\, e^{0.019\,(T - T_0)} \qquad \text{Equation 2-38}$$

where K_{JC} is in MPa√m and T, the assessment temperature, has the unit of $°C$ (i.e. degrees Celsius). It is assumed that both the initiation toughness, K_{JC}, and lower bound approximation of crack arrest toughness, K_{Ia}, data are expected to exhibit the same temperature dependence since the temperature dependence of both toughness values is controlled by the atomic arrangement, or crystal structure of the material. Consequently, the temperature dependence is expected to be common to all ferritic steels[64]. Through analysis of a large amount of experimental data, the following relations which are relevant to this work were proposed in the literature[64,67]:

$$K_{IC} = 51.276 + 51.897\, e^{0.036\,(T - NDTT)} \qquad \text{Equation 2-39}$$

$$K_{Ia} = 49.957 + 16.878\, e^{0.028738(T - NDTT)} \qquad \text{Equation 2-40}$$

where K_{IC} and K_{Ia} are in MPa√m and T, the assessment temperature, has the unit of $°C$ (i.e. degrees Celsius). An alternative correlation which has been developed in previous studies takes the reference temperature from instrumented Charpy testing to describe the arrest toughness using the temperature at which the force after fracture measured by an instrumented Charpy test is 4kN, T_{4kN}[68].

$$K_{Ia} = 30 + 70\, e^{\left(\frac{T - T_{4kN} - 12.3}{52.63}\right)} \qquad \text{Equation 2-41}$$

The pipeline industry typically uses the Battelle Two Curve Method (BTCM) to characterise the pipe's resistance to crack propagation[69]. This method considers the gas decompression curve (driving force) and the dynamic fracture resistance curve which

involves computational fluid dynamics of the fluid in the pipeline[70]. The BTCM is not covered in this review as this kind of ductile fracture is not being considered in this work.

2.6.4 Recent research on small-scale testing

In recent years, there has been some interest in use of small-scale testing to predict brittle crack arrest in the shipbuilding industry, as there is a desire to include it in the IACS unified requirements for brittle crack arrest steels. Much of the recent work on brittle crack arrest has focused on using finite element modelling (FEM) to simulate experimental conditions and predict crack arrest properties. This will be covered in section 2.7. The master curve methods have been investigated by other researchers and generally validated against FEM rather than large scale testing[20,65,71–74]. Modern steels for container ships have been developed to have high crack arrest toughness by rolling using a thermo-mechanically controlled process (TMCP)[75–77]. This texture means that the material properties are not the same throughout the thickness of the steel. It has been proposed that small-scale test methods should sample the near-surface or ¼ wall of the steel to give the best estimate of brittle crack arrest properties for modern shipbuilding steels[77]. An alternative small scale test method to measure brittle crack arrest has been developed in Japan which uses a pressed-notch bend specimen and shows good agreement with ESSO tests[78]. It has not been possible to find a study where a wide range of small-scale test methods were carried out on the same plate of steel to conclusively compare them with one another.

2.7 Finite Element Modelling

In recent years, a number of successful numerical models have been developed to simulate and predict crack arrest in steels. Through adaptation of models used to describe fracture initiation, the mechanism behind crack propagation and arrest is understood to be governed by the local stress criterion[79–88]. That is, crack propagation is determined by the stress state a short distance ahead of the crack tip. This is commonly assessed using the RKR criterion which was originally developed to predict fracture initiation toughness[89]. In this approach, crack propagation is controlled by the crack opening stress shortly ahead of the crack tip, outside of the plastic zone[90]. If the stress ahead of the crack tip exceeds the critical fracture stress, the crack extends forward. This can be further

explained through grain-scale micromechanical models[91–94]. For complex geometries or loading conditions, a local approach to fracture is more reliable than a global approach[85].

The commonly used methods to model a growing crack are element deletion, nodal force release, and XFEM. Other methods include boundary element, meshless, re-meshing, and embedded crack[95]. The element deletion method is quite a basic approximation to the crack growth. When the strain in an element reaches a critical point, its stiffness is reduced to near zero. This causes the element to be insignificant with respect to the other elements and is effectively deleted, therefore the crack front progresses. This method is quite crude, and the crack can only propagate in increments of the element size which limits this approach. Additionally, the crack width is increased by the finite size of the elements which blunts the crack tip and hence reduces the effective stress intensity. The nodal force release method is a generation mode analysis, which means that the crack is modelled following experimental results of crack growth. When the crack propagates, the reaction forces between the nodes at the crack tip are released and the crack grows incrementally. Although this method retains the sharp crack tip, it requires prior knowledge of the crack path because the crack length as a function of time is an input in terms of boundary condition. This method may produce more accurate outputs than the element deletion method, but requires additional inputs in terms of crack propagation behaviour, which may not be known. Both these methods can be improved by re-meshing during the crack propagation, however this requires a projection of the crack growth which is often inaccurate and computationally time-consuming.

A newly developed method of crack modelling is the extended finite element method (XFEM) in which the crack description is unrelated to the meshing or crack location. The crack is established implicitly as the solution of the pair of functions which describe the crack surface and the crack front. These functions evolve to describe the crack as it propagates. The benefits of this method are that the incremental crack extension does not rely on the mesh size, nor is the crack given a finite width (i.e. blunted) due to the element size. However, the material needs to be very well characterised in order to implement XFEM reliably.

Previous studies have modelled brittle crack arrest using a few methods, most commonly using nodal force release to measure the stresses and toughness from experimental crack

growth data[65,87,96–100], or using XFEM to model the crack propagation and arrest[85,95,101–103]. A novel approach has been taken by a group researchers in Japan who have designed a new multi-scale model to predict crack extension, fracture surface, and arrest[79–81,97,104]. One of the issues with modelling cracks is that the crack propagation in a model in the order of 10^0m is controlled by processes happening in the grains, on a scale of 10^{-5}m. This disparity in scale makes the process computationally exhaustive to have a mesh size of 10^{-5}m, or inadequate to be modelled as larger cells. To make sense of this, and bridge the divide, a novel approach was taken to discretize the plate into grain-sized-cells and divide these grains into smaller unit cells. The model was run on the unit cell scale, and the averaged results of this were fed into the grain-sized-cell model in order to predict both the crack length and crack face features accurately.

It was not possible to carry out meaningful FEM as part of this EngD research because the instrumentation of the experiments to measure the crack speed was not successful, which means it would not be possible to validate the FEM.

2.8 Considerations with Testing

There are additional issues when it comes to tough materials, since tunnelling is often more pronounced due to shear lip formation[25,105,106]. However, tunnelling gives more conservative results because it effectively increases toughness/reduces constraint. Tunnelling can be reduced through side-grooving, but it still means that the results can be slightly ambiguous and scatter is increased. Additionally, one could consider a side-grooved specimen to no longer be “full-thickness”.

Cracks typically initiate in localised brittle regions of HAZ and propagate along the weld. Due to the welding residual stress profile available in the plate, or a change to the weld seam, the crack is diverted into, and arrested in, the main plate. The crack is found to almost always arrest in the base metal, hence only base metal needs be considered for K_a testing[11,16]. For this reason, it is common in the test methods described here for the crack to initiate from an embrittled weld and propagate into base metal.

Smaller grain size introduces more grain boundaries into the crack path which increases the resistance to crack growth. Grain size refinement certainly increases initiation toughness and Charpy impact toughness via Hall-Petch grain boundary

strengthening[10,107]. It has been postulated that the same relationship holds for brittle crack arrest toughness[108], however it has recently been suggested that smaller grain size may decrease brittle crack arrest toughness[109].

The most important consideration with testing is the size of the test specimens. It is known that K_a depends on the applied stress, the initial crack length, the plate thickness, the plate width and the temperature. This makes it incredibly difficult to accurately simulate the service conditions, and also means that K_a will vary from plate to plate and application to application. If temperature-based relationships are able to account for the size effects between small-scale and large-scale testing then they can be an effective method of ensuring the crack arrestibility at the service temperature.

2.9 The research gap examined in this research

In any steels which exhibit a ductile-brittle transition, as the temperature decreases the initiation and arrest toughness will also decrease. It needs to be verified that they will be fit for service in any realistic operating conditions. The microstructure is particularly important when it comes to the energy approach, as the grain boundaries contribute towards the material toughness. It has been hypothesised that this may be one of the reasons for the decrease in toughness in higher strength steels.

Crack arrest toughness is believed to be a material property which is measured through large scale (and structurally representative) tests, although smaller CCA tests are also standardised to allow K_{Ia} to be calculated. Although many empirical equations are available in the literature to predict the structural behaviour in terms of crack arrestibility from small-scale test results, very few standards recommend the use of them. The only mention is in the R6 defect tolerance assessment procedure, which recommends the use of drop weight Pellini testing for applications in the UK nuclear industry[62]. This is because as the dimensions and particularly the thickness of the plates employed in many industrial applications increase, the empirical equations are no longer within their limits of validity. There is a need for re-validation of crack arrest behaviour of thick plates of modern steels in terms of reference temperatures determined through small-scale testing. This will increase the accessibility of crack arrest testing, ensuring that materials which are used for shipping applications are safe and preventing catastrophic failures.

References

1. (DNV) Det Norske Veritas. Fatigue Design of Offshore Steel Structures. *Recomm Pract DNV-RPC203*. Published online 2005.

2. Hirdaris SE, Bai W, Dessi D, et al. Loads for use in the design of ships and offshore structures. *Ocean Eng*. Published online 2014. doi:10.1016/j.oceaneng.2013.09.012

3. BS-7910. Guide to methods for assessing the acceptability of flaws in metallic structures. *BSI Stand Publ*. Published online 2013. doi:10.1007/s13398-014-0173-7.2

4. Tassava CJ. Weak seams: Controversy over welding theory and practice in american shipyards, 1938-1946. *Hist Technol*. 2010;19(2):87-108.

5. Hayes B. Classic brittle failures in large welded structures. *Eng Fail Anal*. 1996;3(2):115-127. doi:10.1016/1350-6307(96)00002-7

6. W.S. Pellini. *Guidelines for Fracture-Reliable Design of Steel Structures - The Welding Institute Report*.; 1983.

7. Sumi Y. Structural safety of ships developed by lessons learned from the 100-year history of break-in-two accidents. *Mar Struct*. 2019;64(July 2018):481-491. doi:10.1016/j.marstruc.2018.12.003

8. Martins RF, Rodrigues H, Leal das Neves L, Pires da Silva P. Failure analysis of bilge keels and its design improvement. *Eng Fail Anal*. 2013;27:232-249. doi:10.1016/j.engfailanal.2012.06.002

9. International Association of Classification Societies. Safer and Cleaner Shipping - IACS. http://www.iacs.org.uk/

10. Anderson TL. *Fracture Mechanics: Fundamentals and Applications*. Vol 58.; 2017. doi:10.1016/j.jmps.2010.02.008

11. Kawabata T, Inoue T, Tagawa T, et al. Historical review of research on brittle crack propagation arresting technology for large welded steel structures developed in Japan with the application of Kca parameters. *Mar Struct*.

2020;71(January):102737. doi:10.1016/j.marstruc.2020.102737

12. MAIB. Napoli Report No 9/2008. 2008;(9).

13. Committee on Large Container Ship Safety. *Final Report of Committee on Large Container Ship Safety (English Version)*.; 2015.

14. The Investigative Panel on Large Container Ship Safety - ClasssNK. *Investigation Report on Structural Safety of Large Container Ships*.; 2014.

15. Suresh S. *Fatigue of Materials*.; 1998. doi:10.1017/cbo9780511806575

16. Wiesner C, Hayes B. *A Review of Crack Arrest Tests, Models and Applications*.; 1995.

17. Graville A. *Stress Analysis of Short Crack Arrest Test Report P244/1, Graville Associates Inc.*

18. Kobayashi T. Dynamic photoelastic determination of the a(dot)-K relation for 4340 alloy steel. In: *Hahn GT, Kanninen MF, Editors. Crack Arrest Methodology and Applications. ASTM STP 711. American Society for Testing and Materials;*. ; 1980:189–210.

19. Kalthoff J. Experimental analysis of dynamic effects in different crack arrest test specimens. In: : *: Hahn GT, Kanninen MF, Editors. Crack Arrest Methodology and Applications. ASTM STP 711. American Society for Testing and Materials;*. ; 1980:109–27.

20. Joyce JA, Link RE, Roe C, Sobotka JC. Dynamic and static characterization of compact crack arrest tests of navy and nuclear steels. *Eng Fract Mech*. 2010;77(2):337-347. doi:10.1016/j.engfracmech.2009.04.006

21. ASTM. E1221 Standard Test Method for Determining Plane-Strain Crack-Arrest Fracture Toughness, K Ia, of Ferritic Steels. 2007;96(Reapproved):1-19. doi:10.1520/E1221-12A.2

22. ASTM. E208 Standard Test Method for Conducting Drop-Weight Test to Determine Nil-Ductility Transition Temperature of Ferritic Steels 1. *Test*. 2000;06(Reapproved):1-13. doi:10.1520/E0208-06R12.2

23. Pb C, Ej R. Comparison of Crack Arrest Methodologies. Published online 1980:211-227.

24. International Standards Organisation. *BS ISO 20064 : 2019 BSI Standards Publication Metallic Materials — Steel — Method of Test for the Determination of Brittle Crack Arrest Toughness , K Ca*.; 2019.

25. Funatsu Y, Shirahata H, Otani J, Inoue T, Hashiba Y. The Effect of Shear-lips on the Arrestability of Thicker Steel Plates Longitudinal. *Isope*. 2012;4:63-66.

26. Crosley PB. WELDING RESEARCH Crack Arrest Fracture Toughness of a Structural Steel (A36). Published online 1982.

27. Green G, Knott JF. On effects of thickness on ductile crack growth in mild steel. *J Mech Phys Solids*. 1975;23(3). doi:10.1016/0022-5096(75)90014-9

28. Handa T, Igi S, Oi K, Nishimura K, Tajika H, Tagawa T. Effect of Toughness Distribution in the Thickness Direction on Long Brittle Crack Propagation / Arrest Behavior of Heavy Gauge Shipbuilding Steel Brittle Crack Arrestability of Test Steels Arrestability of Test Steels under Condition of No. Published online 2016:126-131.

29. Sugimoto K. Thickness effect on brittle crack arrest toughness value (Kca)-6. In: *ISOPE - 20th International Offshore and Polar Engineering Conference*. ; 2010.

30. Wallin K. The size effect in KIC results. *Eng Fract Mech*. 1985;22(1):149-163. doi:10.1016/0013-7944(85)90167-5

31. Marschall R. Specimen-Size Considerations in Crack-Arrest Testing of Irradiated RPV Steels. Published online 1986:339-352.

32. Society JWE. *JWES 2815:2014 Test Method for Brittle Crack Arrest Toughness Kca*.; 2014.

33. E1921-15ae1. Standard Test Method for Determination of Reference Temperature , To , for Ferritic Steels in the Transition Range. In: *ASTM Book of Standards*. ; 2016:1-23. doi:10.1520/E1921-15AE01.2

34. Zhu XK, Joyce JA. Review of fracture toughness (G, K, J, CTOD, CTOA) testing

and standardization. *Eng Fract Mech*. 2012;85:1-46. doi:10.1016/j.engfracmech.2012.02.001

35. Yamaguchi Y, Yajima H, Aihara S, et al. Development of Guidelines on Brittle Crack Arrest Design for Large Container Ships (1). In: *ISOPE - 20th International Offshore and Polar Engineering Conference*. ; 2010.

36. International Association of Classification Societies. *W31 YP47 Steels and Brittle Crack Arrest Steels*.; 2019.

37. Barker D. A method for determining the crack arrest fracture toughness of ferritic materials. *Am Soc Test Mater*. Published online 1988.

38. Jutla T. European experience of the proposed ASTM test method for crack arrest toughness of ferritic materials. *Nucl Eng Des*. 1986;96.

39. Sakai Y. A co-operative study for the evaluation of crack arrest toughness of RPV materials in Japan. *merican Soc Test Mater*. Published online 1988.

40. Robertson T. Propagation of brittle fracture in steel. *J Iron Steel Inst*. 1953;175.

41. Feely FJ, Northup MS, Kleep SR, Gensamer M. Studies on the brittle failure of tankage steel plates. *Weld J*. 1955;34:596-607.

42. Hall WJ, Rolfe ST, Barton FW, Newmark NM. *Brittle-Fracture Propagation in Wide Steel Plates, Ship Structure Committee*.; 1961.

43. Wiesner CS, Hayes B, Willoughby AA. Crack Arrest in Modern Steels and their Weldments Comparison between Small and Large Scale Experiments. 1993;56:369-385.

44. ISO. ISO 148-1:2006: Metallic materials -- Charpy pendulum impact test -- Part 1: Test method. *ISO*. Published online 2006.

45. Materials AS for T and. *ASTM E436-86: Standard Method for Drop Weight Tear Tests of Ferritic Steels.*; 1986.

46. Eiber R, A. Duffy, McClure G. Significance of the Drop-Weight Tear Test and Charpy V-Notch Impact Test Results. *Impact Test Met*. Published online

1970:181-191.

47. Tagawa T, Amano T, Hiraide T, et al. Inverse Fracture in DWTT and Brittle Crack Behavior in Large-Scale Brittle Crack Arrest Test. *J Press Vessel Technol Trans ASME*. 2018;140(5):1-9. doi:10.1115/1.4040641

48. Wiesner CS. Predicting structural crack arrest behaviour using small scale material characterisation tests. *Int, J Pres Ves Pip*. Published online 1995.

49. Nichols, R. W. Fast and brittle fracture studies related to steel pressure vessels. *Proc Roy Soc,*. Published online 1965:104-119.

50. Smedley, G. P. & Liston R. Design for forgings. In: *International Forging Conference, Sheffield, UK.* ; 1967.

51. Lessells, J. & Leggett J. Crack arrest properties of C-Mn structural steels. *Met Constr Br Weld J*. Published online 1971:193.

52. Kawaguchi Y. Development of small size test for brittle fracture propagation--arrest characteristics of steel plates--tapered double cantilever beam test. Published online 1973.

53. Kihara, H., Akita, Y. & Ikeda K. Brittle fracture work in Japan--evaluation of ductility for steels and deposited metals in wide plate and industrial tests. *Int Inst Weld*. Published online 1963.

54. Kihara H. Brittle fracture strength of thick steel plates for reactor pressure vessels. *Rep No 9, Sh Res Inst*. Published online 1966.

55. Willoughby A. Crack arrest concept. *Proc Semin Eng Per- formance Welded Joints*. Published online 1986.

56. Hahn G. Crack Arrest Methodology and Applications. *Am Soc Test Mater*. Published online 1980.

57. Pellini W, Puzak P. Fracture analysis diagram procedures for the fracture-safe engineering design of steel structures. *Weld Res Counc Bull*. 1963;88.

58. Institution BS. *BS18:1987: Method for Tensile Testing of Metals.*; 1987.

59. Institution BS. *BS EN10045:1990: Charpy Impact Test on Metallic Materials.*; 1990.

60. Völling A, Kalwa C, Erdelen-peppler M. The misconception of employing cvn toughness as key-measure in ductile crack arrest prediction for modern line-pipe steels. In: *Proceedings of the 2014 10th International Pipeline Conference IPC2014*. ; 2014.

61. Smedley G. Prediction and Specification of Crack Arrest Properties of Steel Plate. *Int, J Pres Ves Pip*. 1989;40:279-302.

62. EDF Energy UK. *R6. Assessment of the Integrity of Structures Containing Defects.*; 2006.

63. Avenue K, Kt S, Berkeley C, Laboratories N, Gli G. R6. Assessment of the Integrity of Structures Containing Defects. *Construction*. 1988;32:3-104.

64. Kirk MT, Natishan ME, Wagenhofer M, et al. A Summary of Wallin ' s Empirical Findings. Published online 2002:729-740.

65. Link RE, Joyce JA, Roe C. Crack arrest testing of high strength structural steels for naval applications q. *Eng Fract Mech*. 2009;76(3):402-418. doi:10.1016/j.engfracmech.2008.11.006

66. Toon: KK. Fracture Toughness Data Analysis Using the Master Curve Method. *WRC Bull 486 Part 3, Nov 2003*. Published online 2003.

67. Pugh CE, Corwin WR, S RHBRYANBRBAS. C.e. pugh, w.r. corwin, r.h. *Nucl Eng Des*. 1986;96:297-312.

68. Wallin K, Karjalainen-roikonen P. Crack Arrest Toughness Estimation for High Strength Steels from Sub-Sized Instrumented Charpy-V Tests. *Proc Twenty-sixth Int Ocean Polar Eng Conf*. Published online 2016:85-91.

69. Maxey WA. *Fracture Initiation, Propagation, and Arrest. 5th Symposium on Line Pipe Research, American Gas Association, Catalog No. L30174. Paper J.*; 1974.

70. C. Lu, Michal G, Godbole A. RE-EXAMINATION OF BATTELLE TWO CURVE METHOD. *Proc 2014 10th Int Pipeline Conf*. Published online 2014.

71. Sathyanarayanan S, Moitra A, Sasikala G, Bhaduri AK, Singh V. Evaluation of Crack Arrest Length and Crack Arrest Toughness of Cold-Worked and Aged Modified 9Cr-1Mo Steel By Application of Key-Curve Method. Published online 2011:6-11.

72. Scibetta M, Link R, Schuurmans J, Lucon E. Towards crack arrest testing using miniature specimens. *ASTM Spec Tech Publ*. 2009;1502 STP(9):49-69. doi:10.1520/JAI101002

73. Mayer U, Mutz A, Ag G, Nicak T. Compact crack arrest tests for the validation of a finite element material model of the reactor pressure vessel steel of the nuclear power plant kkg. *Proc ASME 2018 Press Vessel Pip Conf PVP2018*. Published online 2018:PVP2018-84068.

74. Snartland BD, Østby E, Hauge M, Ren X, Thaulow C. Brittle fracture arrest - The state of art in a multiscale universe. *Proc Int Offshore Polar Eng Conf*. 2016;2016-Janua:296-303.

75. Hase K, Ichimiya K, Ueda K, Handa T, Eto T, Aoki M. Texture-controlled YP460 n/mm2 class heavy thick plate for ultra-large container carriers. *Int J Offshore Polar Eng*. 2019;29(3):315-321. doi:10.17736/ijope.2019.hj31

76. Handa T, Tagawa T, Minami F. Correlation between charpy transition temperature and brittle crack arrest temperature considering texture. *Tetsu-To-Hagane/Journal Iron Steel Inst Japan*. 2012;98(1):32-38. doi:10.2355/tetsutohagane.98.32

77. Okawa T, Shirahata H, Nakashima K, Yanagita K, Inoue T. Simplified evaluation of brittle crack arrest toughness in heavy-thick plate by combined small-scale tests. *Int J Offshore Polar Eng*. 2017;27(2):210-215. doi:10.17736/ijope.2017.hj26

78. Nishizono Y, Kawabata T, Aihara S, Okawa T. A simplified method for evaluation of brittle crack arrest toughness of steels in scaled-down bending tests. *Eng Fract Mech*. 2019;215(November 2018):99-111. doi:10.1016/j.engfracmech.2019.03.047

79. Shibanuma K, Yanagimoto F, Namegawa T, Suzuki K. Brittle crack propagation / arrest behavior in steel plate – Part I : Model formulation. *Eng Fract Mech*.

2016;162:324-340. doi:10.1016/j.engfracmech.2016.02.054

80. Shibanuma K, Yanagimoto F, Namegawa T, Suzuki K. Brittle crack propagation / arrest behavior in steel plate – Part II : Experiments and model validation. *Eng Fract Mech*. 2016;162:341-360. doi:10.1016/j.engfracmech.2016.02.053

81. Shibanuma K, Yanagimoto F, Suzuki K, Aihara S. Brittle crack propagation/arrest behavior in steel plate – Part III: Discussions on arrest design. *Eng Fract Mech*. 2018;190:104-119.

82. Shibanuma K, Yanagimoto F, Namegawa T, Suzuki K, Aihara S. Modeling of Brittle Crack Propagation / Arrest Behavior in Steel Plates in Steel Plates modeling high pressure turbine blade airplane gas turbine engine Modeling of Brittle Crack Behavior PCF Propagation / Arrest. *Procedia Struct Integr*. 2016;2:2598-2605. doi:10.1016/j.prostr.2016.06.325

83. Berdin C, Hajjaj M, Bompard P, Bugat S. Local approach to fracture for cleavage crack arrest prediction. *Eng Fract Mech*. 2008;75:3264-3275.

84. Yanagimoto F, Shibanuma K, Suzuki K, Matsumoto T, Aihara S. Local stress in the vicinity of the propagating cleavage crack tip in ferritic steel. *Mater Des*. 2018;144:361-373.

85. Bousquet A, Marie S, Bompard P. Propagation and arrest of cleavage cracks in a nuclear pressure vessel steel. *Comput Mater Sci*. 2012;64:17-21. doi:10.1016/j.commatsci.2012.04.026

86. Yang X, Marie S, Jacquemoud C, Bompard P. Prediction of cleavage crack propagation path in a nuclear pressure vessel steel. *Eng Fract Mech*. 2018;191(December 2017):486-503.

87. Berdin C. 3D modeling of cleavage crack arrest with a stress criterion. *Eng Fract Mech*. 2012;90:161-171. doi:10.1016/j.engfracmech.2012.05.002

88. Dahl A, Berdin C, Moinereau D. Dynamic modeling of cleavage crack propagation and arrest with a local approach. *Procedia Eng*. 2011;10:1853-1858. doi:10.1016/j.proeng.2011.04.308

89. Ritchie RO, Knott JF, Rice JR. On the relationship between critical tensile stress and fracture toughness in mild steel. *J Mech Phys Solids*. 1973;21(6):395-410. doi:10.1016/0022-5096(73)90008-2

90. Ishihara K, Hamada T, Kikuya N, Meshii T. Applicability Of Modified Ritchie-Knott-Rice Failure Criterion To Predict The Onset Of Cleavage Fracture For The Test Specimen With Residual Stress Introduced To The Crack Tip. *Procedia Struct Integr*. 2016;2:728-735. doi:10.1016/j.prostr.2016.06.094

91. Aihara S, Tanaka Y. A simulation model for cleavage crack propagation in bcc polycrystalline solids. *Acta Mater*. 2011;59(11):4641-4652.

92. Shibanuma K, Suzuki Y, Kiriyama K, Suzuki K, Shirahata H. A model of cleavage crack propagation in a BCC polycrystalline solid based on the extended finite element method. *Acta Mater*. 2019;176:232-241.

93. Qiao Y, Argon AS. Cleavage cracking resistance of high angle grain boundaries in Fe-3%Si alloy. *Mech Mater*. 2003;35(3-6):313-331.

94. Qiao Y, Argon AS. Cleavage crack-growth-resistance of grain boundaries in polycrystalline Fe-2%Si alloy: Experiments and modeling. *Mech Mater*. 2003;35(1-2):129-154.

95. Prabel B, Marie S, Combescure A. Using the X-FEM method to model the dynamic propagation and arrest of cleavage cracks in ferritic steel. 2008;75:2984-3009. doi:10.1016/j.engfracmech.2008.01.008

96. Link R. Analysis of Dynamic Fracture and Crack Arrest of an HSLA Steel in an SE (T) Specimen. 2006;3(1):1-26.

97. Yanagimoto F, Shibanuma K, Suzuki K, Aihara S. A new model to simulate crack arrest behavior in steel plates used for naval structures. Published online 2016:64-69.

98. Nishioka Y, Shibanuma K, Nishioka Y, Yanagimoto F. Finite element model to simulate crack propagation based on local fracture stress criterion. Published online 2016.

99. Kaneko M, Kawabata T, Aihara S. Effect of impact energy in Esso test (Part 2: Proposal of validity criteria of impact condition in Esso test by FEM crack propagation analysis. *J Test Eval*. 2018;46(5):1782-1798. doi:10.1520/JTE20170151

100. Filin VY, Ilyin AV, Mizetsky AV. Crack arrest simulation in steel in account of competing ductile and cleavage fracture. *Procedia Struct Integr*. 2020;28:3-10. doi:10.1016/j.prostr.2020.10.002

101. Marie S, Bompard P. Pvp2014-28422 Cleavage Crack Propagation and Arrest Prediction in French Pwr. Published online 2014:1-11. doi:10.1115/PVP2014-28422

102. O'Hara P, Duarte CA, Eason T. A two-scale generalized finite element method for interaction and coalescence of multiple crack surfaces. *Eng Fract Mech*. 2016;163:274-302. doi:10.1016/j.engfracmech.2016.06.009

103. Suman S, Khan MK, Pathak M, Singh RN. 3D simulation of hydride-assisted crack propagation in zircaloy-4 using XFEM. *Int J Hydrogen Energy*. 2017;42(29):18668-18673. doi:10.1016/j.ijhydene.2017.04.163

104. Yamamoto Y. Multiscale modeling to clarify the relationship between microstructures of steel and macroscopic brittle crack microstructures of steel and macroscopic brittle crack propagation / arrest behavior modeling of a high. *Procedia Struct Integr*. 2016;2:2389-2396. doi:10.1016/j.prostr.2016.06.299

105. Yanagimoto F, Shibanuma K, Suzuki K, Matsumoto T. A physics based model to simulate brittle crack arrest in steel plates incorporating experimental and numerical evidences. *Eng Fract Mech*. 2019;221(August):106660. doi:10.1016/j.engfracmech.2019.106660

106. Aihara S, Shibanuma K, Namegawa T. Numerical Simulation of Brittle Crack Propagation and Arrest in Steels Considering Shear-Lip Formation. 2014;3:98-105.

107. Petch NJ. The Cleavage Strength of Polycrystals. *Iron Steel Inst London*. 1953;173:25–28.

108. Hemmi T, Shibanuma K, Suzuki K, Aihara S, Shirahata H. Experimental and numerical investigation on relationship Experimental and numerical investigation on in relationship between grain size and arrest toughness steels Thermo-mechanical modeling a high pressure turbine blade of an Hemmi of gas turbine engine. *Procedia Struct Integr*. 2016;2:2230-2237. doi:10.1016/j.prostr.2016.06.279

109. Yanagimoto F, Hemmi T, Suzuki Y, Takashima Y, Kawabata T, Shibanuma K. Contribution of grain size to resistance against cleavage crack propagation in ferritic steel. *Acta Mater*. 2019;177:96-106. doi:10.1016/j.actamat.2019.06.038

3 Microstructural analysis of structural steels using optical microscopy, EBSD and neutron diffraction

Abstract

The fracture properties of a material, indeed all properties of a material, are due to its composition – in terms of phase composition, chemical composition, and microstructure. In order to fully understand the behaviour of a material it is essential to fully characterise its properties down to the microscopic level. In this chapter, the microstructures of six batches of steel are investigated through optical microscopy, electron microscopy (EBSD), and neutron diffraction. The results show that the texture of the steel manifests as grain elongation along the rolling direction. The results from this study will be correlated against the materials' key fracture properties which are presented in the following chapter.

Keywords: structural steel, EBSD, neutron diffraction, texture, microstructure

Nomenclature

ΔV	Volume of each cell over which the ODF is determined
EBSD	Electron backscatter diffraction
MAUD	Material Analysis Using Diffraction
ODF	Orientation distribution function
RAL	Rutherford Appleton Laboratory, UK
RoA	Reduction of area
RPV	Reactor pressure vessel
STRA	Short transverse reduction of area
TI	Texture index
TMCP	Thermo-mechanically controlled process
UTS	Ultimate tensile strength

3.1 Introduction

The microstructure of a material dominates its bulk material properties. Small grain sizes can increase the fracture toughness of a metal, strong texture can increase the strength of a material, and the phase structure of a steel can impact various properties such as strength and weldability[1–7]. In order for a material to be fully characterised, that must include an analysis of its microstructural characteristics. Modern steels for container ships have been developed to have high crack arrest toughness by rolling using a thermo-mechanically controlled process (TMCP) which imparts a texture into the materials[1,7,8]. The texture of a material can be measured though multiple different methods including optical microscopy, electron backscatter diffraction (EBSD), neutron diffraction, and X-ray diffraction. The texture can be used to indicate the grain size elongation, or the orientation of the crystal planes of the grains. The latter can be measured through diffraction of radiation through the crystal lattice structure of the material, such as EBSD, neutron diffraction and X-ray diffraction[9,10]. Optical microscopy and EBSD are planar measurement methods which means that they cannot penetrate the depth of the material – only the visible surface. On the other hand, neutrons and x-rays are able to penetrate into the bulk of the material and carry out measurements over a volume - however these methods are more expensive.

The diffraction methods work on the principle of Braggs law, which relates the angle of diffracted waves to the lattice spacing of the crystal structure being imaged[11]. From the diffraction pattern, the crystal's structure can be determined. In order to find the texture of a material, the orientation distribution function (ODF) needs to be determined. The ODF describes the orientation of grains throughout the material and can be determined computationally through various different methods[10–12]. In this work, the microstructure of six batches of steel is investigated through optical microscopy, electron microscopy (EBSD), and neutron diffraction. The results from each method are compared to each other, and will be used to investigate the impact of microstructure on material properties in chapter 4.

3.2 Experimental procedure and specimen manufacture

3.2.1 Optical Microscopy

For the microstructural analysis, optical microscopy was carried out on all materials. The specimens were polished, and etched with 2% nital solution to reveal the grain boundaries. In order to best consider the range of microstructures present throughout the thickness of the materials, the grain size analysis was carried out at the quarter wall location on the plates. It was decided to measure the grain size for each steel by the linear intercept method, following ASTM E112[13], because the grains did not appear to be equiaxed. This method reports the grain size as the average grain diameter which is the geometric mean of the average grain diameter in each of the principal directions. In order to determine the grain aspect ratio, the grain sizes were measured in each of the three orthogonal directions of the plate; rolling direction, through thickness direction, and perpendicular to the rolling direction.

3.2.2 Electron and neutron imaging

EBSD analysis was carried out at Cranfield University (UK) in order to determine the texture index of the steels. The EBSD measurements were taken from the same specimens as the optical microscopy to ensure that they could be directly compared i.e. at the quarter wall of the plates. The data was analysed using AZtecCrystal which is a specialised EBSD software provided by Oxford Instruments.

Neutron diffraction measurements were carried out on the GEM instrument at the Rutherford Appleton Laboratory (RAL, UK) which specialises in determining the bulk texture of crystalline materials. The neutron imaging measurements vary from the electron and optical microscopy in that they measure the bulk material properties rather than the visible surface. The specimen location was chosen as the quarter wall of the plates to ensure that every measurement could be directly comparable to the others. The data was analysed using Material Analysis Using Diffraction (MAUD), which is the preferred software of RAL.

Both of these methods output a texture index (TI) which can have a value between 1 (completely randomly oriented grains) and infinity (single crystal or perfect texture). This

is based on the ODF which represents the statistical distribution of the orientations of each grain in the material[11]. The ODF can be visually represented by pole figures which project the probability density of a particular orientation onto a graphical plot. The texture index is determined by integration of the ODF throughout the sampled region[11]:

$$TI = \frac{1}{8\pi^2}\sum[ODF]^2\Delta V \qquad \text{Equation 3-1}$$

where ΔV is each cell volume where the ODF is determined.

3.2.3 Selected materials

The test programme in this study was carried out on five materials, in six batches, which are summarised in Table 3-1: 1- reactor pressure vessel (RPV) A543 steel with a thickness of 28 mm (denoted M01); 2- RPV A302 steel with a thickness of 28 mm (denoted M02); 3- X65 pipeline steel with a thickness of 30 mm (denoted M03); 4- S355G10+M structural steel plate with a thickness of 90 mm (denoted M04); 5- S355G10+M structural steel plate with a thickness of 50 mm (denoted M05); and 6- EH47 shipbuilding steel with a thickness of 80 mm (denoted M06). The materials selected in this study are widely used in offshore Oil & Gas, nuclear power plants and offshore wind applications, therefore the obtained results and conclusions from this research are expected to have a significant impact on design and life assessment of engineering components and structures employed in a wide range of industries. Traditional tensile tests following BS EN ISO 6892[14] were carried out to determine the yield strength and ultimate tensile strength (UTS) of the materials along with the ductility which was taken as the reduction of area (RoA) or elongation in this work. Additionally, alternative tensile tests, "short transverse reduction of area" (STRA) tests were carried out to measure the ductility in the through-thickness direction following BS EN 10164[15]. This was done to investigate whether the ratio of ductility between the rolling axis and through-thickness axis can be used as a proxy for the material's texture, which is believed to influence crack arrestibility[16,17]. The full tensile test results are given in section 4.4.2, and the ratio of ductility is presented in this chapter.

Table 3-1: Summary of the different steels used in this research.

Material Reference	M01	M02	M03	M04	M05	M06
Material	RPV A543	RPV A302	X65	S355G10+M	S355G10+M	EH47
Thickness (mm)	28	28	30	90	50	80
Ratio of ductility (in terms of RoA)	0.78	0.84	1	0.97	0.93	1

3.3 Results

3.3.1 Microstructure analysis

The micrographs of all six batches of steels considered in this study after polishing and etching are shown in Figure 3-1. The examined slices were extracted from mid-thickness of each batch of material. In Figure 3-1, X indicates the rolling axis and Z indicates the through thickness axis. The micrographs show the variability in carbon contents for each of the materials, with carbide and pearlite regions evident in M01 and M02 which had the greatest carbon contents than the other materials, which show more pure ferritic regions (see table 4-4 in section 4.4.1 for chemical composition). In these micrographs, the grains appear to be elongated along the rolling direction, which is investigated through grain size analysis. The average grain size measured for each steel, which is the combined average, is summarised in Table 3-2. As seen in Table 3-2 and Figure 3-1, the largest and smallest average grain size has been found in RPV A543 (M01) and EH47 (M06), respectively.

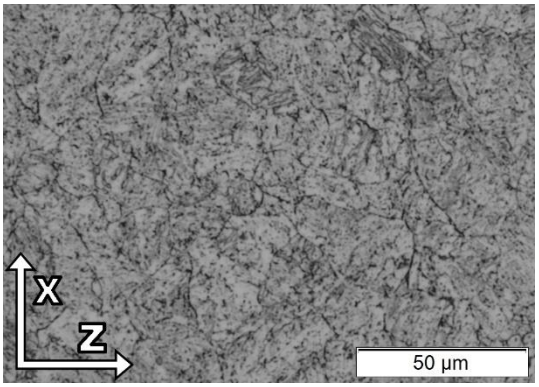

(a)

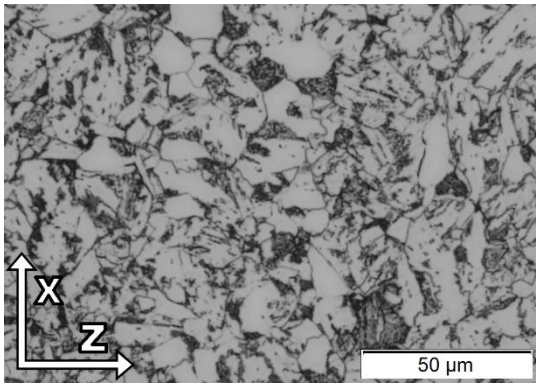

(b)

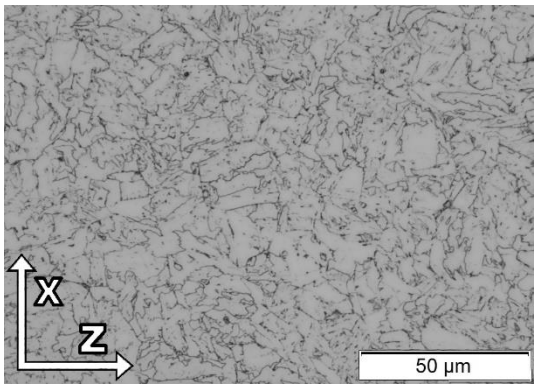

(c)

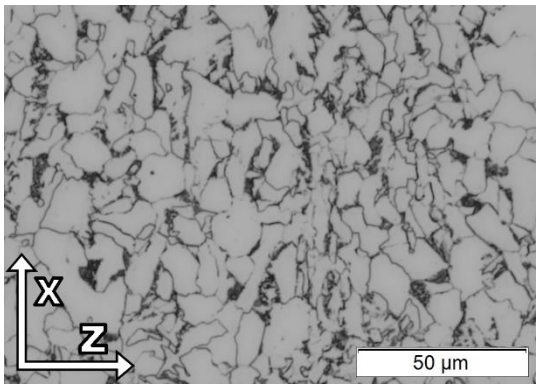

(d)

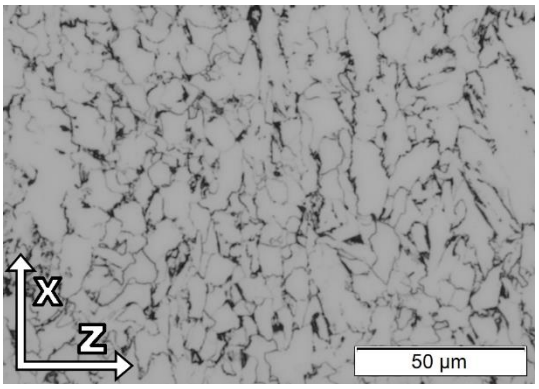

(e)

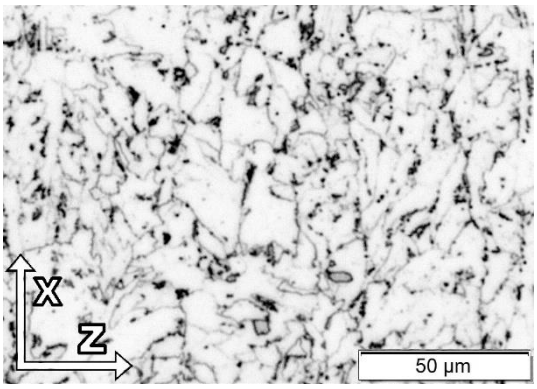

(f)

Figure 3-1: Microstructure of (a) M01, (b) M02, (c) M03, (d) M04, (e) M05, and (f) M06 steels

Table 3-2: Grain sizes of the steels used in this study (measured to ASTM E112)

	M01	M02	M03	M04	M05	M06
Average Grain Size (µm)	9.5 ± 1.4	7.0 ± 1.2	5.2 ± 1.3	5.6 ± 0.9	7.5 ± 0.9	4.1 ± 0.5

Figure 3-2 correlates the aspect ratio of ductility (in terms of RoA) against the aspect ratio of grain size: these values are the ratio of the RoA (or average grain size) along the rolling axis and that along the through-thickness axis. Although the correlation is very weak, there is a slight correlation between the ratio of ductility and the grain elongation. If the anisotropy of the material's tensile properties is due to elongated grains in a certain direction, then this ratio would be expected to follow a 1:1 trend. Hence, although the correlation is weak, the trend follows the behaviour expected for these materials. Other microstructural factors that can contribute to a steels' macroscopic behaviour might include the size and distribution of inclusions, and centreline segregation, which have not been included in the microstructural consideration here. Further analysis of the grain aspect ratio in Figure 3-3 shows that there is no strong correlation between grain size and the aspect ratio, although as these steels are all very finely grained and there is not enough variation between them to make a firm conclusion.

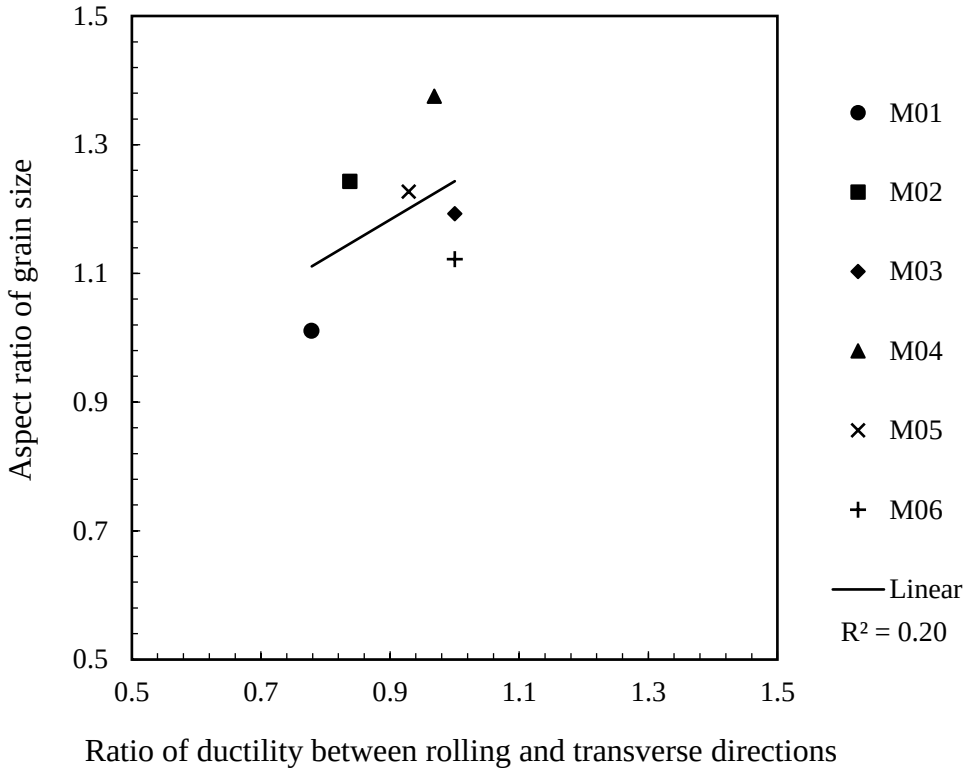

Figure 3-2: Correlation between grain size aspect ratio and ratio of ductility in the rolling direction.

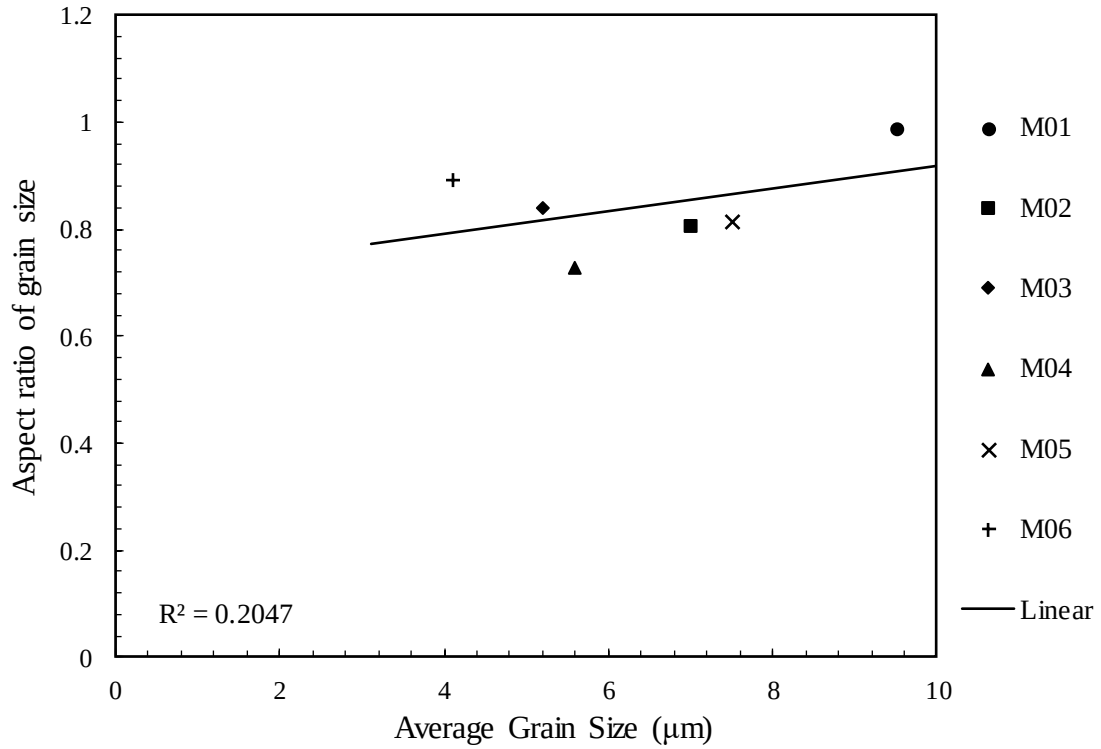

Figure 3-3: Correlation between average grain size and grain aspect ratio in the rolling direction

3.3.2 Texture analysis

The texture index was calculated as a measure of the ODF and this is presented in Table 3-3 for both EBSD and neutron imaging methods.

EBSD maps showing the orientation of the grains are shown in Figure 3-4, where it can be seen that although there are some regions with similarly oriented grains (similar colours), overall the grains seem to be quite randomly oriented. This agrees with the texture index results which are all close to 1, indicating very light texture in the steels. Pole figures for each material are shown in Appendix A.

Table 3-3: Texture measurements of each material.

	M01	M02	M03	M04	M05	M06
EBSD Texture Index	1.13	1.33	1.46	1.99	1.2	1.21
Neutron Imaging Texture Index	1.11	1.09	1.11	1.09	1.14	1.34

Figure 3-5 shows that there is poor correlation between the texture indices measured via neutron diffraction and EBSD. This may be due to statistical scatter since the texture index is very low for all the materials which makes it hard to draw meaningful correlations between the texture indices. Figure 3-6 indicates that the aspect ratio of grains measured through optical microscopy correlates well with the texture measured from EBSD, but poorly with the texture measured from neutron diffraction. This may be because EBSD and optical microscopy are planar measurement methods which agree well, but they do not agree well with the volumetric neutron diffraction measurement method. Figure 3-7 shows that there is minimal correlation between the ratio of ductility in the plates and their texture index. This indicates that the texture present in the material may be manifesting as slight anisotropy in tensile properties.

Figure 3-8 indicates that there is slight correlation between the grain size and texture index. Although a weak relationship, generally the smaller grains have a higher texture index. This may be due to the fact that steels which are designed to have very fine grains undergo more complex processing which imparts a stronger texture into the material. Again, the grain sizes and texture indices are all very small and relatively similar between the steels so it is hard to draw conclusions due to the expected natural scatter of material properties.

Since the scale of texture index ranges from 1 (completely random) to infinity (single crystal), the fact that every steel imaged in this work had a TI value less than 2 is interesting. Low TI in steels is not uncommon, with other researchers reporting similar low values[18,19]. The steels used in this study were typically produced through hot rolling processes, which evidently do not significantly impart a significant texture into the bulk of the steels during manufacturing. It may be that the texture is limited to the surface of the steels which are in contact with the rollers or the centreline of the plates due to heat distribution, and the texture was not captured by this analysis in which specimens were extracted from the quarter wall of the plates.

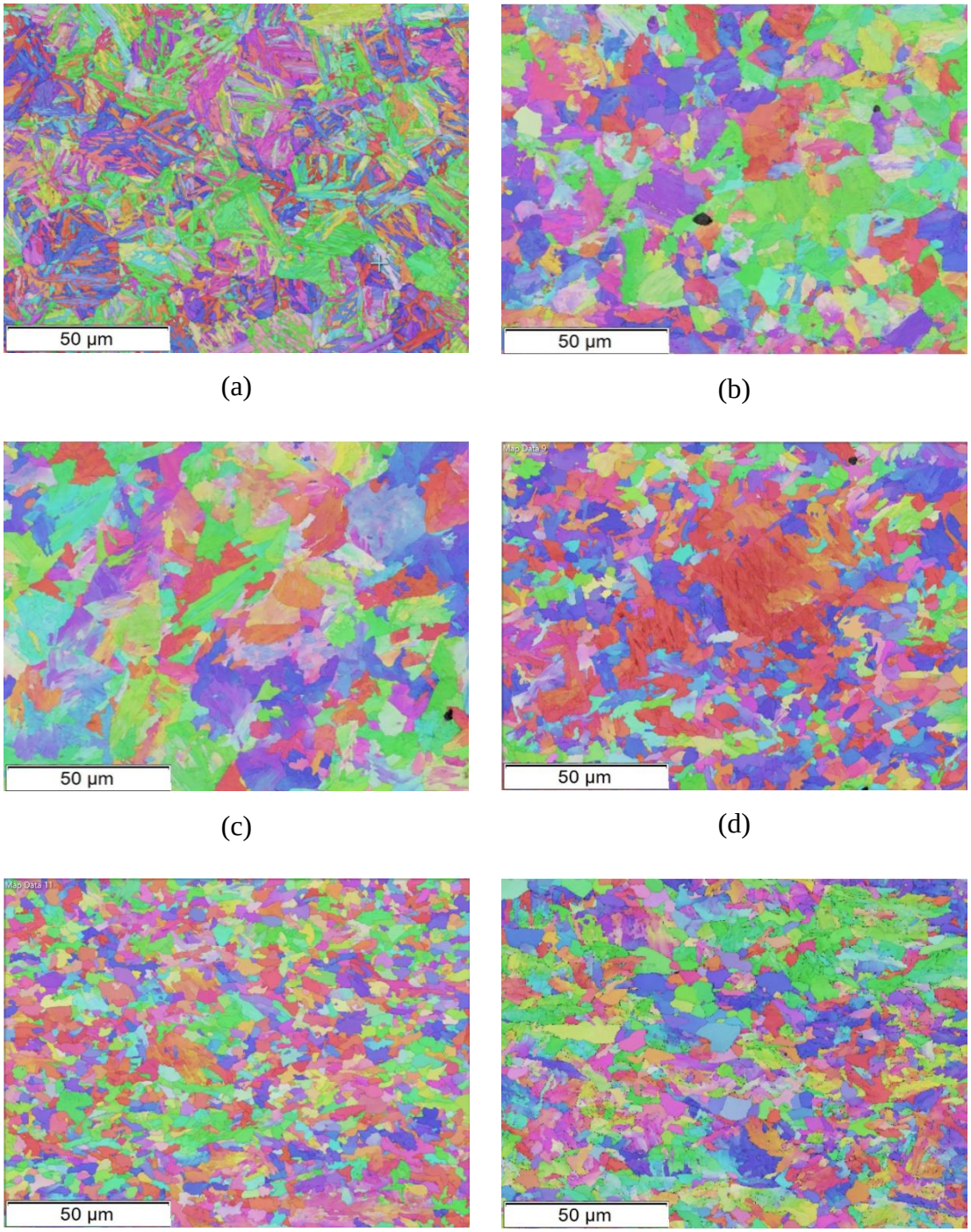

Figure 3-4: EBSD maps of (a) M01, (b) M02, (c) M03, (d) M04, (e) M05, and (f) M06 steels

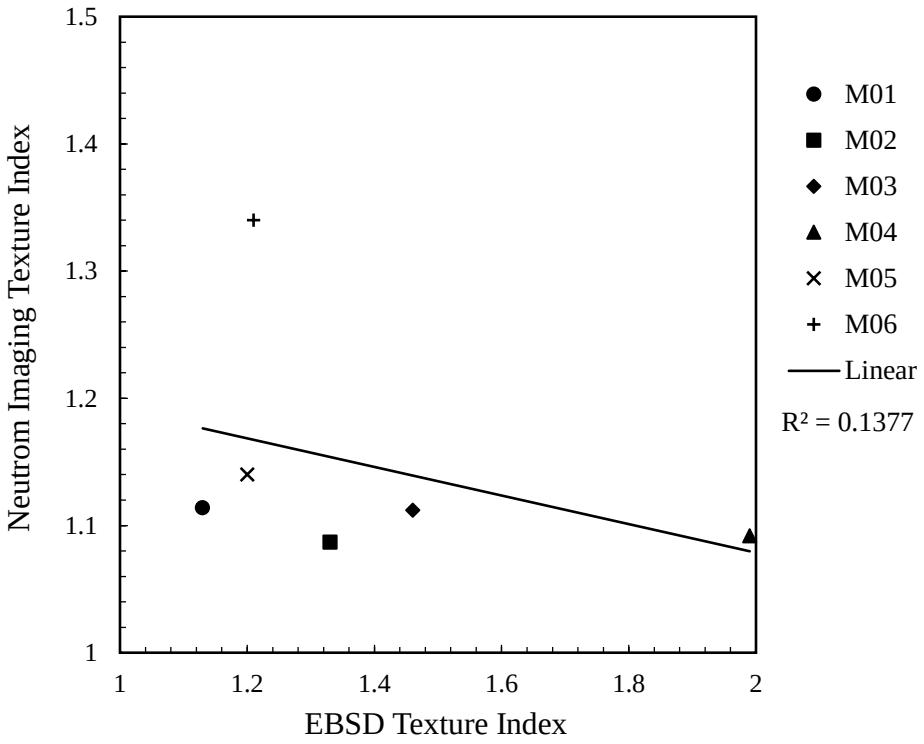

Figure 3-5: Correlation between texture indices measured via neutron diffraction and EBSD.

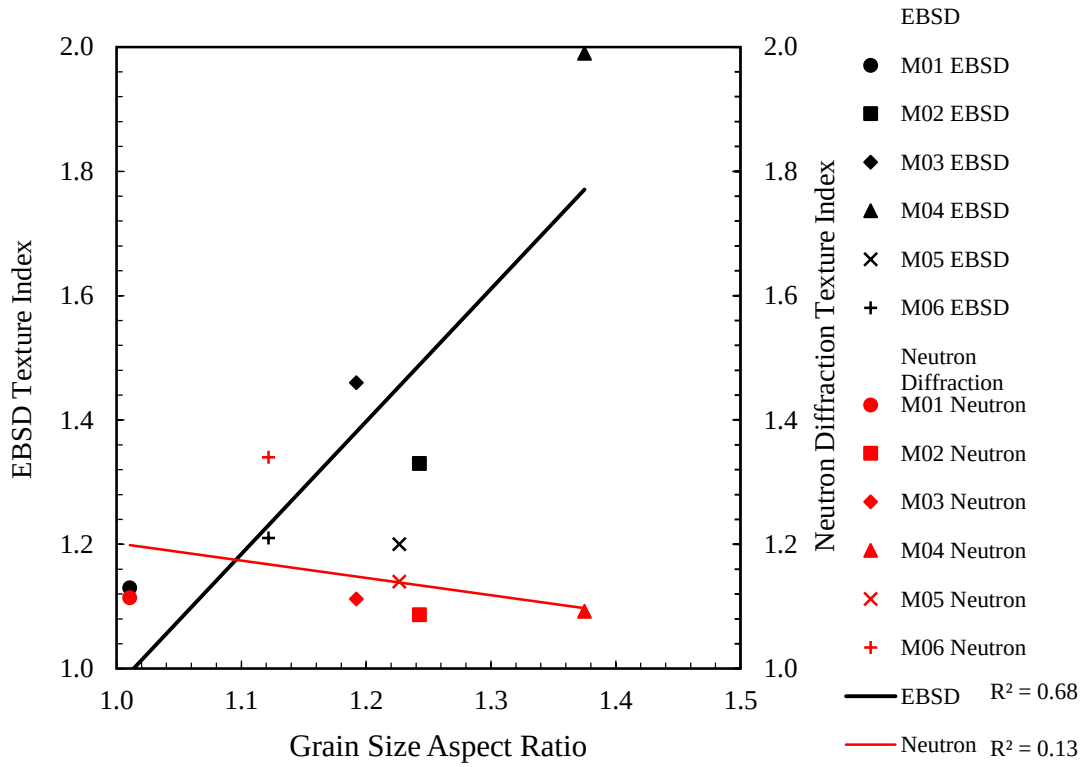

Figure 3-6: Correlation between grain size aspect ratio measured through optical microscopy and texture indices.

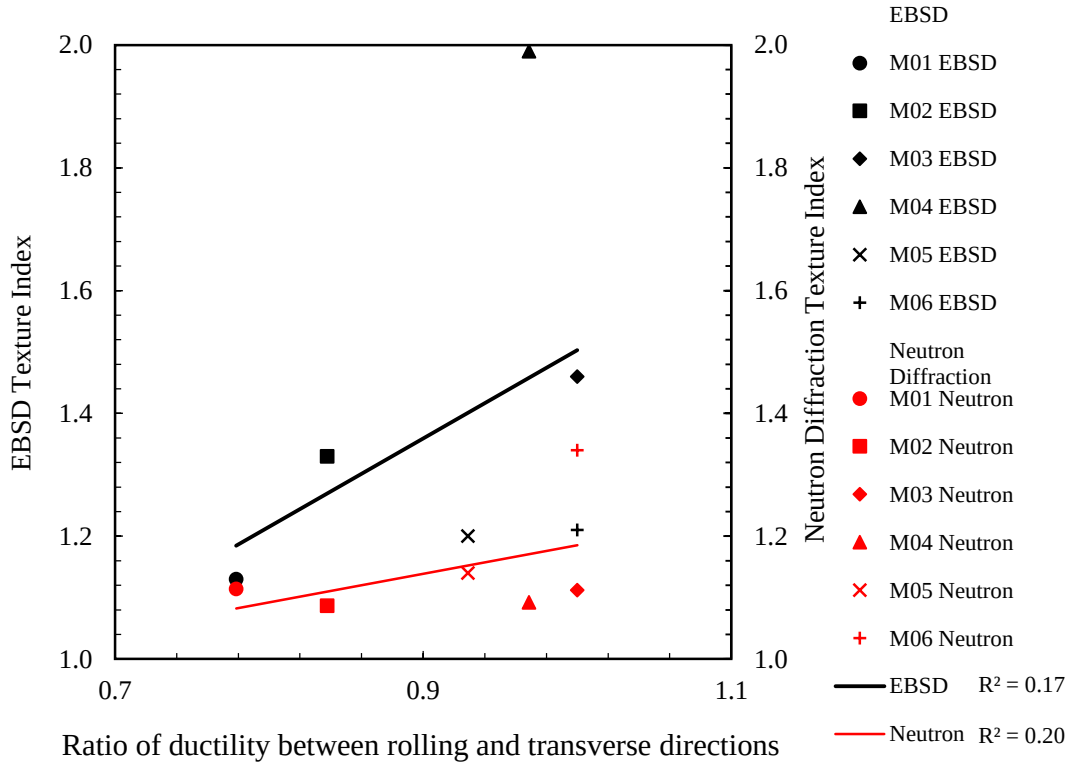

Figure 3-7: correlation between ratio of ductility (in terms of aspect ratio of RoA) and texture indices

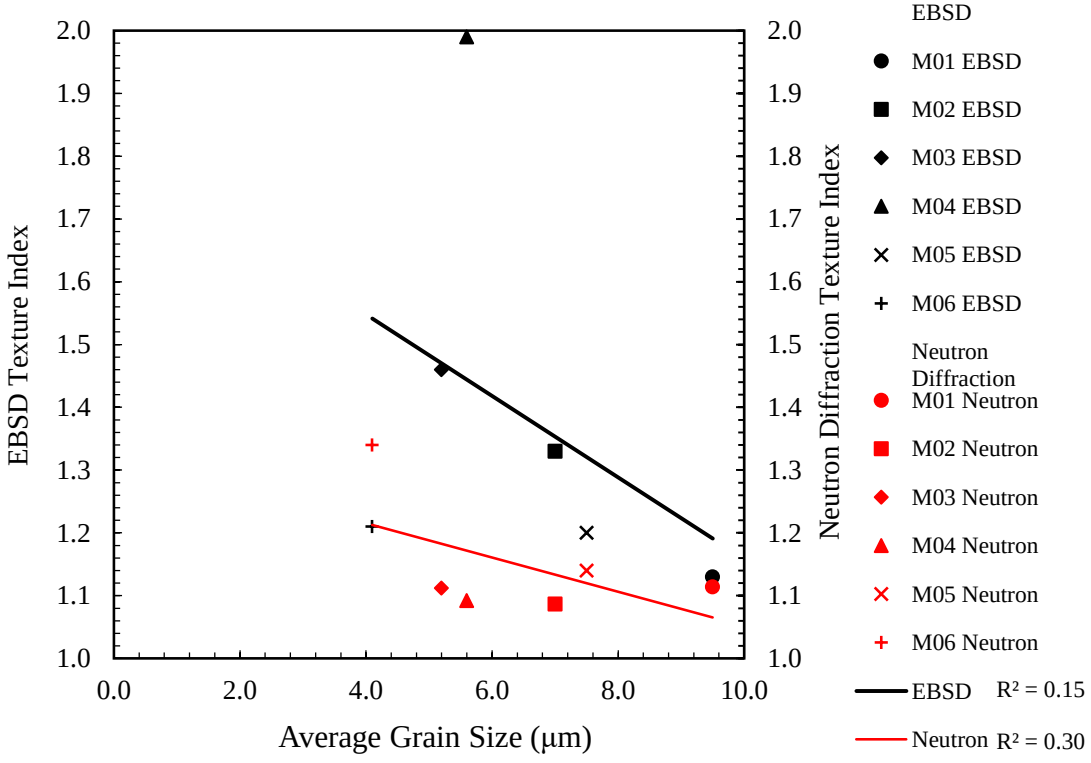

Figure 3-8: correlation between average grain size and texture indices

3.4 Discussion

There was poor agreement between the texture indices measured from EBSD and neutron diffraction. Although neutron diffraction is a bulk measurement method and EBSD is a planar measurement method, it would be expected that there be some correlation between the two since a more textured material should score relatively higher on each scale[10]. Nonetheless, the differences may be attributed to small sample size and local properties of the steels at the location the measurement was taken. It was not possible to make either texture measurement in more than one location or test specimen due to the high demand for neutron imaging facilities and the high cost of EBSD. It would be recommended to carry out texture measurements on a larger number of specimens in future work.

The grain size aspect ratio due to elongation of the grains along the rolling axis was estimated from the material's bulk ductility, in terms of tensile properties, which was correlated against the measured grain size aspect ratio. The observations showed a slight correlation. It would be expected that if the material was isotropic (i.e. tensile properties are identical along each axis), the grains would be equiaxed and not show elongation along the rolling axis. The grain size aspect ratio showed a good correlation with the EBSD texture index, but a poor correlation with the neutron diffraction texture index. This further suggests that the reason for the inconsistency in texture indices is due to the difference between bulk and planar measurement techniques or local inconsistencies as the EBSD analysis was carried out on the exact same specimens as the optical microscopy. It is recommended in future work to extract the steel samples once they have been imaged through optical and electron microscopy for neutron diffraction to ensure the exact same region of interest is being captured.

The texture index was very weak at the quarter wall of the steels, however it has been suggested that a steel's texture is a key factor in ensuring that a brittle crack arrests itself[1,7,8]. This may be due to shear lip formation at the surface of the steels which absorbs energy and prevents continued propagation[20]. This might mean that the texture is limited to the surface of the material which is in contact with the rollers during manufacturing. Alternatively, it has been suggested that hot rolled steels exhibit random texture at the surface and stronger texture at the centreline[19,21]. This is important because it means that although the texture may be influencing the full-thickness material in-service, it cannot

be captured through small-scale testing which samples only a small region of the thickness of the material. It is recommended to carry out a textural analysis at more locations through the plates' thickness to see the full picture more clearly and understand the in-service properties of the steels.

In future work, it is recommended to take further measurements of the texture from multiple specimens and throughout the thickness of the material. This was not possible in this work due to the high demand for neutron imaging facilities and the high cost of EBSD. It was chosen to focus on large scale crack arrest testing which was supplemented by comprehensive material characterisation from small-scale testing. The results given in this chapter are compared against the mechanical and fracture properties in chapter 1.

3.5 Conclusions

In this work, a textural analysis was carried out on 6 different batches of structural steels to investigate the relationship between different measurements of texture. The analysis comprised optical microscopy, electron microscopy, neutron imaging and perpendicular tensile testing. The following key conclusions have been drawn from the present study, and are further developed in chapter 1 in terms of mechanical properties:

- Each of the steels is very fine grained with slight texture which meant it was difficult to draw meaningful conclusions due to natural statistical scatter.
- The texture index measured from EBSD did not show any correlation with the texture index measured from neutron diffraction.
- The grain size aspect ratio correlated well with the texture index measured from EBSD but poorly with the texture index measured from neutron diffraction.
- Grain elongation results in anisotropy in the tensile properties of the steel.
- Texture which is imparted into a steel during manufacturing may not impact the texture in the bulk of the steel, which means it is not possible to accurately measure the effects of texture from small-scale sampling such as Charpy testing.
- It is recommended to carry out a textural analysis at more locations throughout the plates' thickness to see the full picture more clearly, understand the in-service properties of the steels, and investigate how the texture variation affects the resistance to fracture propagation.

References

1. Handa T, Tagawa T, Minami F. Correlation between charpy transition temperature and brittle crack arrest temperature considering texture. *Tetsu-To-Hagane/Journal Iron Steel Inst Japan*. 2012;98(1):32-38. doi:10.2355/tetsutohagane.98.32

2. Handa T, Igi S, Oi K, et al. Effect of toughness distribution in the thickness direction on long brittle crack propagation/arrest behaviour of heavy gauge shipbuilding steel. *Weld Int*. 2018;32(7):460-468. doi:10.1080/01431161.2017.1346884

3. Yanagimoto F, Hemmi T, Suzuki Y, Takashima Y, Kawabata T, Shibanuma K. Contribution of grain size to resistance against cleavage crack propagation in ferritic steel. *Acta Mater*. 2019;177:96-106. doi:10.1016/j.actamat.2019.06.038

4. Wang C, Wang M, Shi J, Hui W, Dong H. Effect of microstructural refinement on the toughness of low carbon martensitic steel. *Scr Mater*. Published online 2008. doi:10.1016/j.scriptamat.2007.10.053

5. Hyzak JM, Bernstein IM. The role of microstructure on the strength and toughness of fully pearlitic steels. *Metall Trans A*. Published online 1976. doi:10.1007/BF02656606

6. Curry DA, Knott JF. The relationship between fracture toughness and microstructure in the cleavage fracture of mild steel. *Met Sci*. Published online 1976. doi:10.1179/030634576790431453

7. Hase K, Ichimiya K, Ueda K, Handa T, Eto T, Aoki M. Texture-controlled YP460 n/mm2 class heavy thick plate for ultra-large container carriers. *Int J Offshore Polar Eng*. 2019;29(3):315-321. doi:10.17736/ijope.2019.hj31

8. Okawa T, Shirahata H, Nakashima K, Yanagita K, Inoue T. Simplified evaluation of brittle crack arrest toughness in heavy-thick plate by combined small-scale tests. *Int J Offshore Polar Eng*. 2017;27(2):210-215. doi:10.17736/ijope.2017.hj26

9. Wright SI, Nowell MM, Bingert JF. A comparison of textures measured using X-ray and electron backscatter diffraction. *Metall Mater Trans A Phys Metall Mater*

Sci. 2007;38(8):1845-1855. doi:10.1007/s11661-007-9226-2

10. Ullemeyer K, Braun G, Dahms M, Kruhl JH, Olesen N, Siegesmund S. Texture analysis of a muscovite-bearing quartzite: A comparison of some currently used techniques. *J Struct Geol*. 2000;22(11-12):1541-1557. doi:10.1016/S0191-8141(00)00103-6

11. Bunge H. *Texture Analysis in Materials Science*. Morris Transactions, Butterworths, London; 1982.

12. Chateigner D. Combined Analysis. *Comb Anal*. Published online 2013. doi:10.1002/9781118622506

13. ASTM. *E112-19 Standard Test Methods for Determining Average Grain Size*.; 2019. doi:10.1520/E0112-13.1.4

14. ISO. *BS EN ISO 6892-1:2016 BSI Tensile Testing Part 1 : Method of Test at Room Temperature*.; 2016.

15. BSI. *BS EN 10164:2004 Steel Products with Improved Deformation Properties Perpendicular to the Surface of the Product — Technical Delivery Conditions*.; 2004.

16. Yamamoto Y. Multiscale modeling to clarify the relationship between microstructures of steel and macroscopic brittle crack microstructures of steel and macroscopic brittle crack propagation / arrest behavior modeling of a high. *Procedia Struct Integr*. 2016;2:2389-2396. doi:10.1016/j.prostr.2016.06.299

17. JFE Steel. Product: Crack Arrest Steel Plate. https://www.jfe-steel.co.jp. Published 2020. Accessed April 15, 2020. https://www.jfe-steel.co.jp/en/products/plate/b02.html

18. Creuziger A, Calhoun CA, Poling WA, Gnäupel-Herold T. Assessment of bias errors caused by texture and sampling methods in diffraction-based steel phase measurements. *J Appl Crystallogr*. 2018;51:720-731. doi:10.1107/S160057671800420X

19. Wiskel JB, Li X, Ivey DG, Henein H. Characterization of X80 and X100

Microalloyed Pipeline Steel Using Quantitative X-ray Diffraction. *Metall Mater Trans B Process Metall Mater Process Sci*. 2018;49(4):1597-1611. doi:10.1007/s11663-018-1298-4

20. Funatsu Y, Shirahata H, Otani J, Inoue T, Hashiba Y. The Effect of Shear-lips on the Arrestability of Thicker Steel Plates Longitudinal. *Isope*. 2012;4:63-66.

21. Juntunen P, Karjalainen P, Raabe D, Bolle G, Kopio T. Optimizing continuous annealing of interstitial-free steels for improving deep drawability. *Metall Mater Trans A Phys Metall Mater Sci*. 2001;32(8):1989-1995. doi:10.1007/s11661-001-0011-3

Appendix A : Pole figures of texture orientation distribution (EBSD and neutron diffraction)

A.1 M01

A.1.1 EBSD

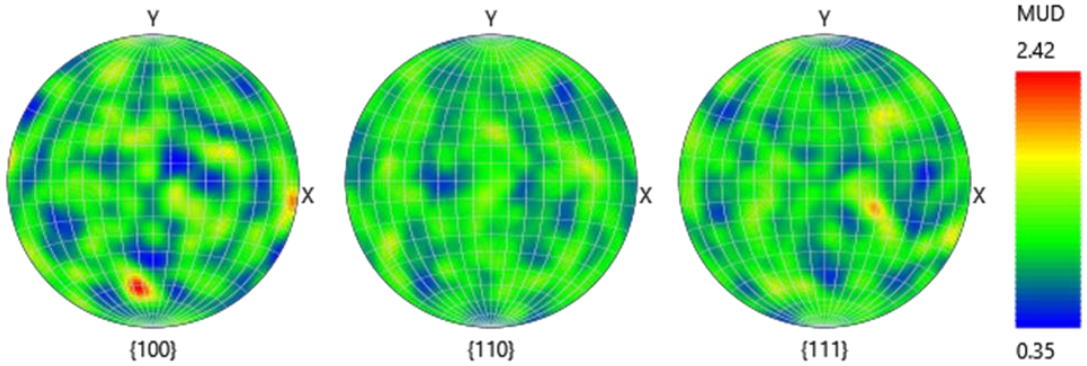

Figure 3-9: Pole figures determined for M01 from EBSD

A.1.2 Neutron Diffraction

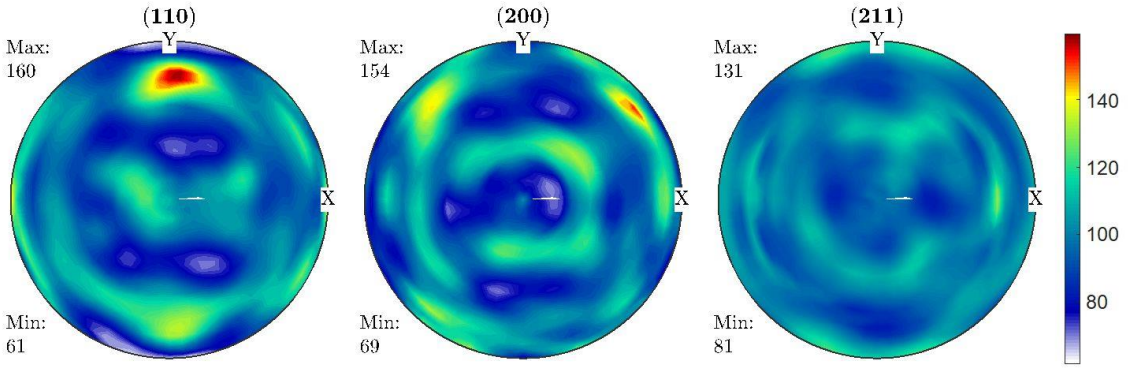

Figure 3-10: Pole figures determined for M01 from neutron diffraction

A.2 M02

A.2.1 EBSD

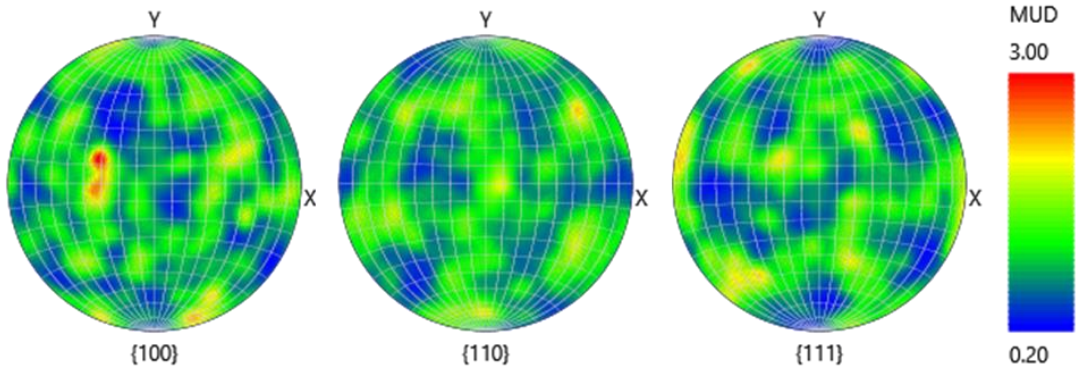

Figure 3-11: Pole figures determined for M02 from EBSD

A.2.2 Neutron Diffraction

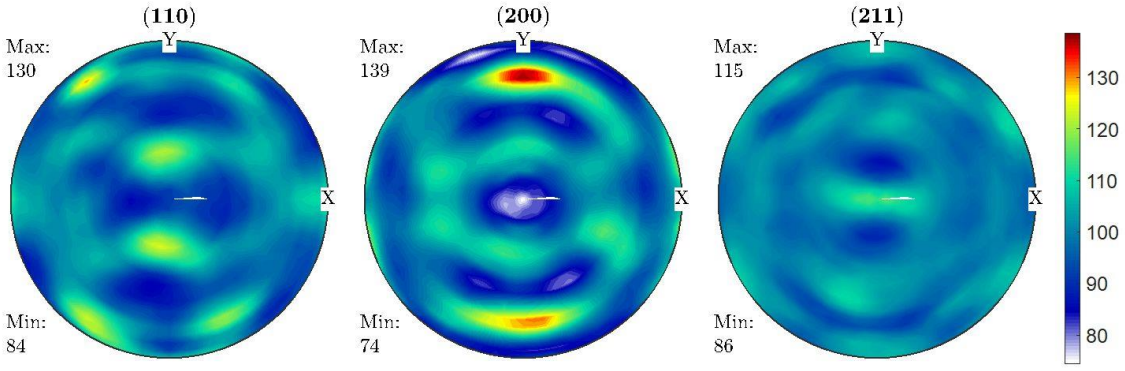

Figure 3-12: Pole figures determined for M02 from neutron diffraction

A.3 M03

A.3.1 EBSD

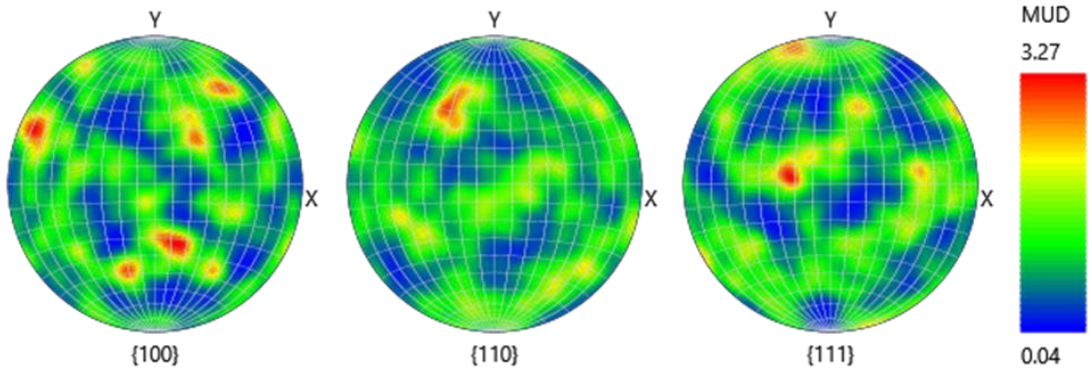

Figure 3-13: Pole figures determined for M03 from EBSD

A.3.2 Neutron Diffraction

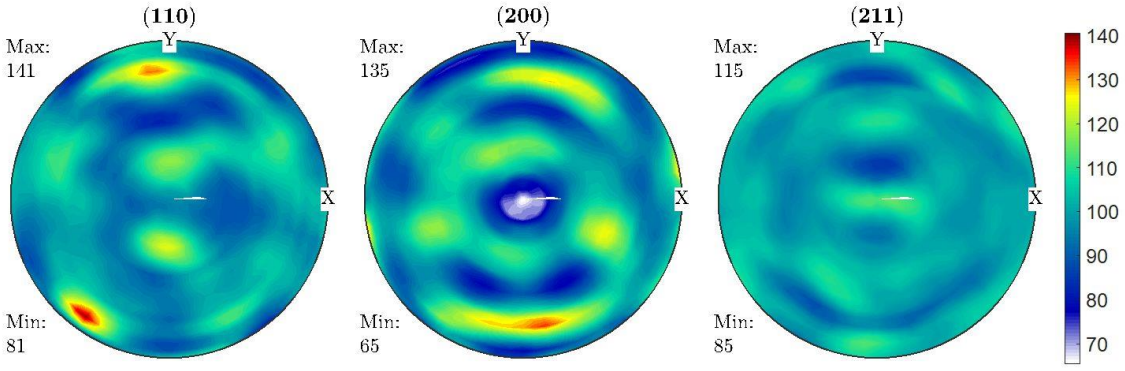

Figure 3-14: Pole figures determined for M03 from neutron diffraction

A.4 M04

A.4.1 EBSD

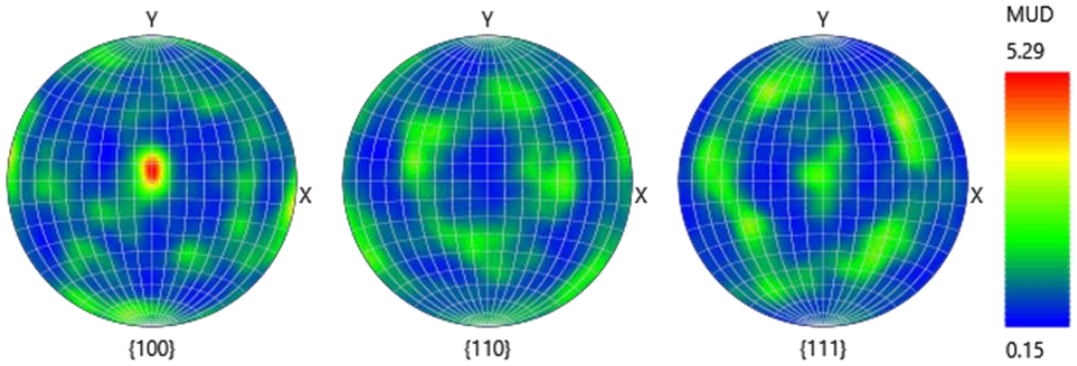

Figure 3-15: Pole figures determined for M04 from EBSD

A.4.2 Neutron Diffraction

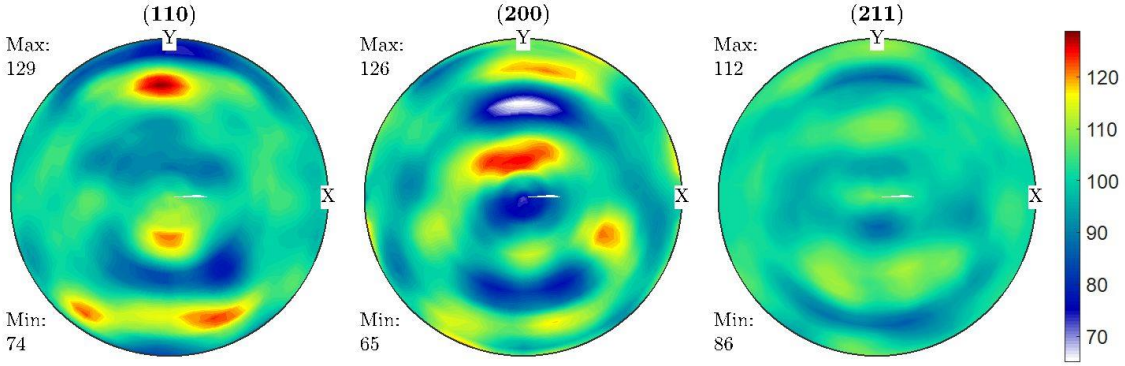

Figure 3-16: Pole figures determined for M04 from neutron diffraction

A.5 M05

A.5.1 EBSD

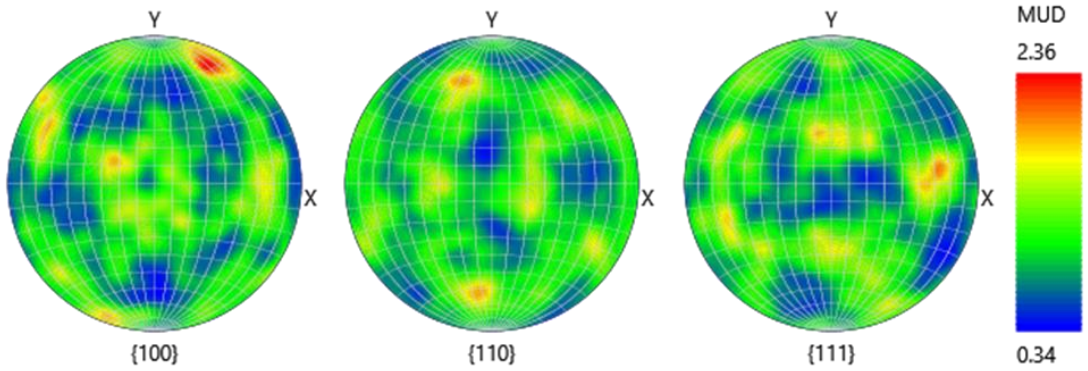

Figure 3-17: Pole figures determined for M05 from EBSD

A.5.2 Neutron Diffraction

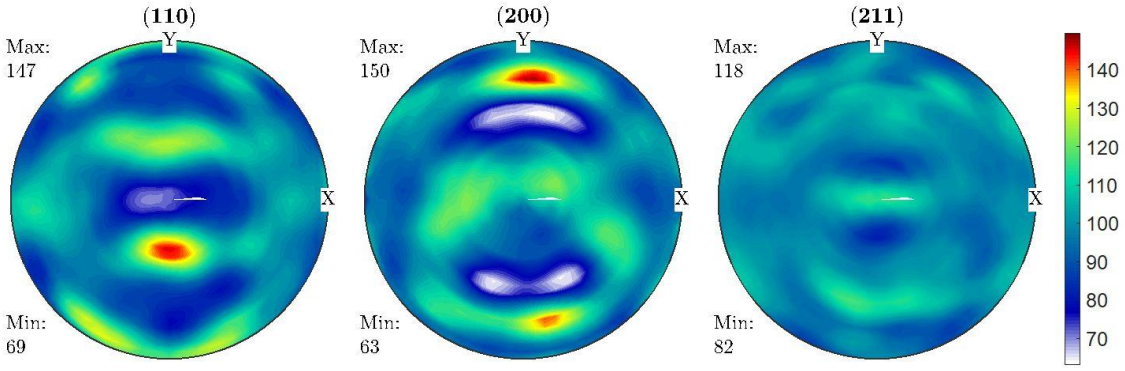

Figure 3-18: Pole figures determined for M05 from neutron diffraction

A.6 M06

A.6.1 EBSD

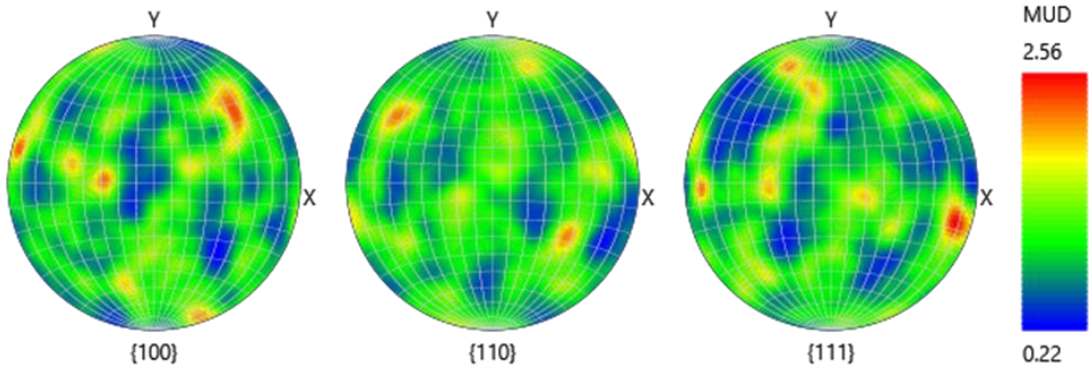

Figure 3-19: Pole figures determined for M06 from EBSD

A.6.2 Neutron Diffraction

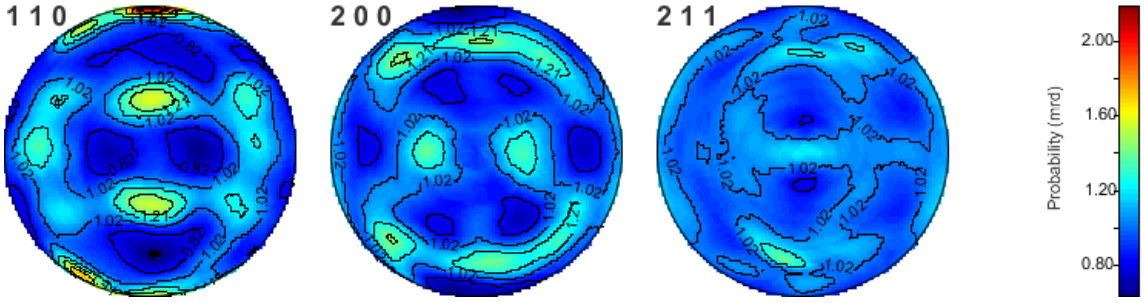

Figure 3-20: Pole figures determined for M06 from neutron diffraction

4 Experimental study of the relationship between fracture initiation toughness and brittle crack arrest toughness predicted from small-scale testing

Abstract

It is vital to prevent brittle cracks in large structures. This is particularly important for a number of industry sectors including offshore wind, Oil & Gas, and shipbuilding where structural failure risks loss of human life and loss of expensive assets. Some modern steels exhibit high Charpy energy – i.e. high initiation fracture toughness, but poor resistance to crack propagation – i.e. low crack arrest toughness. The correlation between initiation and arrest toughness measured through small-scale testing is investigated in five different steels, which include S355 structural steel (with two different thicknesses), X65 pipeline steel, two high strength reactor pressure vessel steels and EH47 shipbuilding steel. Small scale mechanical tests were carried out to characterise the materials' properties and were compared to the materials' microstructures. A wide range of tests were carried out, including instrumented Charpy, drop weight Pellini, fracture toughness, and tensile testing. Nil ductility transition temperature (NDTT) is used to characterise a material's arrest properties. Initiation fracture toughness correlated with higher upper shelf Charpy energy and smaller average grain sizes, as expected, however none of these correlated well with the arrest toughness measured through NDTT. The NDTT correlated most strongly with the T_{27J} temperature which indicates the start of lower shelf of the Charpy curve. This correlation held for all materials including those where the NDTT lies on the upper shelf of the Charpy curve. While initiation fracture toughness can be predicted through high Charpy toughness and operation temperatures on the upper shelf, crack arrest behaviour should be predicted from characteristics of the ductile to brittle transition temperature, for example by using the T_{4kN} from instrumented Charpy tests or T_{27J}.

Keywords: brittle crack arrest, structural steel, small-scale testing, fracture toughness, crack arrest toughness

Nomenclature

a	Crack length
a_0	Initial crack length
B	Thickness
E	Elastic Young's modulus
K_a	Crack arrest toughness
K_{ca}	Crack arrest toughness: critical stress intensity factor for crack arrest under mode I fracture mechanics loading condition
K_{Ia}	Crack arrest toughness: measured via ASTM E1221
K_{IC}	Initiation fracture toughness: critical stress intensity factor for crack initiation under mode I fracture mechanics loading condition
K_{JC}	an elastic-plastic equivalent stress intensity factor derived from the J-integral at the point of onset of cleavage fracture.
σ_y	Yield strength
T	Temperature
T_0	Reference temperature at which a material's mean initiation fracture toughness is 100MPa√m
T_{27J}	Reference temperature at which a material's Charpy impact energy is 27J
T_{4kN}	Reference temperature at which a material's arrest force during instrumented Charpy test is 4kN
T_{KIa}	Reference temperature at which a material's arrest toughness is 100MPa√m
ASME	American Society of Mechanical Engineers
CAT	Crack Arrest Temperature
CTOD	Crack Tip Opening Displacement
CVN	Charpy V Notch
EBSD	Electron Backscatter Diffraction
NDTT	Nil Ductility Transition Temperature
RoA	Reduction of Area
RPV	Reactor Pressure Vessel
SEN(B)	Single Edge Notched Bend fracture toughness test
STRA	Short Transverse Reduction of Area
UTS	Ultimate Tensile Strength

4.1 Introduction

Crack initiation and propagation is often experienced by engineering components and structures subjected to operational loading conditions. An important issue that needs to be understood for design and life assessment of such structures is the ability of a material to arrest a fast-running brittle crack, particularly for structures where a fracture may initiate in areas of high local stress or low toughness, for example in the welds of a large welded offshore structure[1]. This is particularly important for a number of industry sectors including offshore wind, Oil & Gas, and shipbuilding, where structural failure risks loss of human life and loss of expensive assets. A load cannot be transferred through a crack, so once it grows too large the whole structure will fail.

Structures in offshore environments are exposed to very harsh loading conditions, with both wind and wave loading in addition to the operating loads i.e. its own mass and moving components[2,3]. In such structures a crack may initiate around a weld region, which is the part of a structure most susceptible to cracking due to material mismatch, heat input which changes material properties, locked-in residual stresses and increased chance of impurity inclusions during the welding process[4]. Smaller components can be heat-treated after welding, to reduce the damaging effects of welding residual stresses and reset the materials microstructure and larger structures can receive local heat treatment[4]. However, this is simply not commercially viable for very large components such as ships, wind turbine support structures, or long welded pipelines.

An alternative approach to initiation prevention is the crack arrest approach. Using this concept, it can be considered that fracture may occur in a local region of high stress, embrittlement, or under accidental damage. However the material's properties are carefully controlled so it has a sufficient toughness to inhibit fracture propagation outside this region[5]. When the crack arrests before growing too long, catastrophic failure can be prevented. This is vital for a structure with welds, which can be a hotspot for defects or embrittled zones which promote fracture initiation. Moreover, the crack arrest approach can be more reliable than the initiation approach at preventing catastrophic fracture as it accounts for accidental damage and is effective even once a crack is growing[6].

If brittle fracture occurs in a high toughness steel, the initial driving force can be incredibly high, which means the crack will not arrest but propagates until the whole structure fails. This means that some modern steels with very high fracture initiation toughness can be at risk of poor crack arrest behaviour if an accident occurs. This may be a concern for some modern steels which have a very good Charpy toughness, but a poor resistance to fracture propagation[7,8]. In structures made of such materials, accidental damage could result in total structural failure due to the lack of conservatism when brittle crack arrest is not considered. In fact, it has recently been found that although a smaller average grain size improves fracture initiation toughness, it may worsen the brittle crack arrest toughness[9]. In addition, a material's crack arrest properties are heavily temperature dependent for materials which exhibit ductile to brittle transition i.e. ferritic steels. It may be considered that ductile behaviour will occur if a material is operating at a temperature on its upper shelf, but this is not always assured[7]. An example could be impact or dynamic loading where the material experiences a shift upwards of the ductile to brittle transition temperature compared to quasi-static loading behaviour[10];i.e. steels operating at temperatures on their upper shelf can experience brittle crack initiation under dynamic load events such as crash, impact or earthquakes.

There is interest in determining which small-scale test methods are effective at predicting crack arrest behaviour and how a material's different mechanical properties are related to one another. The purpose of this study is to develop a better understanding of the crack arrest behaviour in a range of modern steels by performing mechanical testing and comparing it to metallurgical analysis of the materials' microstructures which is reported in chapter 3, and has been suggested to influence crack arrest properties[9,11,12]. The results from this study correlate the mechanical properties with the microstructure of five different modern structural steels to evaluate the relevant parameters necessary for fracture prevention.

4.2 Empirical test methods for evaluating crack arrest

Crack arrest properties are typically measured by one of the following two parameters: 1- crack arrest toughness, K_a; or 2- crack arrest temperature (CAT). The crack arrest toughness, K_a, can be defined as the critical stress intensity factor for crack arrest under the mode I fracture mechanics loading condition above which a fast-running crack is

arrested, K_{ca}. Alternatively, K_{Ia}, can be used, although this may give a conservative estimate[13–15]. The CAT is the lowest temperature that a fast-running brittle crack will arrest in a certain material under specified conditions. The CAT can be determined by initiating a brittle crack in a material at a range of temperatures and finding the lowest temperature where a brittle running crack arrests[5]. In such experiments, fracture is typically initiated by impacting a region with a notched brittle weld bead. K_{Ia} and K_{ca} can be determined through standardised methods such as those described in ASTM E1221 and JWES 2815[16–18].

Many empirical equations are available in the literature to predict the structural behaviour in terms of crack arrestibility from small-scale test results. However, very few standards recommend the use of them. The only mention is in the R6 defect tolerance assessment procedure, which recommends the use of drop weight Pellini testing for applications in the UK nuclear industry[19]. This is because as the dimensions and particularly the thickness of the plates employed in many industrial applications increase, the empirical equations are no longer valid, and may not fully describe the crack arrest behaviour of actual structures.

Although crack arrest toughness is thought of as a material property, it is strongly dependent on the plate thickness, test temperature, applied stress[20–23]. Furthermore, brittle crack arrest toughness shows a dependence on specimen width as well as manufacturing processes [24–27]. This makes it complex to predict the crack arrest properties of large structures from subsize specimens, thus introducing a need for a sufficiently conservative approach.

4.2.1 Small-scale testing correlations for steels

The ability of a material to resist growth of a propagating brittle crack is analogous to its crack arrest properties. This is measured using the CAT, the minimum temperature where the material arrests a brittle running fracture. Since crack arrest toughness depends on temperature, the ductile to brittle transition of the material must be understood. Reference temperatures taken from the transitional behaviour include the Charpy impact energy (e.g. temperature at onset of lower shelf) and nil-ductility transition temperature (NDTT) which can be determined through small-scale testing. Empirical relationships are

available in the literature to predict the large scale behaviour from these reference temperatures[28,29]. However, the empirical equations are validated for certain specimen dimensions of a given material at a specified thickness, under a certain loading rate. This means that they cannot necessarily be applied to represent a large structure which would almost certainly not meet the strict validity criteria. Therefore some researchers recommend using the NDTT to quantify a material's crack arrest properties[30].

The following relationships were determined by analysing a large amount of data from Charpy-V-Notch (CVN) and drop weight Pellini impact tests. Many other empirical relations are available in the literature and this section highlights just a small number of those[17,31–38]:

$$Pellini\ NDTT\ =\ 120\ J\ CVN\ temperature\ +50°C \qquad \text{Equation 4-1}$$

$$Pellini\ NDTT\ =\ 40\ J\ CVN\ temperature\ +60°C \qquad \text{Equation 4-2}$$

$$Pellini\ NDTT\ =\ 27\ J\ CVN\ temperature\ +60°C \qquad \text{Equation 4-3}$$

Equations 4-1 to 4-3 can be used to predict the crack arrest temperature by using Equation 4-4. This enables use of CVN results to predict the CAT, although of course the NDTT from Pellini testing can be used[5]:

$$CAT\ =\ NDTT\ +\ 40°C \qquad \text{Equation 4-4}$$

From the simple relations given above, a range of tests were carried out to make corrections for a variation in applied stress and thickness[30]. This relationship uses the reference conditions of the CAT for 124 MPa applied stress (σ) on a 25 mm thick (B) plate and adds corrections for other stresses and thicknesses. This leads to the semi-empirical Wiesner equation given below, which is valid up to a thickness of 250 mm[5]:

$$CAT = [NDTT + 10] + [\frac{\ln[\sigma]}{0.046} - 105] + [153(B-5)^{\frac{1}{13}} - 190]\ °C \qquad \text{Equation 4-5}$$

This in turn has led to the formula commonly used today, in the R6 defect tolerance assessment procedure for the UK nuclear industry[19,39]:

$$CAT\ =\ NDTT\ +21.7\ln\sigma\ +\ 173.2(200B\ -\ 1)^{\frac{1}{13}} - 285\ °C \qquad \text{Equation 4-6}$$

The NDTT is the most common parameter which is used to predict the CAT from small-scale test results because there has been a wide range of research into different materials and their weldments. Additionally, the drop weight method measures the ability of the material to resist a propagating brittle crack and can be explained theoretically using fracture mechanics[17,40]. Because of this, NDTT will be used as a measure of crack arrestibility in this work.

4.2.2 Reference curves

Reference curves are used extensively in the pressure vessel industry to give a lower bound crack initiation toughness for all grades of pressure vessel steel at temperatures within the transition region[26]. Originally, the American Society of Mechanical Engineers (ASME) reference curve was used in industry[41], which gives an estimate based on extensive experimental results. The master curve approach is an alternative statistical approximation which gives a higher degree of accuracy[42,43]. These approaches use a reference temperature (for example T_0, the temperature corresponding to a mean initiation fracture toughness of 100 MPa√m) for the material to calculate its toughness at a given temperature[26]. The median fracture toughness, K_{JC} is predicted using the following equation:

$$K_{JC(median)} = 30 + 70\, e^{0.019\,(T - T_0)} \text{ [Ref 26]} \qquad \text{Equation 4-7}$$

where K_{JC} is in MPa√m and T, the assessment temperature, has the unit of $°C$ (i.e. degrees Celsius). It is assumed that both the initiation toughness, K_{JC}, and lower bound approximation of crack arrest toughness, K_{Ia}, data are expected to exhibit the same transition behaviour since the temperature dependence of both toughness values is controlled by the atomic arrangement, or crystal structure of the material. Consequently, this temperature dependence is expected to be common to all ferritic steels[41]. Through analysis of a large amount of experimental data, the following relations which are relevant to this work were proposed in the literature[41]:

$$K_{IC} = 51.276 + 51.897\, e^{0.036\,(T - NDTT)} \text{ [Ref 44]} \qquad \text{Equation 4-8}$$

$$K_{Ia} = 49.957 + 16.878\, e^{0.028738(T - NDTT)} \text{ [Ref 44]} \qquad \text{Equation 4-9}$$

where K_{IC} and K_{Ia} are in MPa√m and *T*, the assessment temperature, has the unit of $°C$ (i.e. degrees Celsius). An alternative correlation which has been developed in previous studies takes a reference temperature from instrumented Charpy testing to describe the arrest toughness using the temperature at which the force after fracture measured by an instrumented Charpy test is 4kN, T_{4kN}.

$$K_{Ia} = 30 + 70\, e^{\left(\frac{T - T_{4kN} - 12.3}{52.63}\right)} \text{ [Ref } ^{45}\text{]} \qquad \text{Equation 4-10}$$

Although K_{Ia} will not be determined in this work, the predictions from these methods will be compared with each other to determine their agreement with one another and likely conservatism using K_{Ia} results from other researchers to give realistic K_{Ia} ranges. For material M06, EH47 shipbuilding steel, a full analysis including K_{Ia} results is given in section 5.3.2.

4.3 Experimental procedure and specimen manufacture

The test program and specimen key information are summarised in Table 4-1, with further details explained below. The small-scale mechanical properties of the steels are compared to a comprehensive microstructural analysis which is presented in chapter 3. The materials used are summarised in Table 4-1.

Where possible, the specimen orientation and extraction location were kept the same for each material, however this was not always possible. For example, no matter the extraction location, a 19 mm thick Pellini specimen will sample a larger proportion of the 28 mm thick steel plate than the 90 mm thick steel plate. Similarly, it was decided to use only subsize SEN(B) fracture toughness tests rather than full plate thickness (as is recommended in the standard) to be able to limit the size effects which could not be captured through the other test methods and make the results more comparable to each other. The specimen extraction plan is shown in Appendix A.

Table 4-1: Summary of small-scale testing carried out and specimen geometries.

Test type	Number of specimens for each material	Extraction location	Orientation (of notch or gauge region)	Thickness, ***B*** (mm)	Width, ***W*** (mm)	Length, ***L*** (mm)
Tensile Roundbar (BS EN ISO 6892-1)	3	Mid-thickness	Along rolling direction	8 (gauge diameter)	n/a	48 (gauge length)
Tensile STRA (BS EN 10164)	3	Through-thickness	Through-thickness	10 (gauge diameter), reduced to 6 (gauge diameter for materials of 30 mm thickness or less)	n/a	Full plate thickness
Instrumented Charpy V Notch (BS EN ISO 148-1)	20	Mid-thickness	Transverse to rolling direction	10	10	55
Pellini - P2 size (ASTM E208)	8+ (if more needed to determine NDTT)	Quarter wall	Through-thickness	19	50	130
SEN(B) Fracture Toughness (BS 7448-1)	3	Mid-thickness	Transverse to rolling direction	20	20	120

Drop weight Pellini testing was carried out using Pellini P2 specimens (with dimensions given in Table 4-1), following ASTM E208[17], to measure the NDTT of each material. Pellini specimens were made up of a small block of material on which a brittle weld bead was laid using a hard-facing electrode and then notched. The specimen was cooled to the desired temperature and was impacted by a dropped weight on the reverse (unwelded) side in order to initiate a brittle crack running from the notched weld into the base metal. The impact energy is specified depending on the material's yield strength: 350 J for σ_y up to 410 MPa and 400 J for σ_y between 410 MPa and 620 MPa. A "no-break" result is where

a brittle crack initiates but does not spread across the full width of the specimen i.e. it initiates and is arrested. If the crack spreads at least across the full width of the specimen, then it was considered to be a "break" result. The test was repeated at a range of temperatures to find the NDTT, which is the highest temperature at which the specimen shows a "break" result i.e. all specimens at temperatures above this show "no-break" results.

Furthermore, instrumented Charpy V notch (CVN) tests were carried out at a range of temperatures, following BS EN ISO 148-1[46], to determine the ductile to brittle transition curve and upper shelf absorbed energy which is commonly used in industry to estimate fracture toughness. Instrumented Charpy tests differ from traditional Charpy tests by measuring the force on the hammer throughout the test as well as the absorbed energy. The post-fracture force, also known as the arrest force, was extracted for each specimen which showed arrest behaviour. This data was analysed to determine (through inter-/extrapolation) at what temperature the post-fracture force would be 4 kN, T_{4kN}.

Tensile testing was carried out on all materials under two different conditions. Traditional tensile tests following BS EN ISO 6892[47] were carried out to determine the yield strength and ultimate tensile strength (UTS) of the materials along with the ductility which was taken as the reduction of area (RoA) or elongation in this work. Additionally, alternative tensile tests, "short transverse reduction of area" (STRA) tests were carried out to measure the ductility in the through-thickness direction following BS EN 10164[48]. This was done to investigate whether the ratio of ductility between the rolling axis and through-thickness axis can be used as a proxy for the material's texture, which is believed to influence crack arrestibility[49,50].

Finally, Single Edge Notched Bend, SEN(B), fracture toughness testing was done on each material, following BS 7448-1[51], to quantitatively determine the fracture toughness as the maximum crack tip opening displacement (CTOD δ_m). The testing was carried out at a temperature on the upper shelf as determined by the Charpy testing so that they can be compared to the upper shelf CVN energy for the material. Typically this was room temperature for most of the steels. In addition to testing all of the steels at their upper-shelf temperatures, half of the steels (M01, M02 and M06) had fracture toughness tests carried out at temperatures within the transition region and lower shelf, to help support

discussions about crack arrest predictions based on the Master Curve. The SEN(B) specimen geometries are summarised in Table 4-1, and each specimen had an initial crack length, a_0, of 0.5W (i.e. 10 mm). The specimens were not side grooved as this is not necessary for small sized specimens like the ones employed in the present study.

4.4 Test Materials

4.4.1 Selected materials

The test programme in this study was carried out on five materials, in six batches, which are summarised in Table 4-2: 1- reactor pressure vessel (RPV) A543 steel with a thickness of 28 mm (denoted M01); 2- RPV A302 steel with a thickness of 28 mm (denoted M02); 3- X65 pipeline steel with a thickness of 30 mm (denoted M03); 4- S355G10+M structural steel plate with a thickness of 90 mm (denoted M04); 5- S355G10+M structural steel plate with a thickness of 50 mm (denoted M05); and 6- EH47 shipbuilding steel with a thickness of 80 mm (denoted M06). The materials selected in this study are widely used in offshore Oil & Gas, nuclear power plants and offshore wind applications, therefore the obtained results and drawn conclusions from this research are expected to have a significant impact on design and life assessment of engineering components and structures employed in a wide range of industries.

Table 4-2: Summary of the different steels used in this research.

Material Reference	M01	M02	M03	M04	M05	M06
Material	RPV A543	RPV A302	X65	S355G10+M	S355G10+M	EH47
Thickness (mm)	28	28	30	90	50	80

4.4.2 Mechanical properties – tensile (roundbar and STRA) and chemical

The tensile and chemical properties of the materials considered in this study are given in Table 4-3 and Table 4-4, with an example tensile curve for each material given in Figure 4-1 and the Young's modulus region emphasised in Figure 4-2. The wide variation in yield stress, σ_y, and the UTS between the different materials is evident in Figure 4-1.

Materials M04 and M05 (both nominally S355 structural steels) are an excellent example to demonstrate the variation in "off-the-shelf" steels. They are the same steel grade and produced through the same manufacturing route, however they show a difference in mechanical properties and chemical composition. This is common for steels because the standard grades allow for a great deal of flexibility[52]. It is worth noting that there is generally low scatter for most of the tensile test results between the 3 specimens of each material although due to the low number of specimens tested, the scatter is of low statistical significance. However, materials M04 and M06 show high scatter in their elastic modulus results. For M04 this is due to one much lower result of 171GPa and for M06 there was one much higher result of 334GPa which is quite an unexpected and extreme value. This kind of scatter in elastic modulus is common for steels and may be due to local inhomogeneities in the material which were picked up during the small sample size of the tensile specimen or minor inconsistencies in test procedure[52–54]. Generally, both the UTS and reduction of area (RoA) were lower in the STRA test (i.e. through thickness direction) as opposed to the tensile tests along the rolling direction. Although for materials M03 and M06, the RoA was the same between the two orientations.

As seen in Figure 4-1, there is generally negative trend between strength and ductility, with the highest strength steel, M01, having a low strain at failure and the lowest strength material, M05, having the highest strain at failure. However, this trend is not consistent for all the steels, for example material M03 which has an intermediate strength but a very low strain at failure. The increased strain at failure for materials M04 and M05 may be due to their low carbon equivalent content which contributes to a higher ductility. As seen in Table 4-3 and Table 4-4, the RPV steels (M01 and M02) have the highest carbon and carbon equivalent content in comparison to the other steels, hence higher yield stress values were observed in RPV steels. Further comparison between the chemical composition of the steels show that there is a variation in Mn and Cr contents: for example, M01 has a far smaller Mn content than the other five batches of steel, which is replaced by a greater Cr and Ni content. Apart from these points of note, the steels have relatively similar compositions. The other variations in tensile properties are likely to be due to microstructural differences between the steels such as their grain size, grain orientation and phase structure.

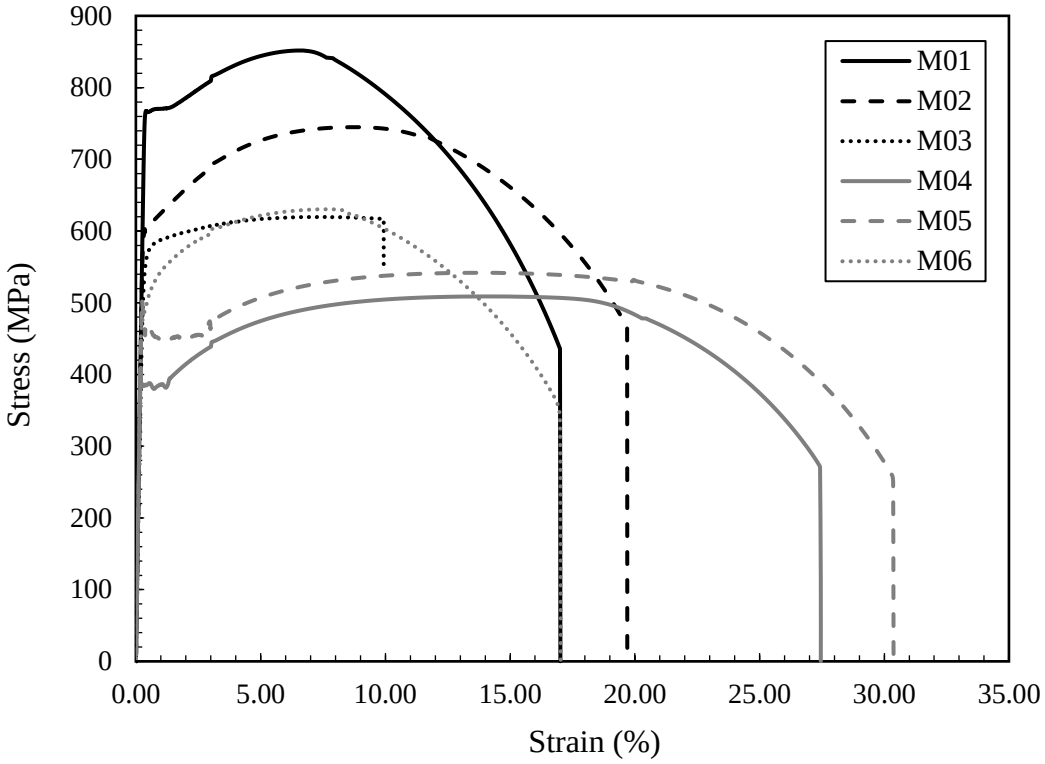

Figure 4-1: Tensile curves for all six materials used in this study.

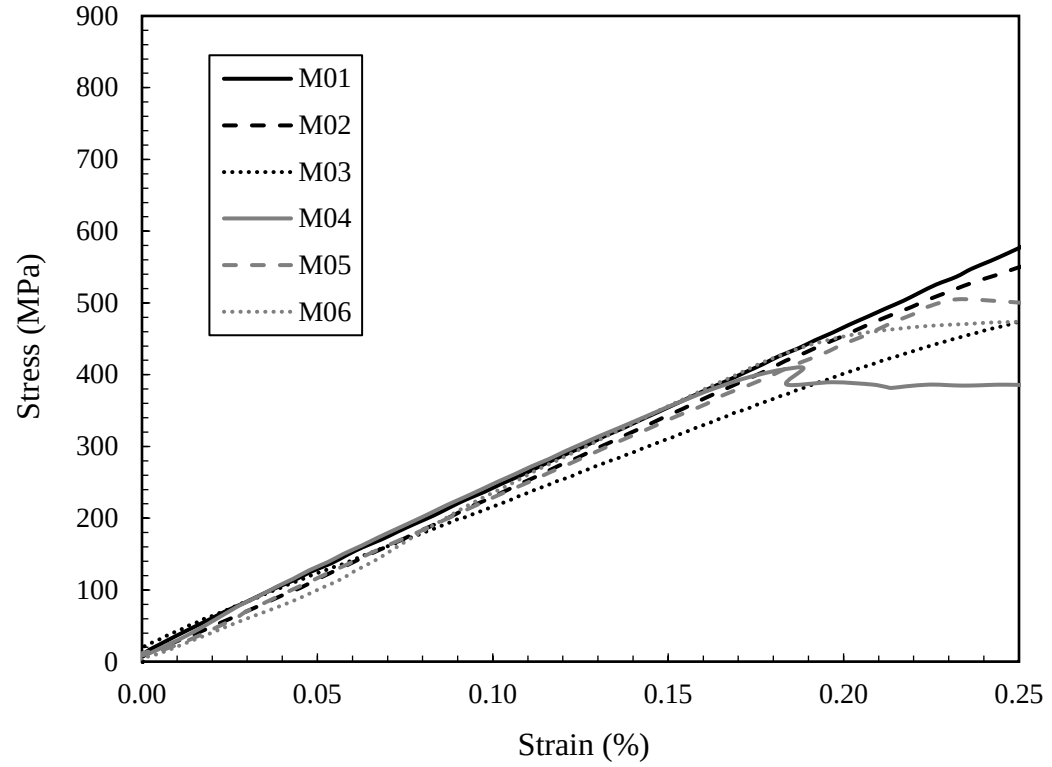

Figure 4-2: Young's modulus region of tensile curves for all six materials used in this study.

Table 4-3: Summary of tensile properties of the steels considered in this research. Uncertainty is taken as two standard deviations of the results.

	M01	M02	M03	M04	M05	M06
Material	RPV A543	RPV A302	X65	S355 G10+M	S355 G10+M	EH47
Thickness (mm)	28	28	30	90	50	80
Average E (GPa)	233 ± 16	227 ± 15	188 ± 5	208 ± 66	217 ± 24	270 ± 112
Average UTS (MPa)	845 ± 31	740 ± 17	613 ± 21	509 ± 2	536 ± 12	622 ± 15
Average σ_y (MPa)	756 ± 34	601 ± 13	566 ± 17	386 ± 4	444 ± 32	490 ± 10
Average RoA (%)	73 ± 4	66 ± 2	81 ± 2	77 ± 1	83 ± 1	78 ± 5
STRA Average UTS (MPa)	835 ± 18	733 ± 7	595 ± 5	501 ± 2	512 ± 1	618 ± 3
STRA Average RoA (%)	57 ± 6	55 ± 4	81 ± 3	75 ± 4	77 ± 5	79 ± 1

Table 4-4: Summary of chemical composition of the steels considered in this research

	M01	**M02**	**M03**	**M04**	**M05**	**M06**
C	0.17	0.19	0.04	0.07	0.06	0.05
Si	0.38	0.31	0.18	0.27	0.35	0.22
Mn	0.3	1.47	1.63	1.57	1.54	1.41
P	0.007	0.012	0.006	0.013	0.012	0.01
S	0.005	0.004	<0.002	<0.002	<0.002	0.005
Cr	1.49	0.23	0.17	0.035	0.16	0.21
Mo	0.46	0.52	0.12	0.007	0.013	0.25
Ni	2.95	0.59	0.48	0.34	0.032	0.78
Al	0.014	0.012	0.027	0.032	0.035	0.039
As	<0.004	<0.004	<0.004	<0.004	<0.004	<0.01
B	<0.0005	<0.0005	<0.0005	<0.0005	<0.0005	<0.003
Co	0.008	0.006	<0.004	<0.004	<0.004	<0.01
Ceq (IIW)[55]	0.81	0.62	0.40	0.36	0.35	0.43

4.5 Experimental results from small-scale tests

4.5.1 Instrumented Charpy V notch impact test results

The key results from the instrumented CVN tests are shown in Table 4-5, with the fit to the Charpy curve for each material shown in Figure 4-3. It is evident that material M02, one of the RPV steels, is designed for use at elevated temperatures as the transition for this material occurs well above room temperature. The other steels show a wide range of upper shelf CVN energy values, but their transition region (with varying slopes) lies in the same window of around -100°C to -50°C, making them suited to work at ambient temperatures. Material M03 has the highest upper shelf Charpy energy, followed by materials M05 and M06 which both have almost the same upper shelf Charpy energy. Despite being the same steel grade as M05, M04 has a markedly lower upper shelf Charpy energy and although they had the highest tensile strength, the RPV steels have the lowest upper shelf Charpy values of any of the materials. The reference temperatures given in Table 4-5 will be discussed later, but suffice to say that there seems to be no relationship between a material's T_{4kN} and its T_{27J} – for example for materials M03, M04 and M06 the T_{27J} is notably higher than the T_{4kN}, however a reverse trend is seen for materials M01 and M02 and no difference is seen between the two for material M05.

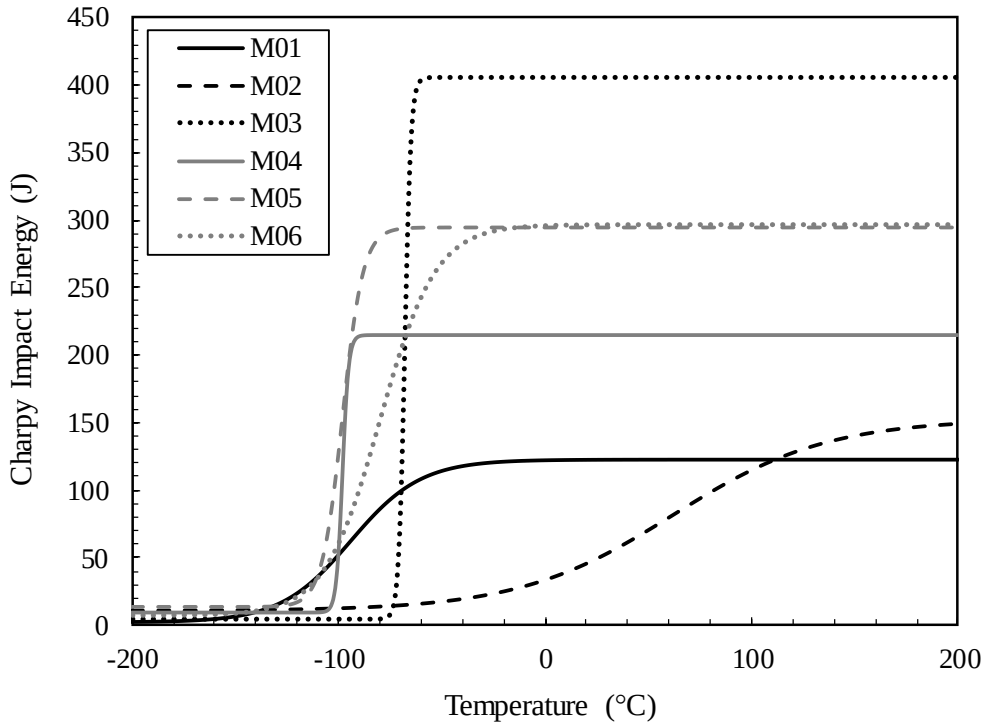

Figure 4-3: Charpy curve for each material determined as a tanh fit to the data.

Table 4-5: Summary of Charpy results for each material, including reference temperatures.

	M01	**M02**	**M03**	**M04**	**M05**	**M06**
CVN Upper Shelf (J)	122	140	410	210	295	297
T_{4kN} (˚C)	-100	14	-90	-113	-112	-156
CVN T_{27J} (˚C)	-117	-13	-72	-102	-113	-115

4.5.2 Pelini test results

The Pellini test results are summarised in Table 4-6, with the full results given in Figure 4-4. In this figure, the open white points indicate that a fracture event occurred at this temperature and the solid black points indicate that no fracture event occurred at this temperature. At some temperatures, both “break” and “no-break” results occurred, and these are indicated with a mix of the two symbols. The arrows indicate the temperature above which no fracture event occurred– i.e. the crack was arrested and it is above the

NDTT of the material. A low NDTT indicates good brittle crack arrestibility for that material.

The two RPV steels, M01 and M02 had the lowest and highest NDTT values respectively. Intermediate NDTT values were seen for the other steels, with material M03 having a slightly higher value followed by materials M04 and M06, and material M05 having a slightly lower value. These results show some similarities with the Charpy results in that materials M01 and M06 had shallower Charpy transition curves than the other materials and here they show some temperatures with both break and no-break results which indicates a wide transition region. However, material M02 which had a shallow Charpy transition curve showed very well defined Pellini behaviour which indicates a narrow transition region and shows disagreement with the Charpy curve.

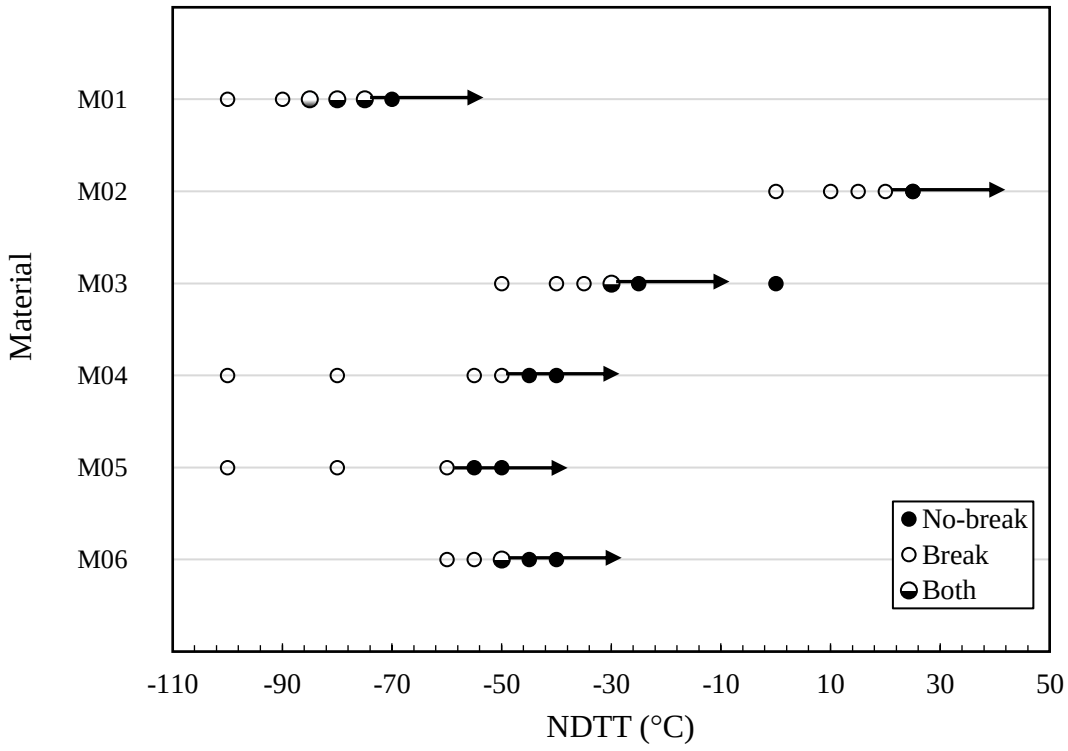

Figure 4-4: Pellini test results for each material.

Table 4-6: Summary of NDTT values determined through Pellini testing

	M01	M02	M03	M04	M05	M06
NDTT	-75˚C	20˚C	-30˚C	-50˚C	-60˚C	-50˚C

4.5.3 SEN(B) fracture toughness test results

The materials' CTOD δ_m results are summarised in Table 4-7, with an example force vs. crack tip opening (CTO) curve for each material given in Figure 4-5. The CTOD δ_m results are calculated from the CTO at which the maximum force is observed using the procedure given in BS 7448-1. This procedure involves using the area under the force/CTO curve along with the specimen dimensions and the material properties in order to calculate CTOD δ_m. It can be seen that the highest CTOD δ_m is found in material M05, followed by material M04 and then by materials M03 and M06. The lowest CTOD δ_m was found in materials M02 and then M01, which had similar results. These results are mirrored in the force/CTO traces which show the same trend of maximum CTOD δ_m for the materials. Additionally, there seems to be a correlation between high CTOD δ_m and low tensile strength. M01 and M02 had the highest UTS values and show the lowest CTOD δ_m, M03 and M06 show the mid range for both properties, and M04 and M05 show the highest CTOD δ_m and the lowest UTS results. Although their material properties have shown differences, it is noticeable that the traces for materials M04 and M05, nominally the same steel grade, overlap. This indicates that they are showing a similar response to fracture, although material M05 has the higher overall toughness. Another notable difference between these materials is the amount of force needed to reach the maximum CTO, with material M01 requiring a large force to reach a relatively low CTOD δ_m compared to material M02, which has a similar CTOD δ_m but took much less force to reach this point.

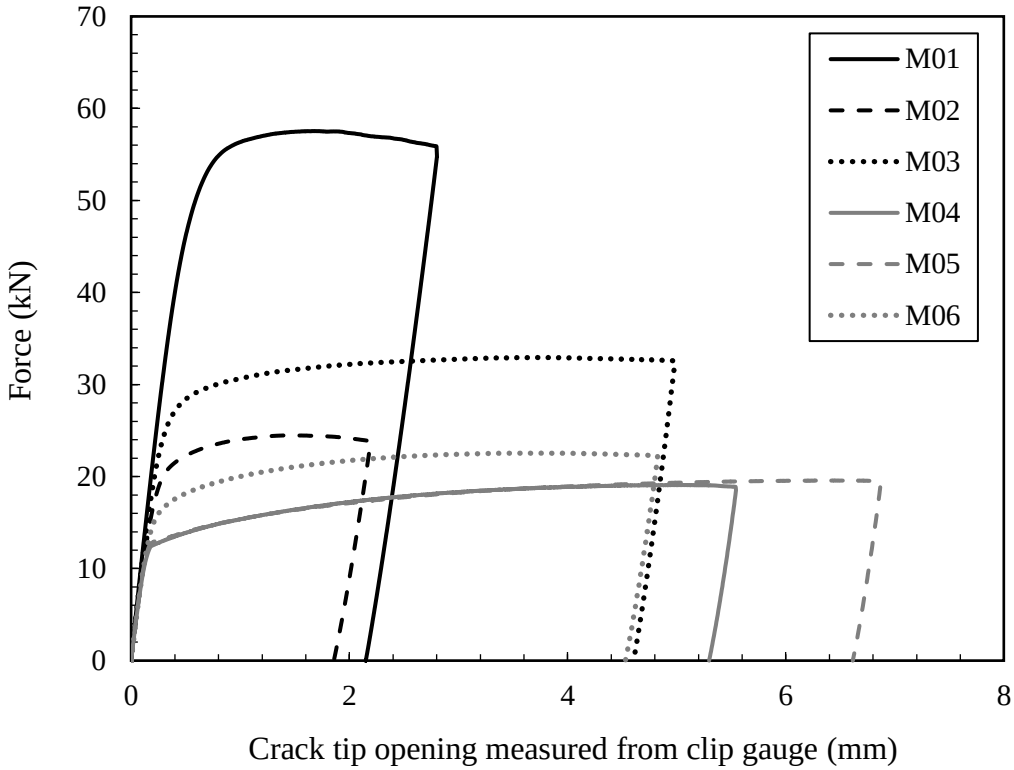

Figure 4-5: Force against CTO plots for each of the materials.

Table 4-7: Summary of results from fracture toughness testing. RT indicates room temperature.

	M01	M02	M03	M04	M05	M06
Test Temperature	RT	120˚C	RT	RT	RT	RT
Average CTOD δ_m (mm)	0.40	0.36	0.86	1.15	1.40	0.86

4.5.4 Comparison of properties between the mid-thickness and quarter-wall locations

As discussed in section 2.6.4, the properties of a steel plate are not uniform throughout its thickness, particularly if it's been rolled during manufacturing. In order to investigate this some of the test programs were carried out at both the mid-thickness and quarter-wall of the plates of EH47 shipbuilding steel. It was chosen to carry out this analysis on the EH47 shipbuilding steel as this material is of the greatest interest to the project sponsors and the plate is of a sufficient thickness for any variation to be captured. Instrumented

Charpy testing and SEN(B) fracture toughness testing was carried out at the mid-thickness and the quarter wall of the plates. Pellini testing was carried out at the mid-thickness and at the surface of the plate (denoted quarter-wall for consistency, and because this region was sampled due to the thickness of the P2 Pellini specimens used). The results, shown in Figure 4-6 and Table 4-8, indicate that there was statistically very little difference between the two locations of the plate with the exception of a slightly reduced upper shelf Charpy energy at the mid-thickness location. Any differences could be considered within the range of normal scatter. In light of this, the testing carried out in this work is deemed to yield results representative of the material properties despite being carried out at a single location. This indicates that taking the Charpy energy at the mid-thickness ensures that the Charpy toughness is measured conservatively.

Table 4-8: Comparison of key material properties between the mid-thickness and quarter-wall of M06

	Mid Thickness	Quarter Wall
CVN Upper Shelf (J)	280	295
CVN T27J (˚C)	-114	-116
NDTT (˚C)	-50	-50
Average CTOD δ_m (mm)	0.87	0.85

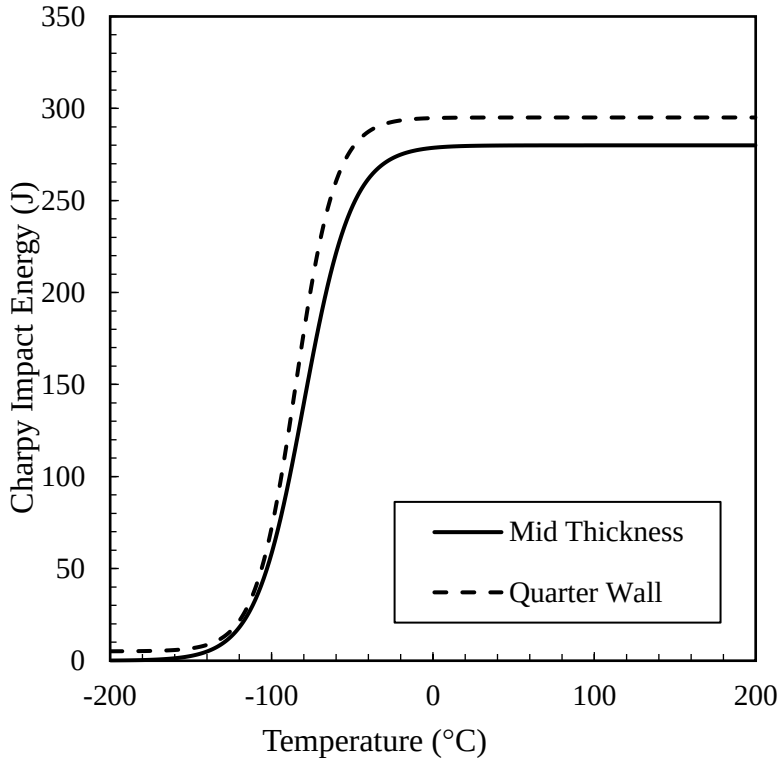

Figure 4-6: Comparison of Charpy curves between mid-thickness and quarter-wall of M06

4.6 Discussion

4.6.1 Correlation between the obtained fracture parameters

The results from fracture toughness and Charpy impact tests are presented and compared with each other in Figure 4-7, Figure 4-8 and Figure 4-9. The correlation between initiation toughness parameters, CTOD δ_m and T_{27J}, with upper shelf Charpy energy has been investigated in Figure 4-7. As seen in this figure, there is a weak linear correlation between upper shelf Charpy energy and CTOD δ_m fracture toughness, excluding M03, which has the highest Charpy energy, but the median fracture toughness compared to the other materials. But overall, the results in Figure 4-7 suggest that an increase in the upper shelf Charpy energy results in an increase in CTOD δ_m as there is a loose linear correlation between these two parameters (R^2=0.32). On the other hand, it is evident from this figure that there is no correlation between the upper shelf Charpy energy and the lower shelf temperature, T_{27J}, as the regression line between these two parameters shows almost no correlation (R^2=0.02).

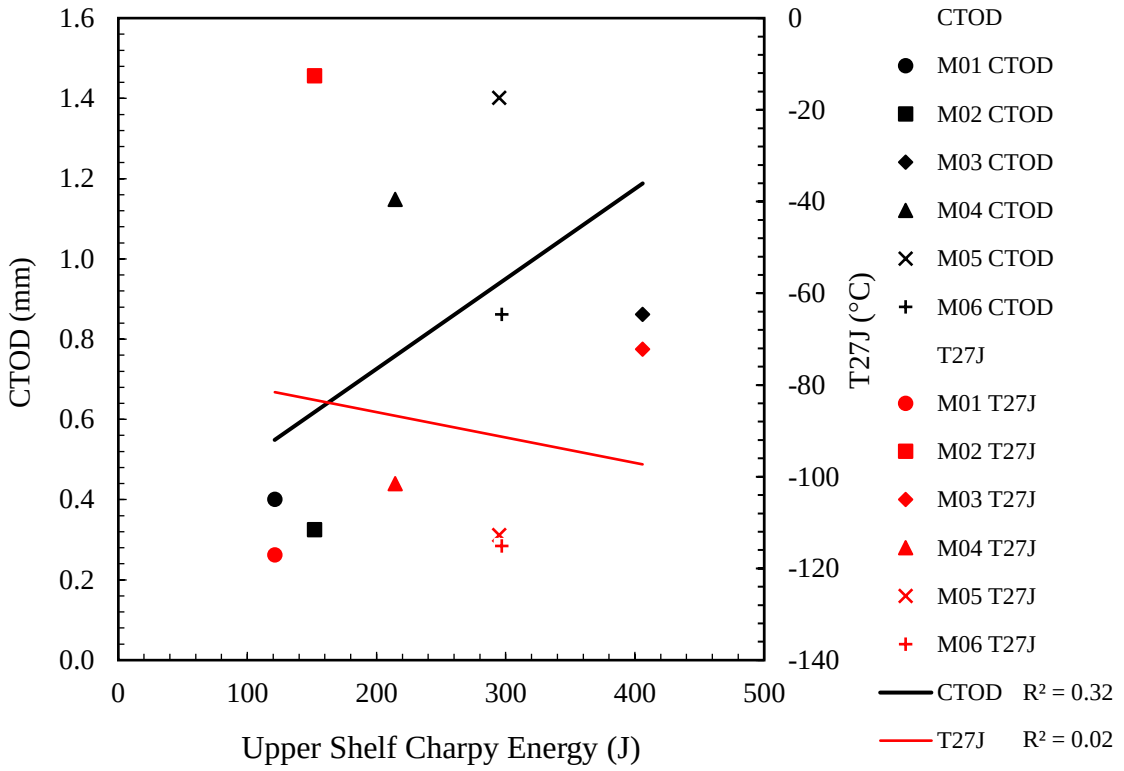

Figure 4-7: Correlation between initiation toughness parameters; CTOD δ_m and T_{27J} with upper shelf Charpy energy

The possible correlation between arrest toughness reference temperatures, T_{27J} and NDTT, with T_{4kN} has been investigated and the results are shown in Figure 4-8. It can be observed in this figure that there is a good linear correlation (R^2=0.69) between parameters indicating arrestibility, NDTT and T_{4kN}, determined through Pellini and Charpy tests. Also seen in this figure is that T_{4kN} shows a strong correlation with the onset of the lower shelf, T_{27J} (R^2=0.85). Comparing the lines of best fits to the data points in Figure 4-8 it can be seen that within the inherent experimental scatter, the slope of the line of best fit made to T_{27J} data is slightly steeper than the NDTT data, when the results are correlated with T_{4kN}.

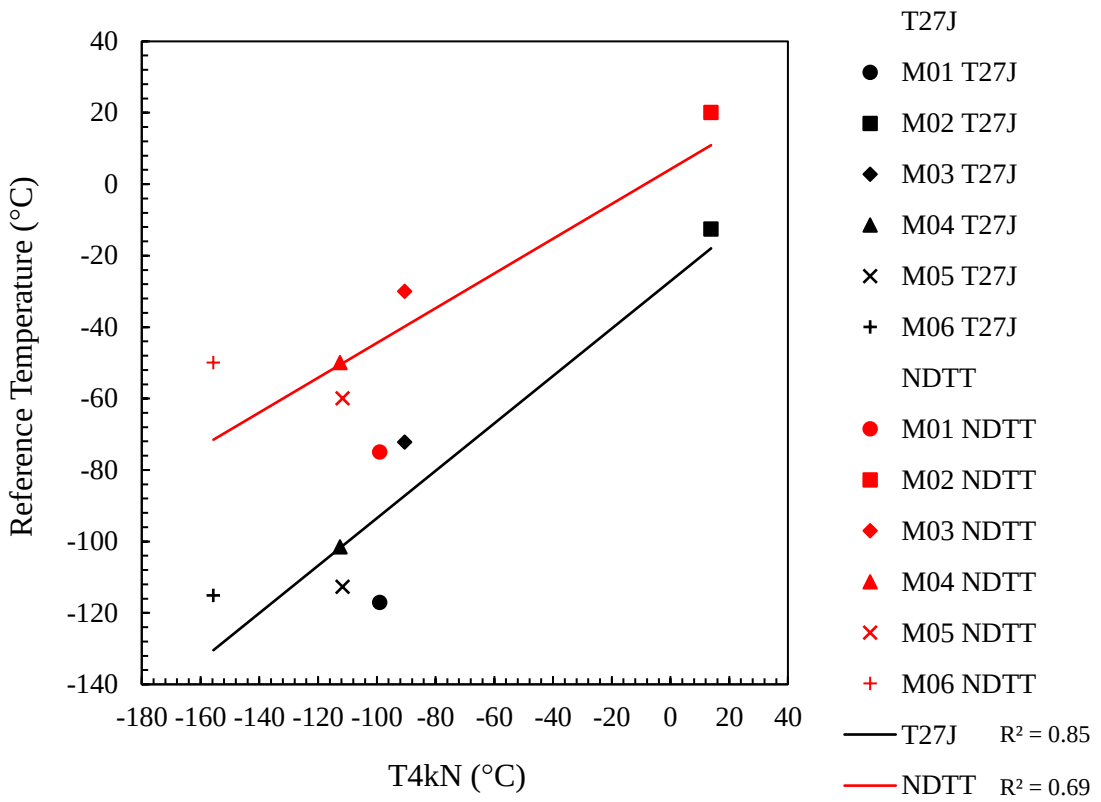

Figure 4-8: Correlation between arrest toughness reference temperatures; T_{27J} and NDTT with T_{4kN}

The CTOD δ_m and upper shelf Charpy energy results are plotted against NDTT data in Figure 4-9. As demonstrated by Figure 4-9, the arrest parameter, NDTT, does not correlate with the fracture initiation toughness parameters when the results from all six batches of steels are considered in the analysis. As an example, material M01 material has the lowest NDTT and T_{27J} of all the steels, which indicates a high arrestability. However this material has the smallest Charpy toughness of any of the materials. Although M02 has approximately the same Charpy toughness as M01, it has the highest NDTT and T_{27J} which indicates very poor arrestibility. This example shows how concerning it is that modern steels can be judged based on their Charpy toughness (which is measured on the upper shelf) although this may not indicate their arrest properties.

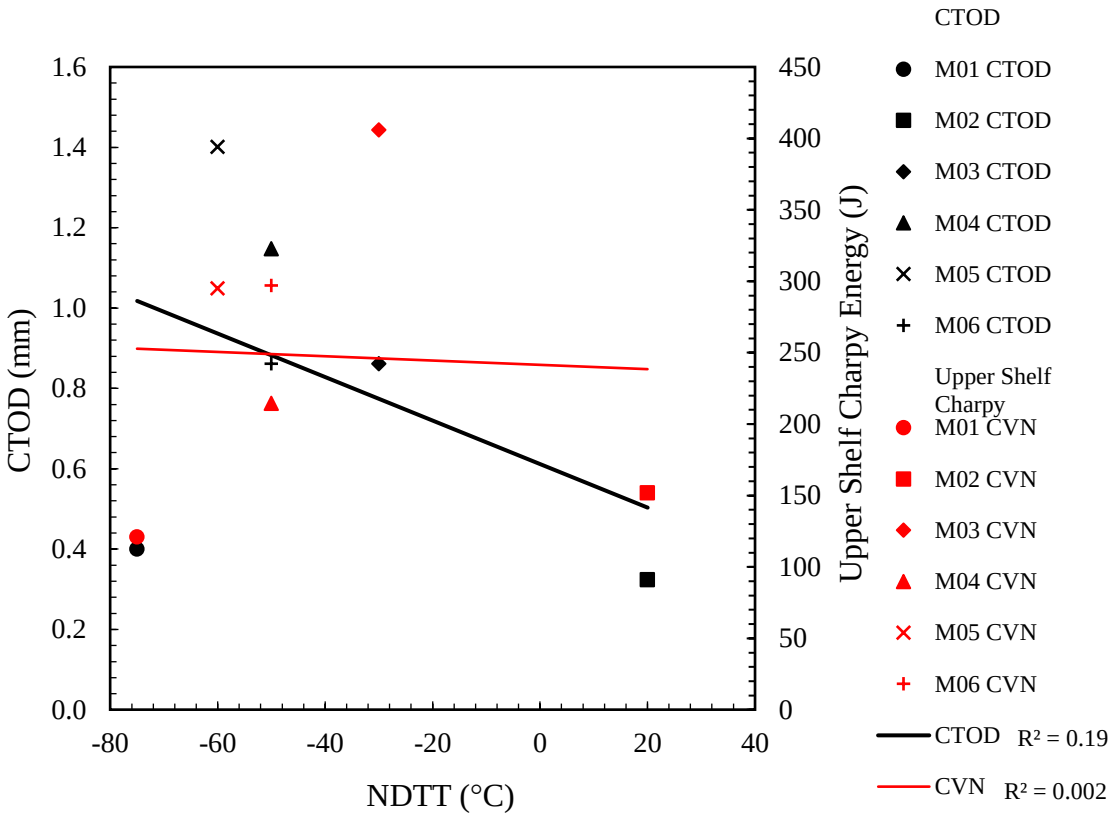

Figure 4-9: Correlation between fracture initiation toughness and crack arrest toughness parameters; CTOD δ_m and upper shelf Charpy energy with NDTT

Since brittle crack arrest properties are heavily dominated by the lower transition region and lower shelf, it is important to investigate these parameters further. Figure 4-10 and Figure 4-11 relate the NDTT to each material's ductile to brittle transition curve. As the NDTT defines the onset of brittle behaviour, it would be expected to lie close to the T_{27J} temperature at the onset of the lower shelf of the Charpy curve. However, the NDTT for each material is located on the upper transition or upper shelf of the Charpy transition curve, except for material M02 which shows the expected behaviour. In spite of this, the NDTT can be strongly correlated (R^2=0.95) against T_{27J}, i.e. as expected, the temperature at the onset of the lower shelf correlates strongly with that of the onset of brittle behaviour. Although this correlation was expected, it holds even for the materials which had their NDTT lie on the upper shelf or transition region of the Charpy curve. However, this correlation is much weaker when the NDTT is correlated against the temperature of the upper shelf., which is probably because the transition region for some of these materials is shallow and for others it is steep. There are concerns with the NDTT of some materials

lying on the upper shelf of the Charpy curve because these materials are at a risk of behaving in a brittle manner at a higher temperature than is predicted from the Charpy transition curve. This is a concern because it means that a running brittle crack would not be arrested if it initiated, for example through accidental damage.

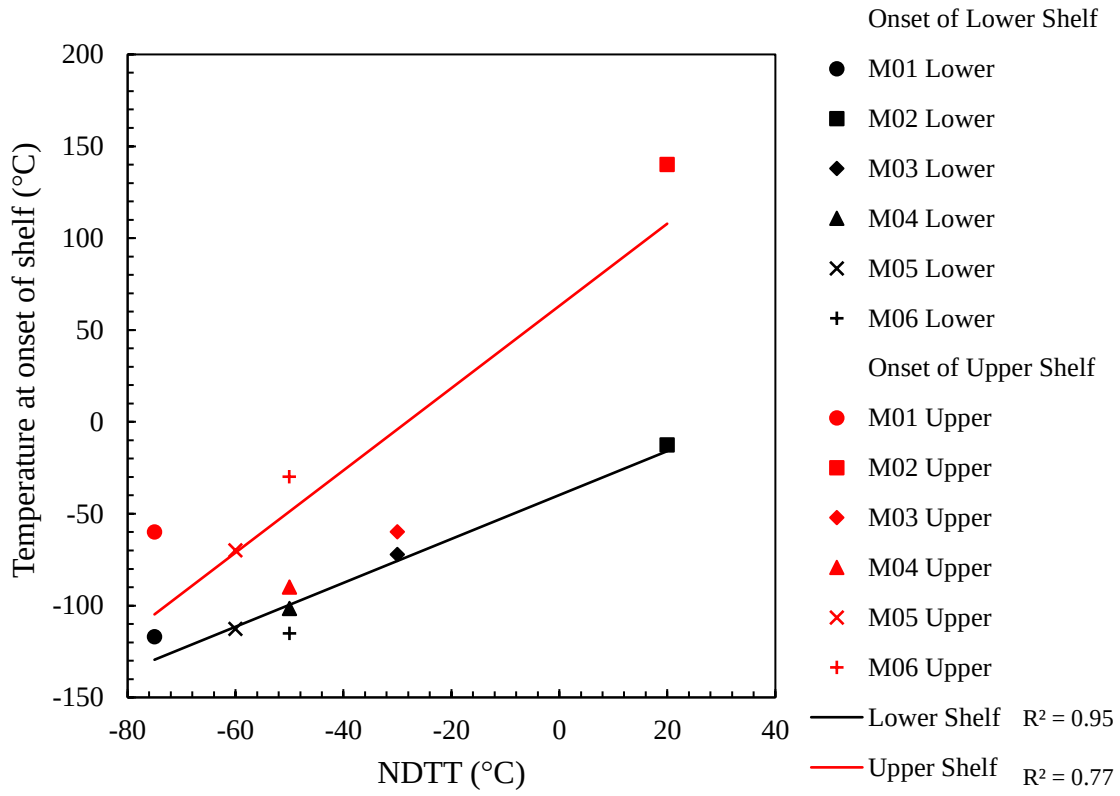

Figure 4-10: Correlation between arrest toughness parameter NDTT and transition temperatures for both the upper and lower shelf of the Charpy transition curve

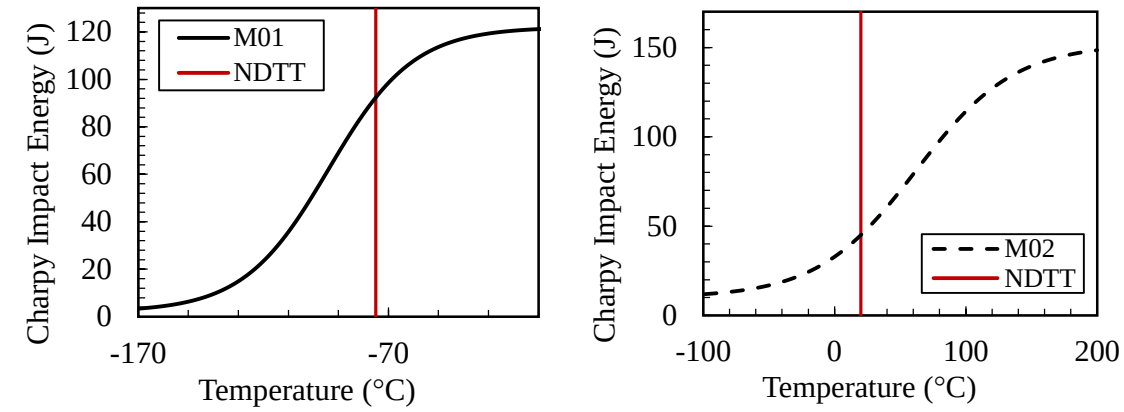

(a)

(b)

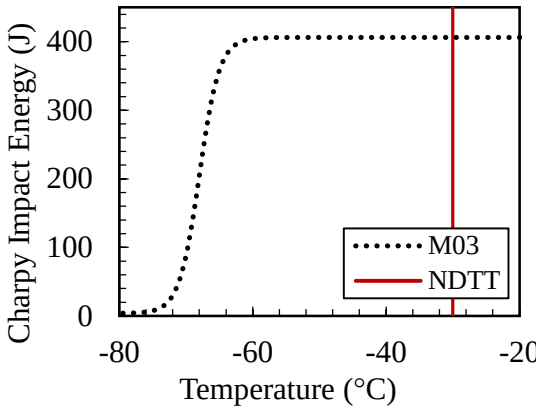

(c)

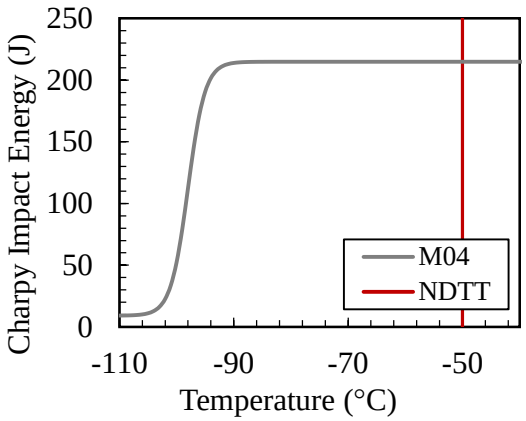

(d)

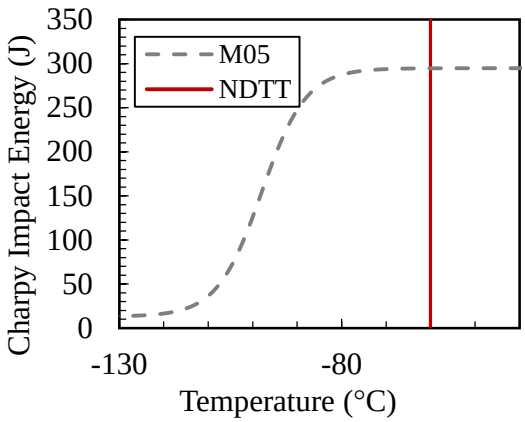

(e)

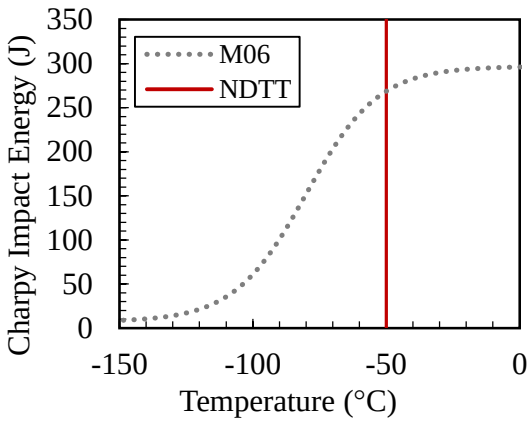

(f)

Figure 4-11: The location of the NDTT on the Charpy transition curve for (a) M01, (b) M02, (c) M03, (d) M04, (e) M05, and (f) M06 steels

4.6.2 Correlation between mechanical properties and microstructure

The small-scale mechanical properties of the steels are compared to a comprehensive microstructural analysis which is presented in chapter 3. The steels examined in this study all have small grain sizes, which makes it more complex to correlate the mechanical properties against the microstructural characteristics due to the cluster of grain size values giving high uncertainty. Figure 4-12 shows that the average grain size correlates loosely against the upper shelf Charpy energy, and very weakly against the CTOD δ_m fracture toughness. It is well-accepted that grain refinement provides improved tensile properties and initiation fracture toughness for steels and this is likely to be the reason why these steels are designed to have very fine grain sizes on average. Although only a weak correlation, this observation is consistent with the results presented in the open literature by other researchers[56–58].

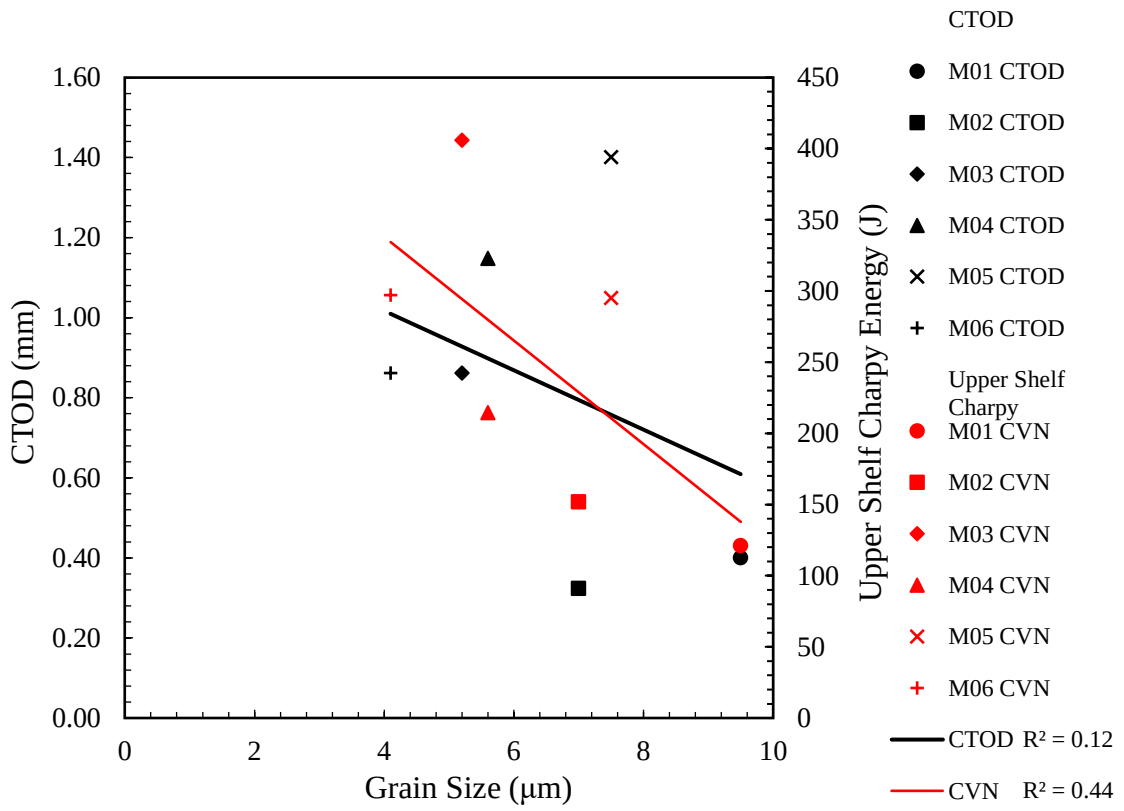

Figure 4-12: Correlation between grain size and initiation toughness parameters; CTOD δ_m and upper shelf Charpy energy

The grain size and aspect ratio are plotted against NDTT in Figure 4-13. It can be seen in this figure that no strong correlations can be made between the average grain size or aspect ratio of grain sizes and the material's arrest properties when all six batches of steels are considered in the analysis. However, by excluding the largest value of NDTT, which is associated with material M02, the overall trends indicate an increase in NDTT with a reduction in grain size and aspect ratio with the average grain size having a more pronounced effect (i.e. steeper trend) on the NDTT results. This would mean that a smaller grain size gives poorer brittle crack arrest properties than a larger grain size, which contradicts the observations seen on the relationship between grain size and initiation toughness. This is in agreement with recent results from other researchers[9]. Additionally, the grain aspect ratio does not seem to affect the arrest parameter NDTT significantly.

The influence of texture in terms of texture index (see section 3.3.2) on key fracture-related properties can be seen in Figure 4-14 (NDTT), Figure 4-15 (CVN), and Figure 4-16 (CTOD). In all cases there is very little correlation between either measure of texture and the key fracture properties. This implies that the texture in the materials is not strongly contributing to its ability to prevent fracture initiation or propagation. The microstructural texture has not been shown to be a factor in the crack arrest behaviour on its own, and other factors such as composition, inclusion size and distribution, plate centreline and surface microstructures, might also be influential.

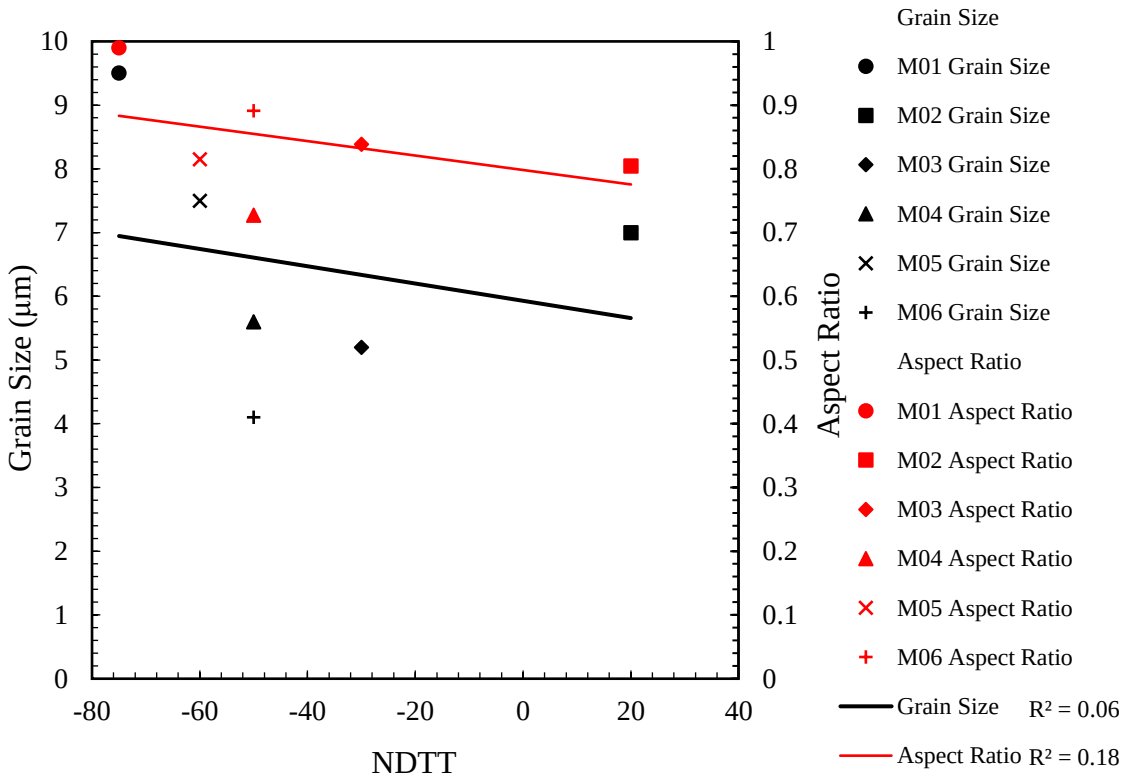

Figure 4-13: Correlation between arrest toughness parameters and microstructural characteristics; average grain size and grain aspect ratio with NDTT

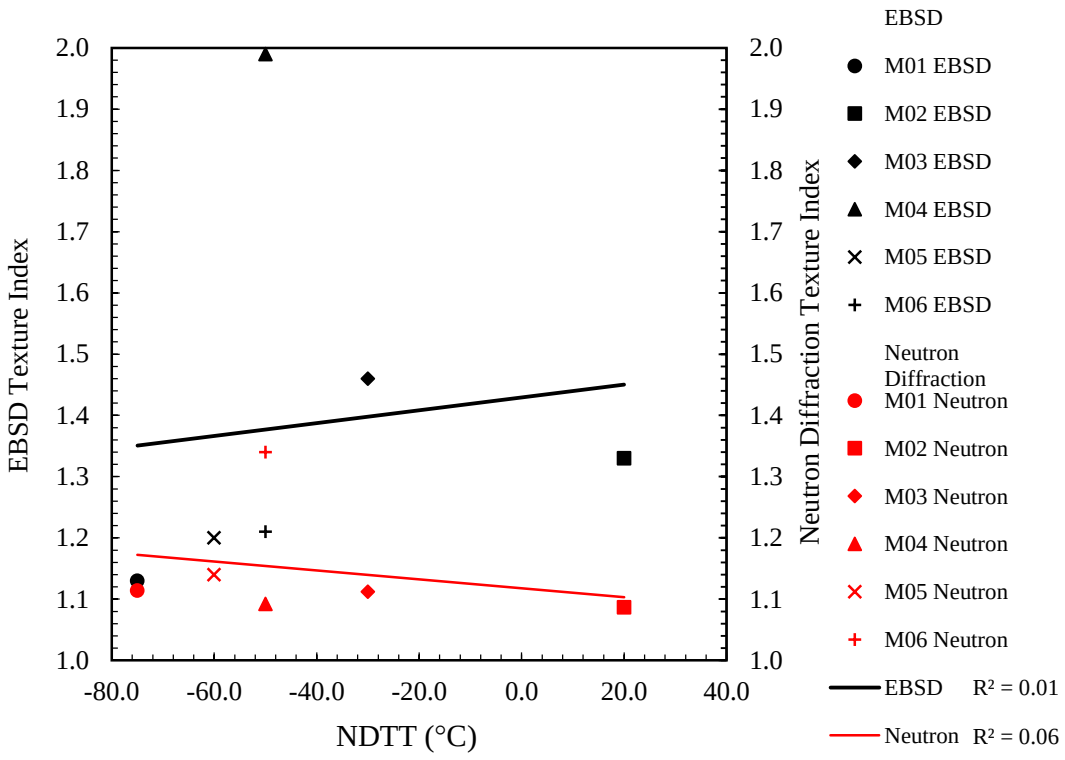

Figure 4-14: correlation between NDTT for each material and its texture indices.

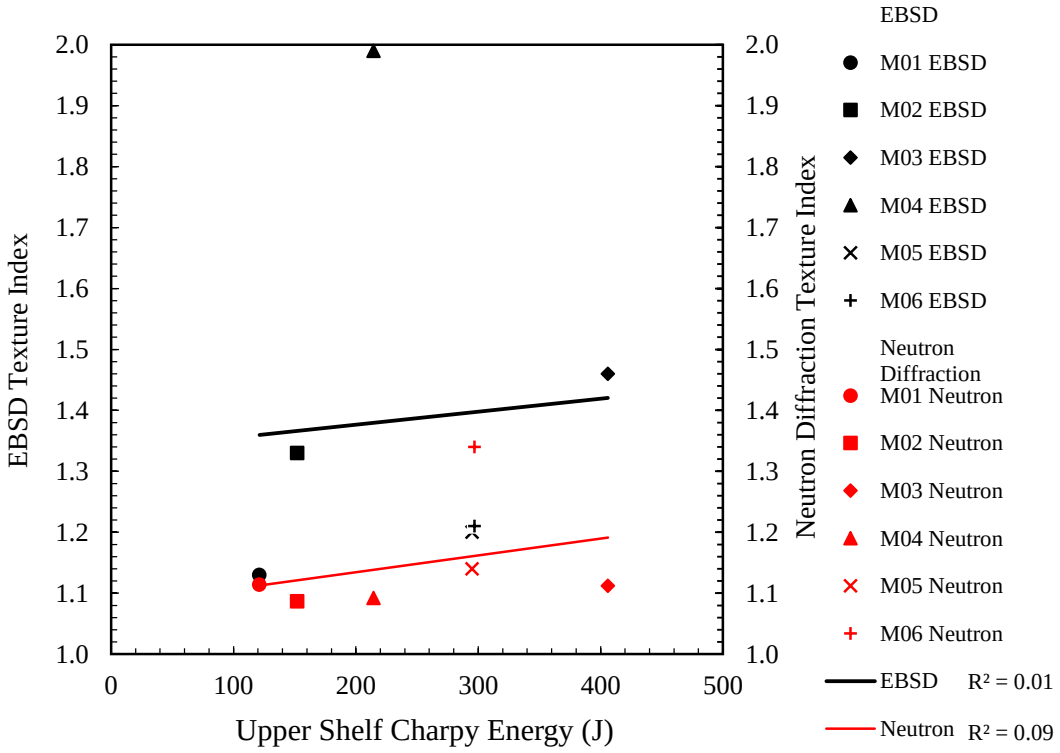

Figure 4-15: Correlation between upper shelf Charpy energy and texture indices.

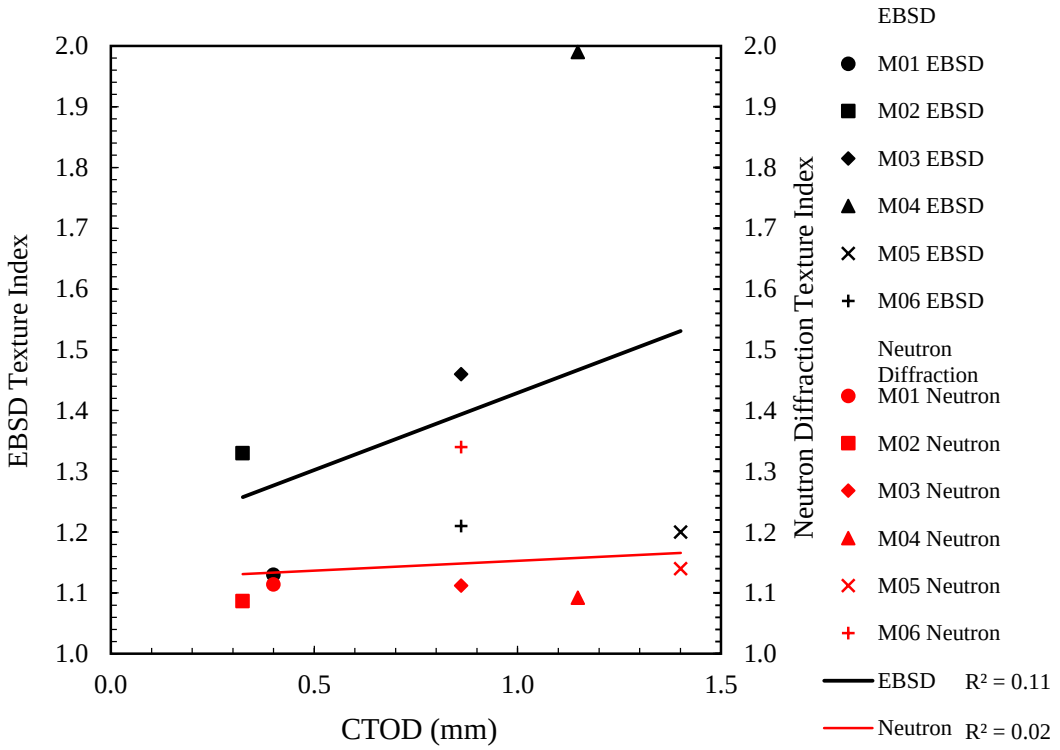

Figure 4-16: correlation between CTOD fracture toughness and texture indices.

4.6.3 Comparison of the experimental results with empirical predictions

The relationship between NDTT and T_{27J} shown in Figure 4-10 is not 1:1, which means that Equations 4-1 to 4-3 cannot be considered valid for modern steels, and using these equations results in over-predicting the NDTT in almost every case, which is shown in Figure 4-17. For the materials studied here, there is an offset between the NDTT and T_{27J} of approximately 40°C ± 10°C, which is similar to Equation 4-4 and the offset between the NDTT and CAT. It is recommended that the CAT is measured through large-scale crack arrest testing to determine the validity of these predictions, but it can be seen that the reference temperatures do indeed show strong agreement with each other. It is recommended to carry out Pellini tests to determine the NDTT of the material rather than relying on Charpy data.

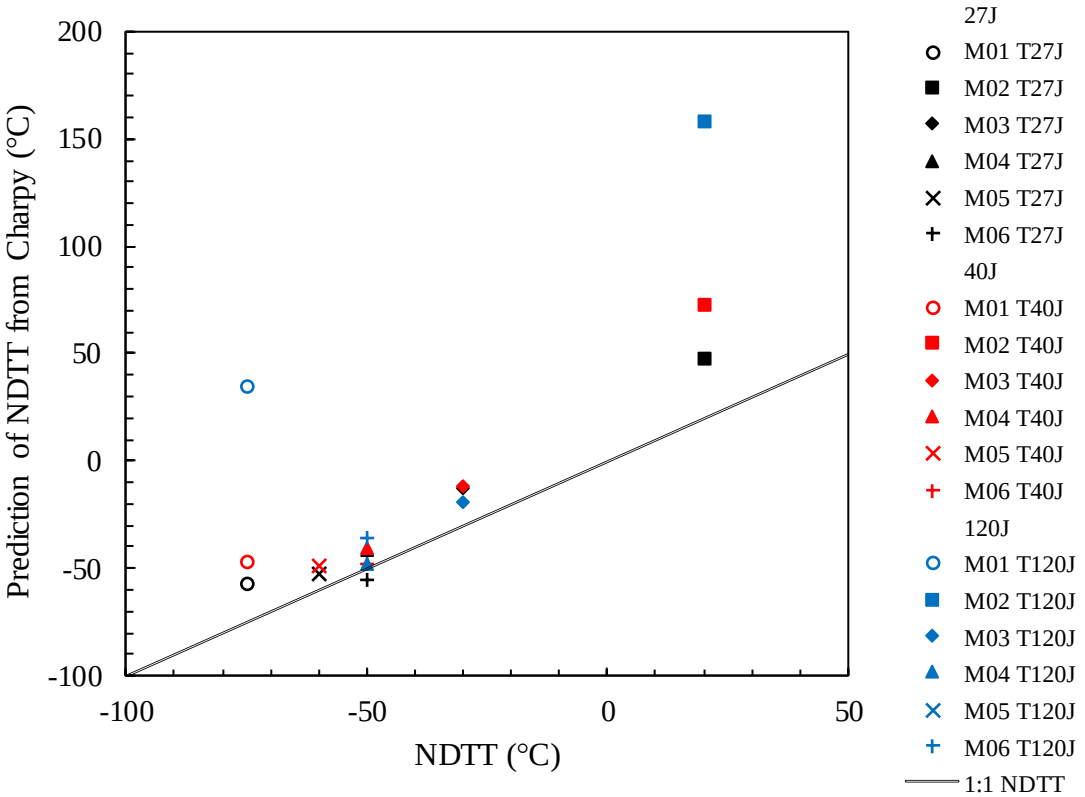

Figure 4-17: Prediction of NDTT from Charpy reference temperatures

The master curve method given in Equation 4-7 to Equation 4-10 gives the predicted lower bound toughness shown in Figure 4-18 using M06 as an example. In order to give an indication of the accuracy on these relationships, additional SEN(B) tests were carried out at low temperature between -50 °C and -120 °C and the results are in good agreement with the K_{IC} prediction from the master curve (MC) approach at low temperatures. The points listed as "K, MC" were measured using standard small-scale master curve specimens following ASTM 1921[59] with a concentration around T_0, the 100 MPam^{½} measurement. This shows strong agreement close to and below the 100 MPam^{½} mark, until the lower transition region. However, as expected, the agreement is limited to the lower end of the transition region and agreement is poor at -50 °C. Furthermore, the master curve predicted from small scale specimens, $K_{JC(median)}$, agrees well with the full-thickness SEN(B) results close to the 100 MPam^{½} value. A more conservative prediction of K_{IC} is given by the prediction from NDTT, which indicates that the NDTT gives a conservative prediction of the materials' toughness. The small-scale master curve results, "K, MC" indicate the scatter in toughness measured at a single temperature. At -85°C, which was indicated to be T_0 from the multiple-temperature approach, the toughness was measured in a wide range between 79 MPam^{½} and 110 MPam^{½}, with an average of 98 MPam^{½}.

These results are compared against the K_{Ia} results in chapter 5, where large-scale testing results are presented for further comparison. For brevity, master curves for other materials are not shown here but can be found in Appendix B. Generally, for the other materials, K_{Ia} prediction from NDTT gave the most conservative toughness estimate. Low temperature SEN(B) fracture toughness tests on materials M01 and M02 show a similar trend of good agreement on the lower shelf and lower transition, and poor agreement in the upper transition region. This is a limiting factor on the use of these predictions at ambient temperatures.

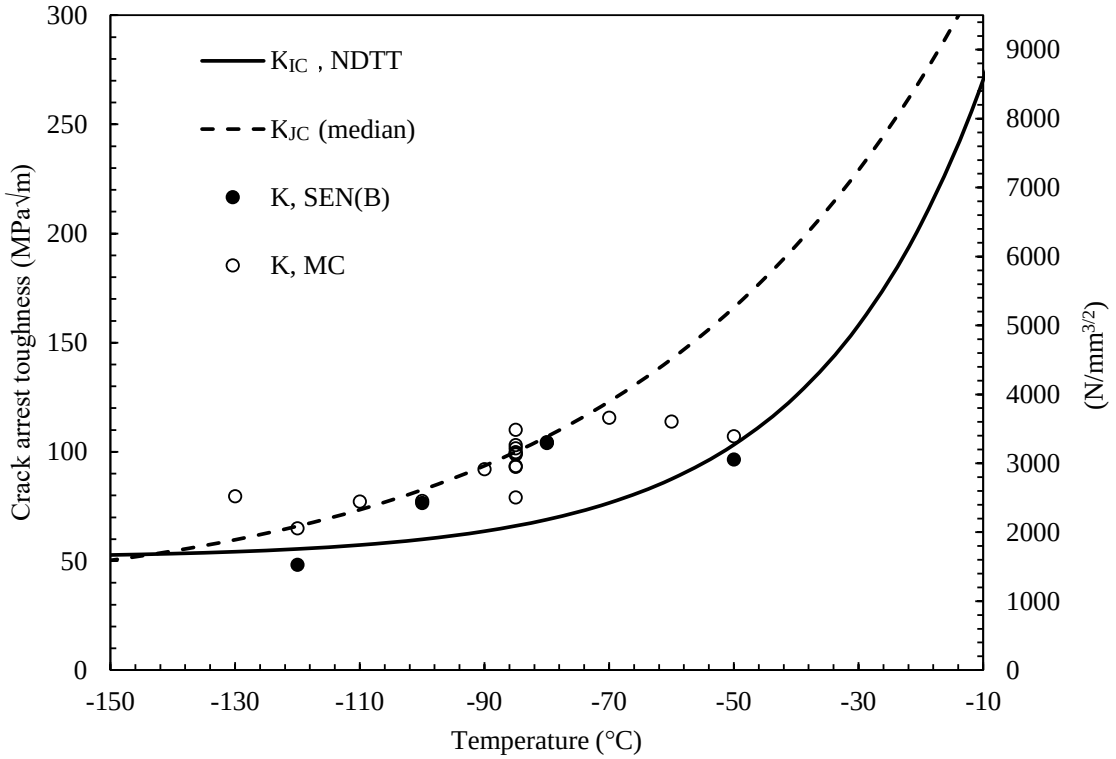

Figure 4-18: Master curve predictions of toughness at a range of temperatures for M06.

4.7 Conclusions

In this work, a wide range of mechanical testing was carried out on 6 different batches of structural steels to investigate the relationship between mechanical properties and microstructure with respect to fracture initiation and brittle crack arrest. The following key conclusions have been drawn from the present study:

- Improved fracture initiation behaviour of a steel (i.e. high CTOD δ_m and upper shelf Charpy toughness) correlates with a smaller average grain size, but improved crack arrest behaviour does not.
- There was a low correlation between microstructural measures of texture and macroscopic fracture parameters of the steels, indicating that the texture does not play a large role in fracture initiation and arrest.
- High CTOD δ_m fracture toughness or upper shelf Charpy energy does not indicate whether a material is protected from unstable brittle fracture because this is independent from high crack arrest toughness.

- For modern steels, the criteria that result in good crack arrest properties are not the same as those which result in a high upper shelf initiation fracture toughness. Therefore, it is suggested to avoid using upper shelf fracture toughness parameters such as CTOD δ_m and Charpy energy to indicate crack arrestibility of modern steels due to poor correlation.
- The crack arrestibility of a material is most strongly correlated with reference temperatures based on the onset of brittle behaviour (such as T_{27J} and T_{4kN} from Charpy tests or NDTT from drop weight Pellini tests) – even for a steel where the NDTT is located at a temperature on the upper shelf of the Charpy transition curve.
- It is recommended to characterise the crack arrest properties of steels using lower shelf parameters such as drop weight Pellini or Charpy impact testing to determine NDTT, T_{4kN}, or T_{27J}.

References

1. Anderson TL. *Fracture Mechanics: Fundamentals and Applications*. Vol 58.; 2017. doi:10.1016/j.jmps.2010.02.008

2. (DNV) Det Norske Veritas. Fatigue Design of Offshore Steel Structures. *Recomm Pract DNV-RPC203*. Published online 2005.

3. Hirdaris SE, Bai W, Dessi D, et al. Loads for use in the design of ships and offshore structures. *Ocean Eng*. Published online 2014. doi:10.1016/j.oceaneng.2013.09.012

4. BS-7910. Guide to methods for assessing the acceptability of flaws in metallic structures. *BSI Stand Publ*. Published online 2013. doi:10.1007/s13398-014-0173-7.2

5. Wiesner C, Hayes B. *A Review of Crack Arrest Tests, Models and Applications*.; 1995.

6. Graville A. *Stress Analysis of Short Crack Arrest Test Report P244/1, Graville Associates Inc.*

7. Moore P, Duncan G, Singh N, Bakthavathsalam B. Comparing Small-Scale Testing Approaches to Determine Crack Arrest in High Strength Steel. In: *Proceedings Structural Integrity 2018*. ; 2018.

8. Völling A, Kalwa C, Erdelen-peppler M. The misconception of employing cvn toughness as key-measure in ductile crack arrest prediction for modern line-pipe steels. In: *Proceedings of the 2014 10th International Pipeline Conference IPC2014*. ; 2014.

9. Yanagimoto F, Hemmi T, Suzuki Y, Takashima Y, Kawabata T, Shibanuma K. Contribution of grain size to resistance against cleavage crack propagation in ferritic steel. *Acta Mater*. 2019;177:96-106. doi:10.1016/j.actamat.2019.06.038

10. Burdekin M, Zhao W, Tkach Y, Wiesner C, W Xu. *The Effects of Dynamic Loading on Structural Integrity Assessments*.; 2004.

11. Handa T, Tagawa T, Minami F. Correlation between charpy transition temperature

and brittle crack arrest temperature considering texture. *Tetsu-To-Hagane/Journal Iron Steel Inst Japan*. 2012;98(1):32-38. doi:10.2355/tetsutohagane.98.32

12. Handa T, Igi S, Oi K, et al. Effect of toughness distribution in the thickness direction on long brittle crack propagation/arrest behaviour of heavy gauge shipbuilding steel. *Weld Int*. 2018;32(7):460-468. doi:10.1080/01431161.2017.1346884

13. Kobayashi T. Dynamic photoelastic determination of the a(dot)-K relation for 4340 alloy steel. In: *Hahn GT, Kanninen MF, Editors. Crack Arrest Methodology and Applications. ASTM STP 711. American Society for Testing and Materials;*. ; 1980:189–210.

14. Kalthoff J. Experimental analysis of dynamic effects in different crack arrest test specimens. In: : *: Hahn GT, Kanninen MF, Editors. Crack Arrest Methodology and Applications. ASTM STP 711. American Society for Testing and Materials;*. ; 1980:109–27.

15. Joyce JA, Link RE, Roe C, Sobotka JC. Dynamic and static characterization of compact crack arrest tests of navy and nuclear steels. *Eng Fract Mech*. 2010;77(2):337-347. doi:10.1016/j.engfracmech.2009.04.006

16. ASTM. E1221 Standard Test Method for Determining Plane-Strain Crack-Arrest Fracture Toughness, K Ia, of Ferritic Steels. 2007;96(Reapproved):1-19. doi:10.1520/E1221-12A.2

17. ASTM. E208 Standard Test Method for Conducting Drop-Weight Test to Determine Nil-Ductility Transition Temperature of Ferritic Steels 1. *Test*. 2000;06(Reapproved):1-13. doi:10.1520/E0208-06R12.2

18. Pb C, Ej R. Comparison of Crack Arrest Methodologies. Published online 1980:211-227.

19. EDF Energy UK. *R6. Assessment of the Integrity of Structures Containing Defects.*; 2006.

20. Green G, Knott JF. On effects of thickness on ductile crack growth in mild steel. *J*

Mech Phys Solids. 1975;23(3). doi:10.1016/0022-5096(75)90014-9

21. Handa T, Igi S, Oi K, Nishimura K, Tajika H, Tagawa T. Effect of Toughness Distribution in the Thickness Direction on Long Brittle Crack Propagation / Arrest Behavior of Heavy Gauge Shipbuilding Steel Brittle Crack Arrestability of Test Steels Arrestability of Test Steels under Condition of No. Published online 2016:126-131.

22. Sugimoto K. Thickness effect on brittle crack arrest toughness value (Kca)-6. In: *ISOPE - 20th International Offshore and Polar Engineering Conference*. ; 2010.

23. Wallin K. The size effect in KIC results. *Eng Fract Mech*. 1985;22(1):149-163. doi:10.1016/0013-7944(85)90167-5

24. Marschall R. Specimen-Size Considerations in Crack-Arrest Testing of Irradiated RPV Steels. Published online 1986:339-352.

25. Society JWE. *JWES 2815:2014 Test Method for Brittle Crack Arrest Toughness Kca*.; 2014.

26. E1921-15ae1. Standard Test Method for Determination of Reference Temperature , To , for Ferritic Steels in the Transition Range. In: *ASTM Book of Standards*. ; 2016:1-23. doi:10.1520/E1921-15AE01.2

27. Zhu XK, Joyce JA. Review of fracture toughness (G, K, J, CTOD, CTOA) testing and standardization. *Eng Fract Mech*. 2012;85:1-46. doi:10.1016/j.engfracmech.2012.02.001

28. Funatsu Y, Shirahata H, Otani J, Inoue T, Hashiba Y. The Effect of Shear-lips on the Arrestability of Thicker Steel Plates Longitudinal. *Isope*. 2012;4:63-66.

29. Crosley PB. WELDING RESEARCH Crack Arrest Fracture Toughness of a Structural Steel (A36). Published online 1982.

30. Wiesner CS. Predicting structural crack arrest behaviour using small scale material characterisation tests. *Int, J Pres Ves Pip*. Published online 1995.

31. Willoughby A. Crack arrest concept. *Proc Semin Eng Per- formance Welded Joints*. Published online 1986.

32. Hahn G. Crack Arrest Methodology and Applications. *Am Soc Test Mater*. Published online 1980.

33. Pellini W, Puzak P. Fracture analysis diagram procedures for the fracture-safe engineering design of steel structures. *Weld Res Counc Bull*. 1963;88.

34. Robertson T. Propagation of brittle fracture in steel. *J Iron Steel Inst*. 1953;175.

35. Institution BS. *BS18:1987: Method for Tensile Testing of Metals.*; 1987.

36. Institution BS. *BS EN10045:1990: Charpy Impact Test on Metallic Materials.*; 1990.

37. Materials AS for T and. *ASTM E436-86: Standard Method for Drop Weight Tear Tests of Ferritic Steels.*; 1986.

38. Wiesner CS, Hayes B, Willoughby AA. Crack Arrest in Modern Steels and their Weldments Comparison between Small and Large Scale Experiments. 1993;56:369-385.

39. Avenue K, Kt S, Berkeley C, Laboratories N, Gli G. R6. Assessment of the Integrity of Structures Containing Defects. *Construction*. 1988;32:3-104.

40. Puzak P, Eschbacher E, Pellini W. Initiation and Propagation of Brittle Fracture in Structural Steels. *Weld J*. 1952;31(12):561-581.

41. Kirk MT, Natishan ME, Wagenhofer M, et al. A Summary of Wallin ' s Empirical Findings. Published online 2002:729-740.

42. Link RE, Joyce JA, Roe C. Crack arrest testing of high strength structural steels for naval applications q. *Eng Fract Mech*. 2009;76(3):402-418. doi:10.1016/j.engfracmech.2008.11.006

43. Toon: KK. Fracture Toughness Data Analysis Using the Master Curve Method. *WRC Bull 486 Part 3, Nov 2003*. Published online 2003.

44. Pugh CE, Corwin WR, S RHBRYANBRBAS. C.e. pugh, w.r. corwin, r.h. *Nucl Eng Des*. 1986;96:297-312.

45. Wallin K, Karjalainen-roikonen P. Crack Arrest Toughness Estimation for High

Strength Steels from Sub-Sized Instrumented Charpy-V Tests. *Proc Twenty-sixth Int Ocean Polar Eng Conf*. Published online 2016:85-91.

46. ISO. ISO 148-1:2006: Metallic materials -- Charpy pendulum impact test -- Part 1: Test method. *ISO*. Published online 2006.

47. ISO. *BS EN ISO 6892-1:2016 BSI Tensile Testing Part 1 : Method of Test at Room Temperature*.; 2016.

48. BSI. *BS EN 10164:2004 Steel Products with Improved Deformation Properties Perpendicular to the Surface of the Product — Technical Delivery Conditions*.; 2004.

49. Yamamoto Y. Multiscale modeling to clarify the relationship between microstructures of steel and macroscopic brittle crack microstructures of steel and macroscopic brittle crack propagation / arrest behavior modeling of a high. *Procedia Struct Integr*. 2016;2:2389-2396. doi:10.1016/j.prostr.2016.06.299

50. JFE Steel. Product: Crack Arrest Steel Plate. https://www.jfe-steel.co.jp. Published 2020. Accessed April 15, 2020. https://www.jfe-steel.co.jp/en/products/plate/b02.html

51. ISO. BS7448-1: Fracture mechanics toughness tests. *BS EN*. 1991;(November).

52. Mehmanparast A, Taylor J, Brennan F. Experimental investigation of mechanical and fracture properties of offshore wind monopile weldments : SLIC interlaboratory test results. *Fatigue Fract Eng Mater Struct*. 2018;(April):1-17. doi:10.1111/ffe.12850

53. Ingelbrecht CD, Loveday M. *The Certification of Ambient Temperature Tensile Properties of a Reference Material for Tensile Testing According to EN 10002-1, CRM661*.; 2000.

54. Lord JD, Roebuck B, Orkney L. *Validation of a Draft Tensile Testing Standard for Discontinuously Reinforced MMC. VAMAS Report No.20*.; 1995.

55. British Standards Institution. *EN 1011-2, "Welding - Recommendations for Welding of Metallic Materials - Part 2: Arc Welding of Ferritic Steels."*; 2001.

56. Wang C, Wang M, Shi J, Hui W, Dong H. Effect of microstructural refinement on the toughness of low carbon martensitic steel. *Scr Mater*. Published online 2008. doi:10.1016/j.scriptamat.2007.10.053

57. Hyzak JM, Bernstein IM. The role of microstructure on the strength and toughness of fully pearlitic steels. *Metall Trans A*. Published online 1976. doi:10.1007/BF02656606

58. Curry DA, Knott JF. The relationship between fracture toughness and microstructure in the cleavage fracture of mild steel. *Met Sci*. Published online 1976. doi:10.1179/030634576790431453

59. ASTM. ASTM 1921: Standard Test Method for Determination of Reference Temperature , To , for Ferritic Steels in the Transition Range. *Annu B ASTM Stand*. Published online 2005:1-20. doi:10.1520/E1921-19B.2

Appendix A – Specimen extraction plan

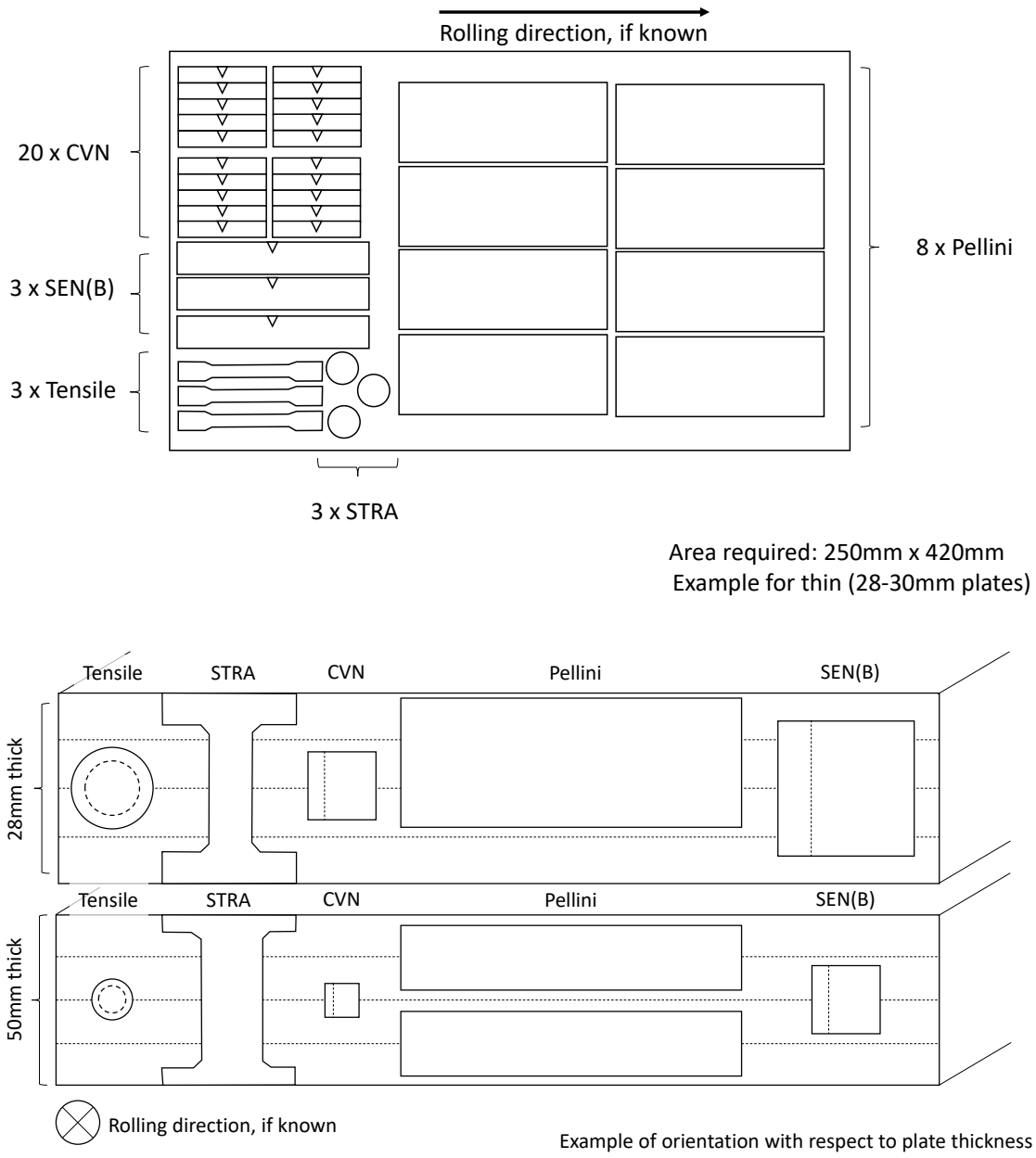

Figure 4-19: Sectioning plan to show the specimen orientations with respect to rolling direction and plate thickness for a thin plate (28mm) and thick plate (over 50mm).

Appendix B – Master curves for all materials

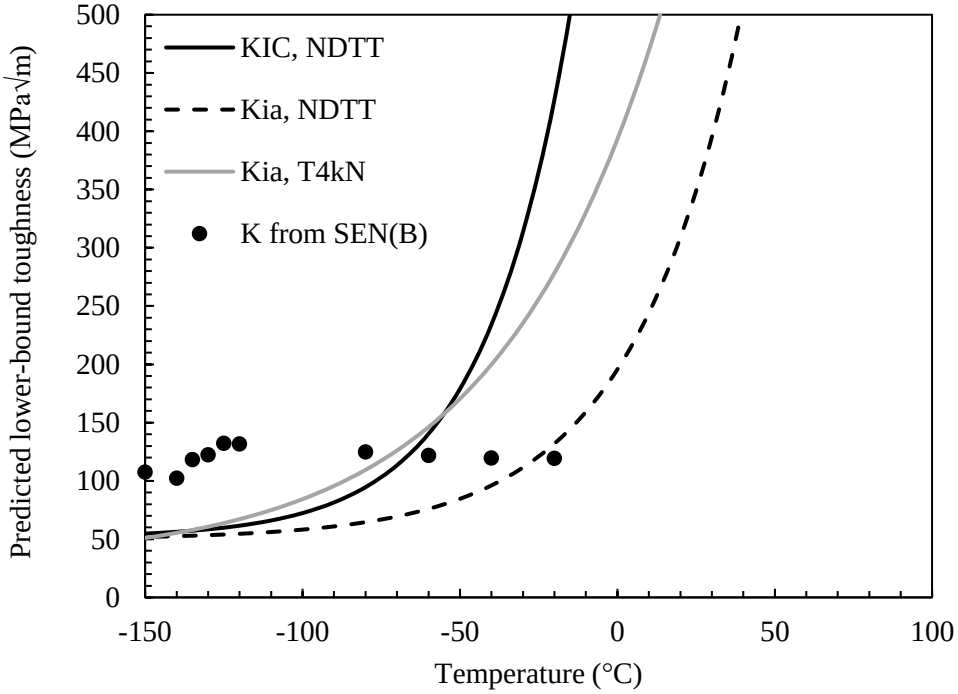

Figure 4-20: Master curves for material M01

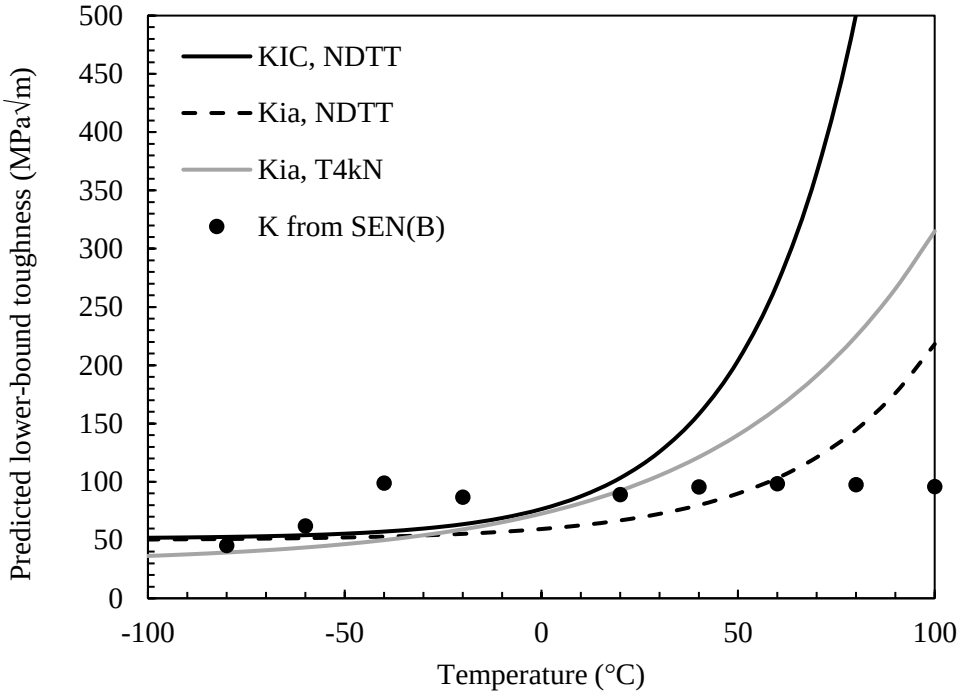

Figure 4-21: Master curves for material M02

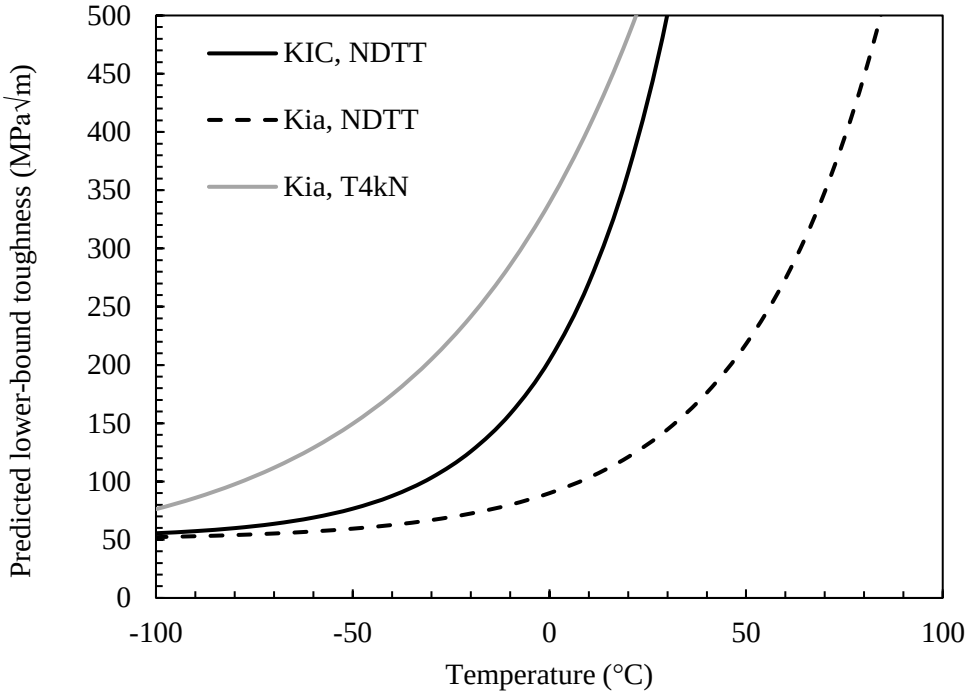

Figure 4-22: Master curves for material M03

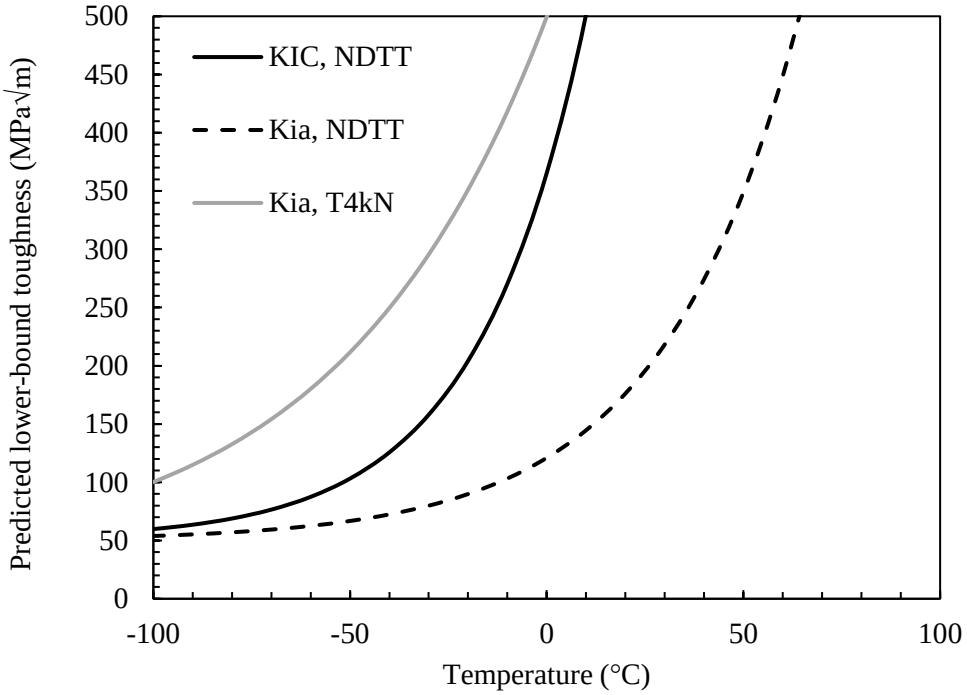

Figure 4-23: Master curves for material M04

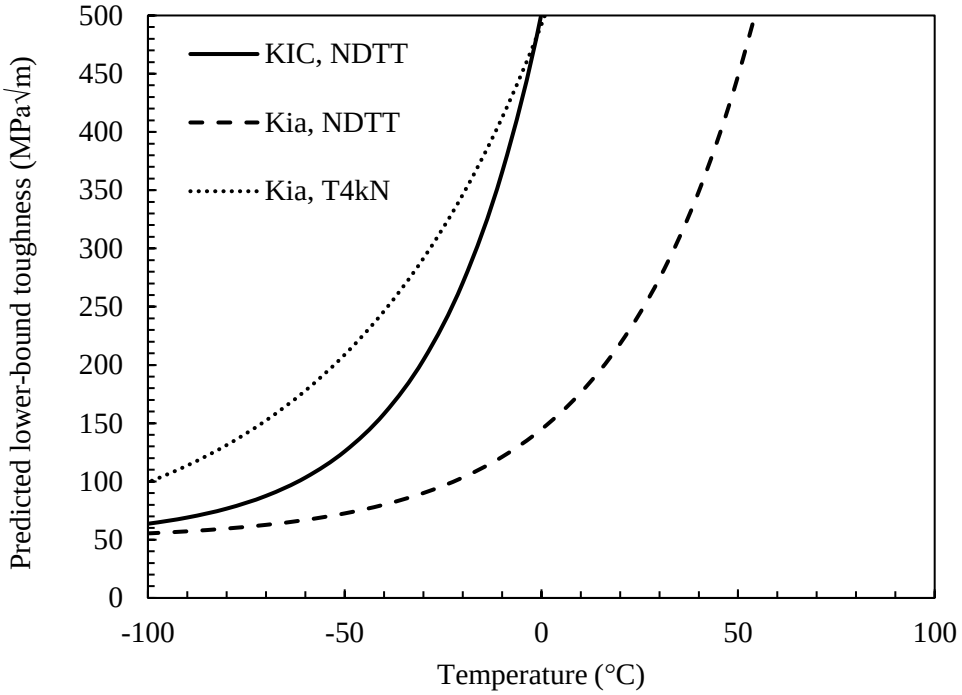

Figure 4-24: Master curves for material M05

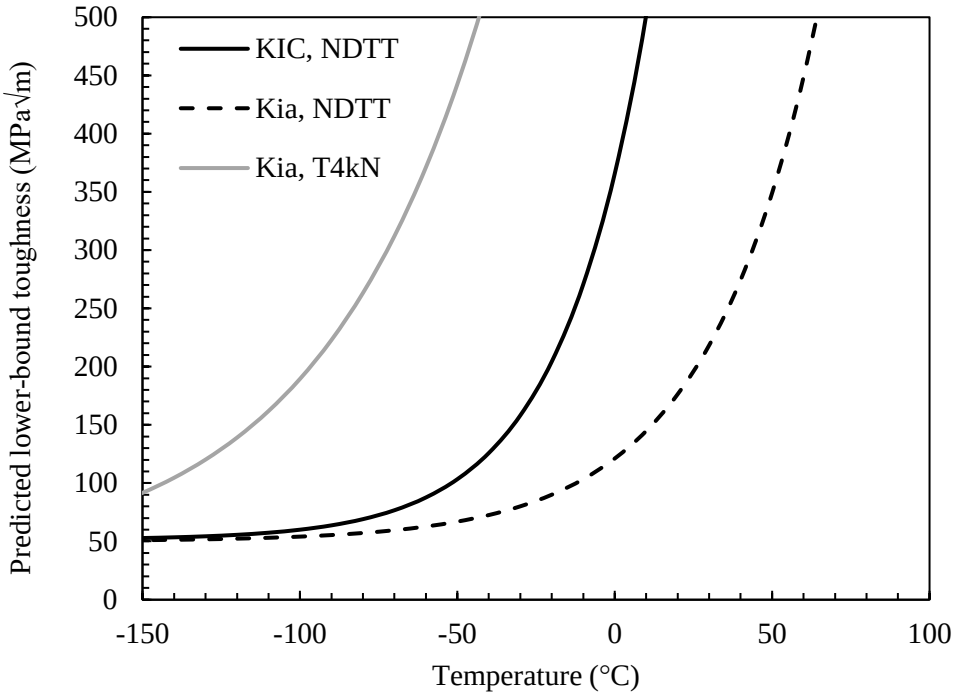

Figure 4-25: Master curves for material M06

5 Compact Crack Arrest Testing and Analysis on EH47 Shipbuilding Steel

Abstract

It is vitally important to measure the brittle crack arrest properties of shipbuilding steels to ensure that accidental damage will not result in total structural failure. Wide-plate test methods allow for direct measurement of the crack arrest toughness but this kind of testing is incredibly expensive. Therefore, there is a need for cheaper and simpler test methods which are able to measure a material's brittle crack arrest toughness. In this work, Compact Crack Arrest (CCA) testing, which is standardised in ASTM E1221, has been successfully used to measure the crack arrest toughness of thick sections of EH47 shipbuilding steel. The results from this study have been compared to small-scale test methods. It was found that instrumented Charpy testing gives an overprediction of the CCA results, and Nil-ductility transition temperature (NDTT) from Pellini tests gives a conservative estimate. The results presented in this study have been discussed in terms of the effectiveness of the CCA test method for measurement of brittle crack arrest toughness and integrity assessment of large-scale structures.

Keywords: brittle crack arrest, shipbuilding steel, CCA, compact crack arrest testing

Nomenclature

a	Crack length
a_0	Initial crack length before test
a_a	Arrested crack length
B	Thickness of the CCA test specimen
B_N	Net thickness between side-grooves
D	Diameter of wedge loading hole
E	Elastic Young's modulus
H	Height of the CCA test specimen
K	Stress intensity factor
K_0	Crack initiation toughness
K_a	Crack arrest toughness
K_{ca}	Crack arrest toughness: critical stress intensity factor for crack arrest under mode I fracture mechanics loading condition
K_{Ia}	Crack arrest toughness: measured via ASTM E1221
L	Length from loading hole to CMOD measurement location
N	Slot width in CCA test specimen
S	Side-groove depth (on each side) in CCA test specimen
T	Temperature
T_{4kN}	Reference Temperature at which a material's arrest force during instrumented Charpy test is 4kN
T_{KIa}	Reference temperature at which a material's arrest toughness is 100MPam^{½}
W	Width of the CCA test specimen
Y	Shape factor
δ	Experimental crack mouth opening displacement
σ_{UTS}	Ultimate tensile strength
σ_{Ys}	Static Yield Strength
σ_{Yd}	Dynamic Yield Strength
CCA	Compact crack arrest
CMOD	Crack Mouth Opening Displacement
EDM	Electrical discharge machining

5.1 Introduction

The issues associated with brittle fracture of shipbuilding steels were first brought to light by the premature failure of some of the Liberty ships during WWII[1]. In modern days, the requirements for shipbuilding steels are set by the International Association of Classification Societies (IACS), which includes assurance organisations worldwide. There is a drive to reduce carbon emissions of the shipping industry by using larger ships which can carry more cargo per journey[2]. These ships require stronger and thicker plates of steel for their hulls, and this carries with it an increased risk of brittle fracture, particularly in the case of bad weather or accidental damage[3,4]. A brittle crack can be prevented from causing catastrophic failure of the structure by ensuring that the materials used have a sufficient resistance to a propagating fracture i.e. high brittle crack arrest toughness[5].

The first standard which was developed for measurement of brittle crack arrest toughness was ASTM E1221:1988[6], which utilises relatively large-scale Compact Crack Arrest (CCA) test specimens. In recent years, the most common method to measure brittle crack arrest toughness is using wide-plate testing[7–17] such as ESSO tests or double-tension tests which have been incorporated into International Standard ISO 20064:2019[18]. It has been shown in previous studies that CCA testing gives a lower-bound approximation to the brittle crack arrest toughness, K_{Ia}, whereas wide-plate testing usually enables the crack arrest toughness, K_{ca}, to be directly measured[19]. Due to the experimental difficulties involved in CCA testing, there has been a limited amount of published results available in the public domain using this test method. The limited CCA test data which are publicly available are entirely limited to specimens with thicknesses of below 50mm[20–24]. Some researchers noted that it was difficult to get valid results from this test method and there was high scatter in the test data, which is why wide-plate methods are generally preferred[15,22,25].

Although wide-plate test methods are more likely to give a better prediction of brittle crack arrest toughness, there are many advantages to using CCA testing. Primarily, CCA testing is much cheaper than wide-plate testing. CCA testing requires less extensive instrumentation and set-up of the test, for example it is usually done isothermally rather than under a temperature gradient. Additionally, due to the smaller size and use of wedge

loading, there is a lower force requirement for the test machine. For these reasons, it is of interest to carry out CCA tests on modern shipbuilding steels to determine their viability, with an aim to reduce the cost of brittle crack arrest testing.

In this paper, CCA testing was carried out on 80mm thick EH47 shipbuilding steel to measure the brittle crack arrest toughness over a range of temperatures. The results from this study provide a unique set of data on relatively large thickness plates using the CCA test method. The obtained results have been compared to predictions of the crack arrest toughness from small-scale testing which are reported in chapter 1[26]. These predictions rely on determination of reference temperatures and are based on the master curve approach. The specimen preparation, test procedure, experimental challenges, and the analysis of the test data have been comprehensively explained and discussed in the following sections.

5.2 Compact Crack Arrest Test Methodology

The experimental studies in this work were carried out on EH47 shipbuilding steel, supplied by a steel manufacturer, which is widely used in industrial applications. EH47 steel was chosen due to the fact that it has been well characterised by other researchers which enables the CCA results obtained from this study to be compared to wide-plate test results available from other researchers' works[17,27]. The mechanical and fracture behaviour of the supplied EH47 steel employed in this study was characterised using small-scale mechanical testing in chapter 1[26]. The main material properties including the upper shelf Charpy energy, room temperature yield strength, σ_{Ys}, and ultimate tensile strength, σ_{UTS}, the nil-ductility transition temperature (NDTT), and average grain size are summarised in Table 5-1.

Table 5-1: Material properties for EH47 shipbuilding steel employed in this study

Upper shelf Charpy energy (J)	Yield strength (MPa)	Ultimate tensile strength (MPa)	Nil-ductility transition temperature (°C)	Average grain size (µm)
297	490	622	-50	4.1

Compact crack arrest testing was carried out in accordance with ASTM E1221[6] on 80mm thick EH47 shipbuilding steel plates. In total, 8 specimens were prepared and tested in this study, denoted CCA1−8. The CCA specimens consisted of a full-thickness piece of material which had a notched slot machined into them. The notch was opened using a wedge load through the hole in the specimen to initiate a brittle crack within a brittle weld bead deposited at the base of the notch.

The predictions of crack arrest toughness using small-scale tests which were made in chapter 1[26] have been compared against the results from CCA test data obtained from the present study.

5.2.1 Specimen design

The mechanical properties of the material, shown in Table 5-1, were used to choose appropriate specimen dimensions which would meet the strict criteria given in the ASTM E1221 standard[6] and give the best chance of calculating K_{Ia}. The key specimen dimensions are summarised in Table 5-2 and schematically shown in Figure 5-1. As seen in Table 5-2, all 8 specimens had the thickness of B = 80 mm, width of W = 260 mm, height of H = 156 mm, wedge loading hole diameter of D = 50.8 mm, length from loading hole to CMOD measurement location of L = 65 mm, slot width of N = 8.28 mm, and initial crack length of a_0 = 55 mm. Also included in Table 5-2 are the normalised dimensions for each parameter with respect to the width of the specimen, X/W. According to the guidelines provided in ASTM E1221 standard[6], the thickness, B, of CCA test specimens must be sufficiently large to satisfy plane strain conditions, with the width of the test specimen, W, within the range of $2B \leq W \leq 8B$; and the height, H, is $0.6W$.

In order to make the best use of the available material, it was chosen to use a B/W ratio of 0.31, which gives a width of W = 260 mm for the plates with the thickness of B = 80 mm. The initial normalised crack length, a_0/W, was kept very low to increase the stress intensity around the crack tip and facilitate brittle crack initiation. It was decided to use an a_0/W of just over 0.2 which is at the lower end of the allowed range recommended by the ASTM E1221 standard[6]. As seen in Figure 5-1, all test specimens were side-grooved following the recommendation in the ASTM E1221 standard[6]. Six out of eight specimens were side-grooved on both sides to promote a straight crack front. The remaining two

specimens were side-grooved only on one face so that crack propagation monitoring wires could be soldered to the other face of the specimen to measure the crack speed as it propagated. As shown in Table 5-2, the side-groove depth of S = 10 mm was implemented on each side of the test specimens with the net thickness between side grooves of B_N = 60 mm in those six specimens with double side-grooves, and B_N = 70 mm in those with a single side-groove. As shown in Figure 5-1, the test specimens were side-grooved at 45° angle using an Electrical Discharge Machining (EDM) technique.

Table 5-2: CCA specimen dimensions

	Dimension (mm)	Ratio to width, *X/W*
B	80	0.31
W	260	1.00
H	156	0.60
D	50.8	0.20
L	65	0.24
N	8.28	0.03
B_N	60	0.23
S	10	0.04
a_0	55	0.21

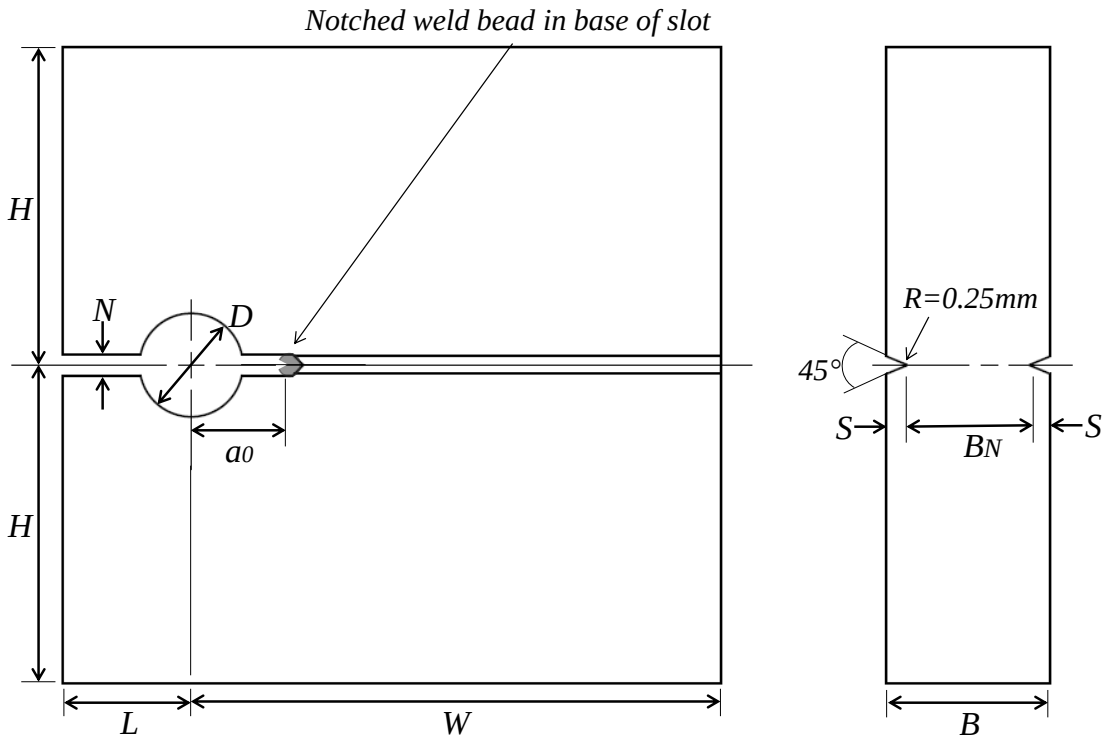

Figure 5-1: Schematic illustration of the CCA test specimen design.

5.2.2 Introduction of weld beads

A brittle weld bead was laid in the bottom of the slot to give an embrittled material in the starter notch to facilitate brittle crack initiation. The numerous challenges with producing suitable welds of high quality are explained in this section. Due to the large thickness of the specimens, magnetism was introduced in the specimen during the machining and welding processes. The magnetism caused the weld to be uneven due to arc blow or arc wander[28]. This was combatted through a combination of surface peening and careful welding technique. Before welding, the entire specimen was surface peened using a 2lb ball hammer with a focus around the bottom of the slot where the weld would be laid. The manual metal arc welding technique was used to deposit a brittle weld bead at the bottom of the slot for each specimen using the hard-facing electrode Bohler FoxDur 350 with a heat input of about 1.5kJ/mm. The weld was notched to 2 mm depth using the EDM technique to introduce a starter notch in the test specimens.

There were challenges with ensuring a sufficient thickness of the weld deposit as it was necessary to complete the weld in a single pass. It was necessary to increase the heat input

from that recommended in the standard (from 1kJ/mm to 1.5kJ/mm) to ensure the weld deposit was thick enough to be notched. Some of the specimens which had poor quality of welds were re-welded by initially using EDM to remove the old weld deposit before introducing the weld bead again. Although this gives a concern that the excess heat input may affect the test results, this was localised to the crack initiation region, hence this process is believed not to have affected the bulk of the specimen where the crack is propagating and, most importantly the arresting region which is further away from the initial crack tip. Through an iterative welding process, the deposition of the weld beads on test specimens was finalised. An example of a test specimen with the weld bead, before performing the test, is shown in Figure 5-2.

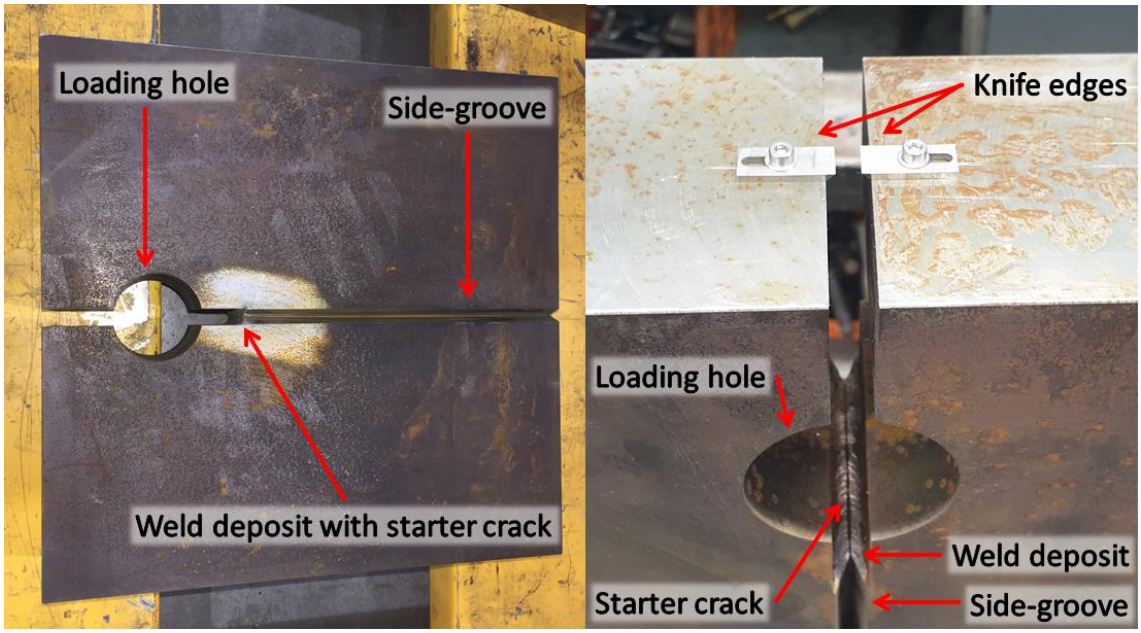

Figure 5-2: Example CCA specimen showing the weld bead and machined starter crack.

5.2.3 Test procedure

According to the experimental approach detailed in the ASTM E1221 standard, side-grooved CCA specimens are slowly cyclically loaded under crack-line wedge loading to incrementally increasing peak loads, in order to achieve a rapid run-arrest of a crack with a nearly straight crack front. The temperature range for the CCA testing was chosen based on the ductile to brittle transition behaviour of the material, with the NDTT (-50°C) chosen as the initial test temperature and subsequent temperatures chosen iteratively. In order to perform CCA experiments, the sample was initially cooled down to the desired

test temperature using liquid nitrogen, and subsequently loaded and unloaded repeatedly to a higher load point each cycle. This loading and unloading sequence continued until a brittle crack initiated and arrested itself. This was evident through the loud noise it made and also a steep drop-off in the load reading as the crack jumped. Once the experiment was completed, the specimens were heat tinted to highlight the notch and arrested crack clearly on the fracture surface once the specimen was broken open, so that the arrested crack length could be measured. The arrested crack length was measured as the average of 3 points equally distributed across the thickness of the specimen, as suggested by the ASTM E1221 standard[6].

To facilitate the experiments, a bespoke test rig was designed and fabricated at TWI Ltd., UK, using high strength steel based on the design suggested in the ASTM E1221 standard[6], which is shown in Figure 5-3. The test rig included cooling coils embedded into the support block through which liquid nitrogen was pumped to ensure a consistent temperature throughout the specimen. Due to the large thickness of the material being tested, the whole rig was scaled up, including the wedge and split pin assembly, to ensure sufficient strength in the test rig. This was directly scaled from the example dimensions which are given in the standard.

Each stage of the experimental set-up is shown in Figure 5-3. Figure 5-3-a shows the test rig, which is fully set up on TWI's 500kN capacity machine in Figure 5-3-b. The specimen was inserted into the test rig and instrumented as shown in Figure 5-3-c. The instrumentation included temperature measurements for all specimens and crack propagation monitoring wires which were used to measure the crack speed in two of the experiments. The case shown in Figure 5-3-c is that with crack propagation monitoring wires applied to the surface of the specimen. As the crack propagates past the wire, it is broken and the signal is recorded and its speed can be measured. During the experiment, the low temperature was maintained by covering the specimen in thick layers of insulation, which is shown in Figure 5-3-d.

Figure 5-3: Experimental set up of CCA tests showing: (a) the test rig assembly, (b) the fully assembled test rig on the machine, (c) the specimen is placed in the test rig and instrumented, (d) during the test.

5.2.4 Data analysis procedure

Equation 5-1 to Equation 5-5 are used to calculate the stress intensity factor, *K*, shortly after arrest, which would be equivalent to K_{Ia} when particular requirements are met as described by Equation 5-6 to Equation 5-10. In order to perform a CCA test, the wedge is loaded cyclically into the specimen with increasing peak load, and the crack mouth opening displacement (CMOD) is used to find *K* once an arrest event has occurred. According to the ASTM standard, the stress intensity factor for standard CCA specimen geometry can be calculated using Equation 5-1 to Equation 5-5:

$$K = E\delta Y\sqrt{\frac{B}{B_N W}} \qquad \text{Equation 5-1}$$

$$Y = (1-x)^{\frac{1}{2}}(0.748 - 2.176x + 3.56x^2 - 2.55x^3 + 0.62x^4) \qquad \text{Equation 5-2}$$

$$x = \frac{a}{W} \qquad \text{Equation 5-3}$$

where *E* is the elastic Young's modulus in MPa, *B* is the specimen thickness in mm, B_N is the net thickness between the side grooves in mm, *W* is the specimen width in mm, δ is calculated from the CMOD using Equation 5-4 or Equation 5-5, and *a* is the crack length in mm (i.e. a_0 is the initial crack length and a_a is the arrested crack length). In order to calculate K_0, which is the stress intensity factor at initiation point (known as crack initiation toughness), the crack length is taken as $a = a_0$, and $\delta = d_0$. Similarly, K_a which is known as the crack arrest toughness is calculated using $a = a_a$ and $\delta = d_a$.

δ, used in Equation 5-1, is calculated from the equations below using Figure 5-4 as a reference to show how the parameters are calculated from the load-displacement curve over multiple cycles.

$$d_0 = \delta_0 - (\delta_p)_{n-1} \qquad \text{Equation 5-4}$$

$$d_a = 0.5\left[\delta_0 + \delta_a - (\delta_p)_1 - (\delta_p)_{n-1}\right] \qquad \text{Equation 5-5}$$

where n is the number of load cycles to the run-arrest event, δ_0 is the CMOD at the crack initiation point, $\delta_{p(n-1)}$ is the CMOD at the start of the nth loading cycle when the load has been reset to 0, and δ_a is the CMOD after the crack has arrested. It can be seen that as the crack propagates, the crack mouth widens before it arrests.

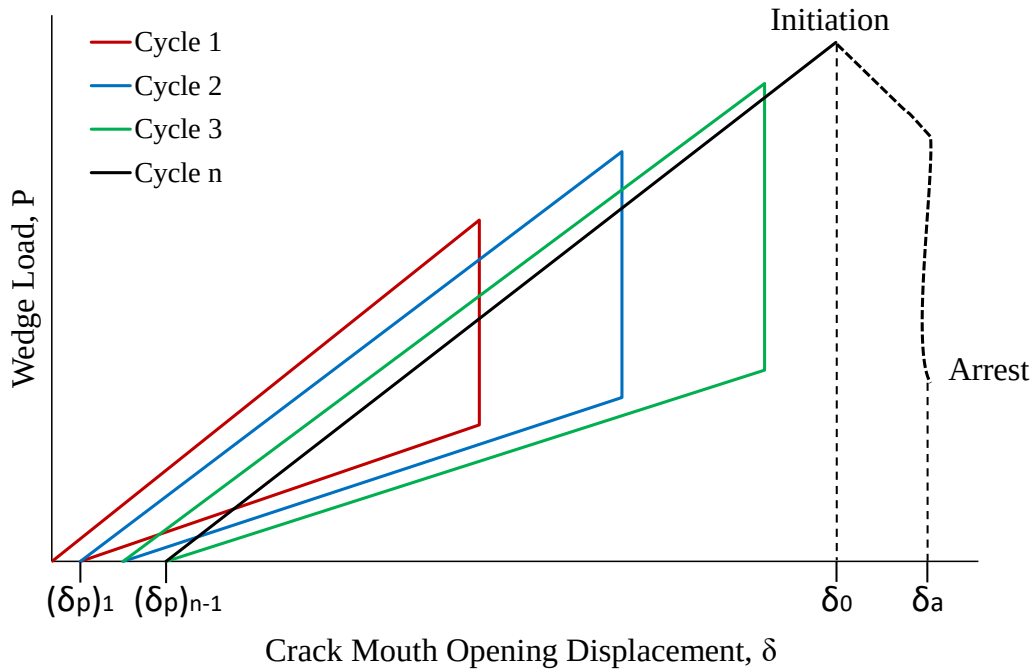

Figure 5-4: Wedge force vs. CMOD using cyclic loading technique. Each loading cycle is shown in a different colour until the final "cycle n" the where the crack propagates and arrests.

According to ASTM E1221, when the following criteria are met K_a can be taken as K_{Ia} which is the critical stress intensity factor for crack arrest under the mode I fracture mechanics loading condition.

$$W - a_a \geq 0.15W \qquad \text{Equation 5-6}$$

$$W - a_a \geq 1.25\left(\frac{K_a}{\sigma_{Yd}}\right)^2 \qquad \text{Equation 5-7}$$

$$B \geq 1.0\left(\frac{K_a}{\sigma_{Yd}}\right)^2 \qquad \text{Equation 5-8}$$

$$a_a - a_0 \geq 2N \qquad \text{Equation 5-9}$$

$$a_a - a_0 \geq \left(\frac{K_0}{\sigma_{Ys}}\right)^2 / 2\pi \qquad \text{Equation 5-10}$$

where N is the machined slot width, $W\text{-}a$ is the uncracked ligament, σ_{Yd} is the dynamic yield stress and σ_{Ys} is the static yield stress. These criteria ensure that the specimen is of a sufficiently large size to satisfy plane strain conditions, and that the assumption of static behaviour during the crack jump event is appropriate i.e. dynamic effects are not present.

5.2.5 Small-scale testing

Following chapter 1[26], where small-scale testing was carried out, the predictions of the crack arrest toughness obtained from smaller size samples were validated against the large-scale results presented in this study. The small-scale tests in the previous study consisted of instrumented Charpy V notch testing to determine the post-fracture force during impact, and drop weight Pellini testing to measure the nil-ductility transition temperature (NDTT). These predictions rely on determination of reference temperatures and are based on the principles of the master curve approach. The master curve is a statistical approach which gives a lower bound estimate of fracture toughness of ferritic steels for temperatures in the transition region and lower shelf from a limited amount of test data. This has been adapted by other researchers[25,29–32] to predict brittle crack arrest toughness from small-scale testing using the following relationships:

$$K_{Ia} = 49.957 + 16.878\, e^{0.028738(T - NDTT)} \text{ [Ref 32]} \qquad \text{Equation 5-11}$$

$$K_{Ia} = 30 + 70\, e^{\left(\frac{T - T_{4kN} - 12.3}{52.63}\right)} \text{ [Ref 30]} \qquad \text{Equation 5-12}$$

where T is the calculation temperature, $NDTT$ is measured from Pellini testing[33], and T_{4kN} is the temperature at which the instrumented Charpy post-fracture force is 4kN. These curves can be compared to the fit to the CCA data, which uses T_{KIa} as the reference temperature and is given in ASTM E1221[6] by:

$$K_{Ia(median)} = 30 + 70\, e^{0.019(T - T_{KIa})} \qquad \text{Equation 5-13}$$

where T_{KIa} is the temperature corresponding to a median crack arrest toughness of 100 MPam^{½}.

5.3 Compact Crack Arrest Test Results

5.3.1 Validity of the test results

The results obtained from the CCA tests are summarised in Table 5-3 and compared against the predictions from small-scale testing in Figure 5-5. While CCA2, CCA3, CCA4 and CCA8 specimens were tested satisfactorily according to ASTM E1221 and accurate crack arrest results were obtained from these four specimens, the remaining four samples resulted only in indicative crack arrest data as they were not fully qualified, due to number of different reasons.

In the test on the CCA1 specimen, which was the first experiment conducted in this study, it was discovered that part of the loading rig had deformed during the loading of the specimen. This meant that the load recorded during the experiment was higher than the load applied onto the specimen, as some was lost to the loading rig. This did not affect the calculated crack arrest toughness as the load is not used as an input parameter into the calculation and the CMOD measurement was not affected. Although this issue was unlikely to have impacted the results, the test data obtained from this experiment was assumed to be indicative. The issue with the loading rig was fixed after this first test and this problem did not occur again in any of the other tests.

In the test on the CCA5 specimen, the crack did not propagate through the entire thickness of the test geometry, presumably due to the comparatively high temperature in this specimen, which meant that the crack was arrested easily in the material. Therefore, the results obtained from this experiment were considered to be indicative. Finally, CCA6 and CCA7 test specimens were side-grooved in a single side, to be able to accommodate wiring on the opposite plane side of the test piece for measurement of the crack propagation speed. Although this was taken into account during the calculation of K_{Ia}, which includes consideration for the thickness between the side-grooves, the results obtained from these two test specimens were also considered indicative rather than strictly qualified to the standard.

5.3.2 Presentation of the test results

It is evident from Figure 5-5 that there is a large scatter in the toughness results, and that not all of the test data points are valid. However, it can also be seen that both valid and indicative test data follow the same trend when the toughness data are correlated with the arrest temperature. Also seen in Figure 5-5 is that the data points obtained from the CCA tests are entirely bounded by the two prediction lines which were made from small-scale testing. The prediction of the crack arrest toughness from NDTT gives a lower bound estimate, and the prediction from T_{4kN} gives an upper bound estimate with the CCA test data falling in between these two extreme trends. Also seen in Figure 5-5 is that when the trend obtained from the test data points from this study is extrapolated to higher toughness values, the CCA trend remains between the prediction lines from NDTT and T_{4kN}. This suggests that the NDTT can be used to give a conservative estimate of CCA toughness results. However, more tests need to be conducted in future work to confirm the obtained trend from this study for higher and lower toughness values. The K_{IC} and K_{JC} curves show very similar shapes to the K_{Ia} curves measured from similar methods, translated upwards. This indicates that for this material the initiation toughness is higher than the crack arrest toughness at a given temperature. Full analysis of the initiation master curves is given in section 4.6.3.

Table 5-3: Summary of the CCA test results

Specimen ID	Temperature (°C)	Average arrested crack length, a_a (mm)	K_{Ia} (MPam^{½})
CCA1	-50	180.0	93.4
CCA2	-50	141.7	123.9
CCA3	-90	159.4	73.7
CCA4	-70	161.8	89.0
CCA5	-10	85.0	145.9
CCA6	-70	113.1	110.4
CCA7	-50	137.1	130.4
CCA8	-30	129.3	99.4

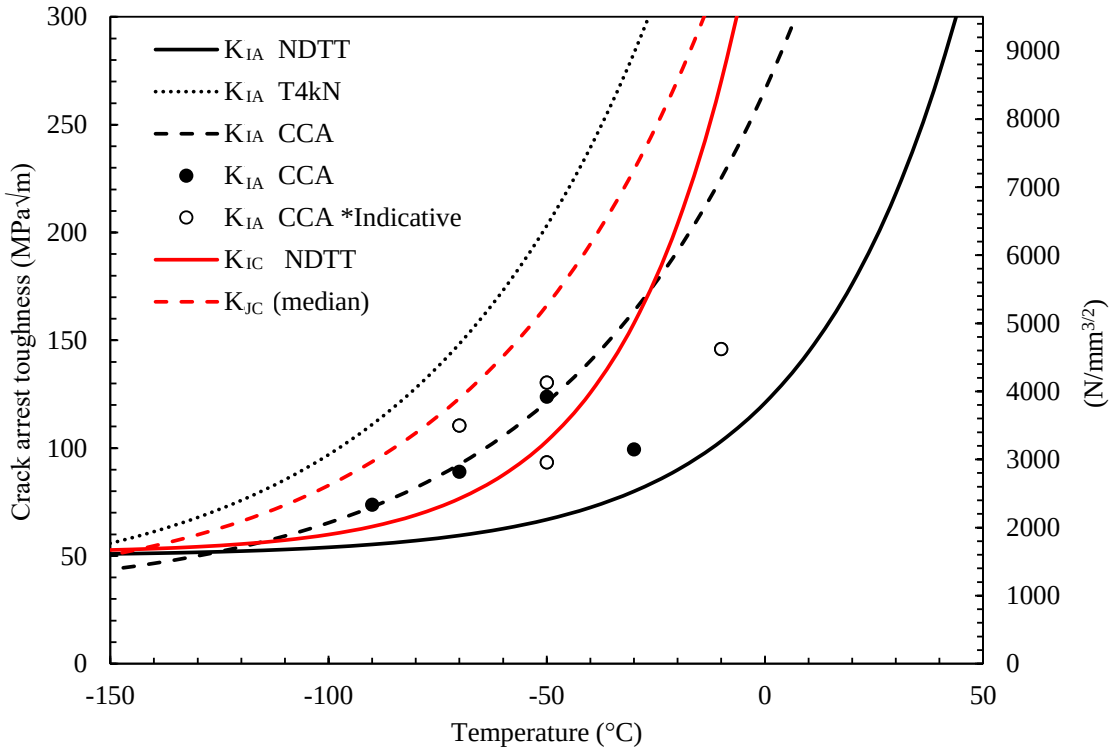

Figure 5-5: Comparison of the CCA test results with predictions from small-scale testing

5.3.3 Fractography

Fractography analysis was carried out on all specimens post-testing. The fracture surfaces of one half of specimens CCA1−8 are shown in Figure 5-6. It can be seen on the fracture surface of all specimens that heat tinting was an effective approach to mark the extent of crack growth during testing and before the specimen was broken open. The crack propagation occurred in a brittle manner in all specimens, which is evident from the relatively smooth and flat crack path observed in the fractography analysis on all test specimens. In specimens CCA6 and CCA7 (Figure 5-6(f) and Figure 5-6(g)), the crack showed tunnelling away from the surface, which meant that the crack propagation monitoring wires were not broken as the crack propagated. This indicates that although these two specimens were instrumented for crack speed measurement, this could not be achieved in practice due to the lack of crack growth along the plane-sided face of the CCA specimen geometry.

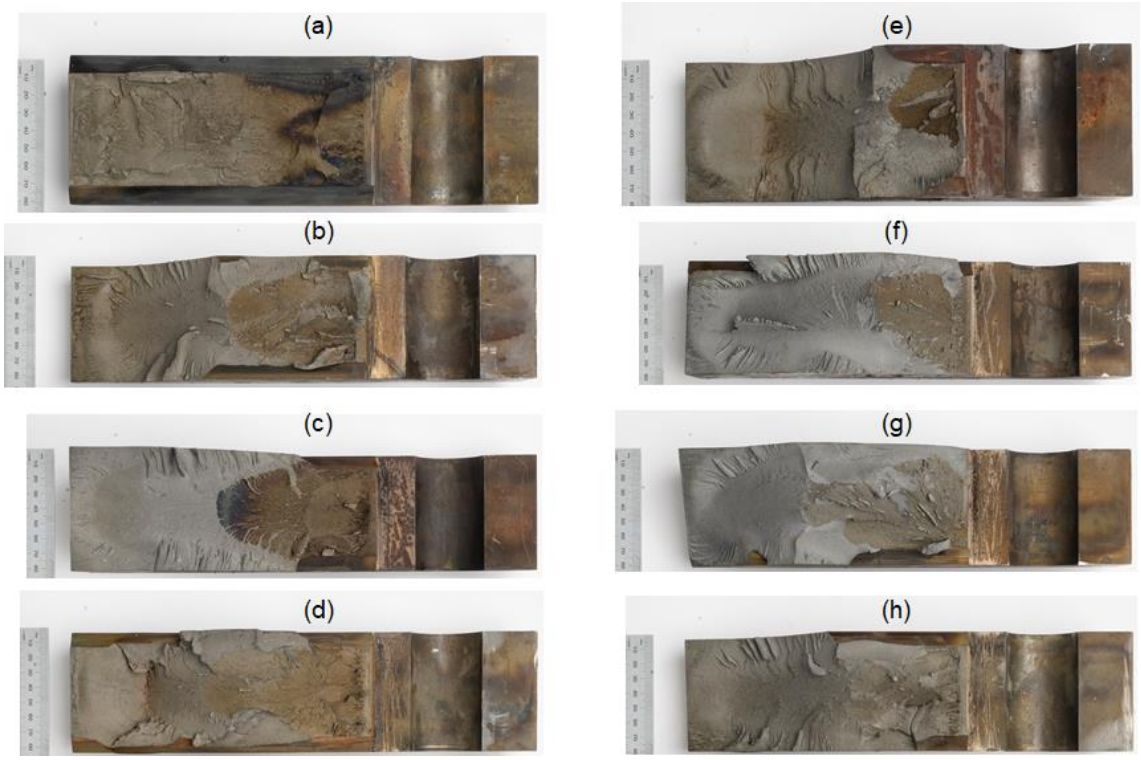

Figure 5-6: Fracture surface of (a) CCA1, (b) CCA2, (c) CCA3, (d) CCA4, (e), CCA5 (f), CCA6 (g), CCA7, (h) CCA8 specimens

5.4 Discussion

It was not possible to measure the crack velocity from these specimens. Due to the very low test temperatures (between -10°C and -90°C) it was necessary to keep the specimen under insulation which meant that it was not possible to use visual crack speed measurement methods (e.g. digital image correlation). For that reason, use of crack propagation monitoring wires is the recommended approach to measuring the crack speed. The focus of this research was on measurement of crack arrest toughness and ensuring that it was possible to get valid results before attempting to measure the crack speed, hence only two specimens were instrumented in this way. Now that the compact crack arrest testing approach has been proven successful, future work should focus on ensuring that the crack speed can be measured during these tests.

It is important to measure the crack propagation speed throughout the test as this is an important input into finite element modelling of brittle crack arrest which has been successfully carried out by other researchers [34–44].The most common technique for finite

element modelling of brittle crack arrest is using the nodal release method to replicate the propagating crack and extract the stress shortly ahead of the crack tip[40–42,45]. The critical stress just ahead of the crack tip is taken as the criterion for crack propagation, following a local stress approach[34,46]. Using this critical stress, predictive models can be developed. In future work, finite element modelling should be used to validate the experimental results.

The CCA results obtained from this study can be compared to those of other researchers who have carried out quantitative crack arrest testing on the same material. Although these experiments have never been done before on such thick sections of shipbuilding steels, other wide-plate tests have been carried out in previous studies using different methods[15]. Other researchers have consistently shown crack arrest toughness exceeding 6000 $N/mm^{3/2}$ at -10°C (which is equivalent to 190 $MPam^{½}$) and this has been incorporated as a requirement of the International Association of Classification Societies[17,47,48]. Comparison of the results available on wide-plates to those obtained from CCA specimen geometries from the present study reveals that other test methods give a much higher threshold of brittle crack arrest toughness for the material examined in this study. This raises concerns that the CCA method may under-predict brittle crack arrest toughness results. Given the high strength and Charpy toughness of this material, it seems likely that it is the test method which is resulting in a low prediction of crack arrest toughness rather than the material itself. It would be necessary to carry out CCA testing and wide-plate testing on the same batch of steel in future work to have confidence in the agreement between the results of these two test methods. Alternatively, it may be possible to apply a correction factor to relate the CCA test results to wide-plate results for integrity assessment of large-scale structures. This correction factor would likely comprise a combination of specimen geometry (a, W, B), along with factors. In order to determine a correction factor, a large test program would need to be carried out to determine the dependence of the toughness on different factors involved in CCA testing. Nonetheless, CCA testing is a viable alternative to wide-plate testing and could be used to verify the quality of a batch of steel plates without the need for expensive wide-plate testing every production run. This would reduce the cost of testing while maintaining high quality of steel plates.

5.5 Conclusions

CCA testing was successfully carried out on 80mm thick EH47 shipbuilding steel to measure the brittle crack arrest toughness in this material. The results obtained from these tests were compared to the toughness predictions from small-scale testing and also wide-plate test results available from other researchers. The following conclusions were made from this study:

- The present study has proved the possibility of achieving valid results from CCA testing on relatively thick (i.e. 80 mm) steel plates
- Relatively smooth arrested fracture surfaces were observed in all CCA test specimens confirming that brittle crack arrest occurred in these experiments
- The results show that Pellini NDTT data from small-scale tests can be used to obtain a conservative estimate of CCA test results
- The results show that instrumented Charpy testing provides an over-estimation of the CCA test results
- Master curve predictions of K_{Ia} are more conservative when using NDTT than T_{4kN} so using the NDTT is recommended to give a safer estimate of crack arrest properties, although this prediction is only valid at low temperatures
- The wide-plate test results available in the literature on the EH47 steel indicates that more conservative values of brittle crack arrest toughness may be achieved from CCA tests
- More experiments should be conducted in future work on the same material batch to directly compare the CCA and wide-plate
- Crack speed monitoring in CCA tests is challenging and may not be achieved by instrumenting a plane sided face of the specimen

References

1. Tassava CJ. Weak seams: Controversy over welding theory and practice in american shipyards, 1938-1946. *Hist Technol*. 2010;19(2):87-108.

2. International Association of Classification Societies. Safer and Cleaner Shipping - IACS. http://www.iacs.org.uk/

3. (DNV) Det Norske Veritas. Fatigue Design of Offshore Steel Structures. *Recomm Pract DNV-RPC203*. Published online 2005.

4. Hirdaris SE, Bai W, Dessi D, et al. Loads for use in the design of ships and offshore structures. *Ocean Eng*. Published online 2014. doi:10.1016/j.oceaneng.2013.09.012

5. Anderson TL. *Fracture Mechanics: Fundamentals and Applications*. Vol 58.; 2017. doi:10.1016/j.jmps.2010.02.008

6. ASTM. E1221 Standard Test Method for Determining Plane-Strain Crack-Arrest Fracture Toughness, K Ia, of Ferritic Steels. 2007;96(Reapproved):1-19. doi:10.1520/E1221-12A.2

7. Shibanuma K, Yanagimoto F, Namegawa T, Suzuki K, Aihara S. Modeling of Brittle Crack Propagation / Arrest Behavior in Steel Plates in Steel Plates modeling high pressure turbine blade airplane gas turbine engine Modeling of Brittle Crack Behavior PCF Propagation / Arrest. *Procedia Struct Integr*. 2016;2:2598-2605. doi:10.1016/j.prostr.2016.06.325

8. Handa T, Matsumoto T, Yajima H, et al. Effect of S tructural D iscontinuities of W elded J oints on B rittle C rack P ropagation B ehavior - Brittle C rack A rrest D esign for L arge C ontainer S hips -3 - Steel Plates Used for Tests. 2010;7:88-94.

9. An GB, Park JS, Ryu KM, et al. Brittle Crack Arrest Technique of Thick Steel Plate Welds in Container Ship. 2009;1:357-360.

10. Kawabata T, Matsumoto K, Ando T, et al. Development of Brittle Crack Arrest Toughness Kca Test Method - Brittle Crack Arrest Design for Large Container

Ships -2 - Review of Wide Plate Test Method for Arrest Toughness. 2010;7:80-87.

11. Funatsu Y, Shirahata H, Otani J, Inoue T, Hashiba Y. The Effect of Shear-lips on the Arrestability of Thicker Steel Plates Longitudinal. *Isope*. 2012;4:63-66.

12. Kawabata T, Namegawa T, Kaneko M, et al. Numerical analyses of press-notched bend tests and applicability to simplified method of arrest toughness evaluation. *Proc Int Offshore Polar Eng Conf*. 2015;2015-Janua:169-176.

13. Handa T, Igi S, Oi K, et al. Effect of toughness distribution in the thickness direction on long brittle crack propagation/arrest behaviour of heavy gauge shipbuilding steel. *Weld Int*. 2018;32(7):460-468. doi:10.1080/01431161.2017.1346884

14. Handa T, Tagawa T, Minami F. Correlation between charpy transition temperature and brittle crack arrest temperature considering texture. *Tetsu-To-Hagane/Journal Iron Steel Inst Japan*. 2012;98(1):32-38. doi:10.2355/tetsutohagane.98.32

15. Kawabata T, Inoue T, Tagawa T, et al. Historical review of research on brittle crack propagation arresting technology for large welded steel structures developed in Japan with the application of Kca parameters. *Mar Struct*. 2020;71(January):102737. doi:10.1016/j.marstruc.2020.102737

16. Aihara S, Watabe Y, Shibanuma K, Inoue T, Koseki T. Numerical and Experimental Analysis of Brittle Crack Propagation and Arrest in Steels. 2012;4:90-97.

17. Shibanuma K, Yanagimoto F, Namegawa T, Suzuki K. Brittle crack propagation / arrest behavior in steel plate – Part II : Experiments and model validation. *Eng Fract Mech*. 2016;162:341-360. doi:10.1016/j.engfracmech.2016.02.053

18. International Standards Organisation. *BS ISO 20064 : 2019 BSI Standards Publication Metallic Materials — Steel — Method of Test for the Determination of Brittle Crack Arrest Toughness , K Ca*.; 2019.

19. Wiesner C, Hayes B. *A Review of Crack Arrest Tests, Models and Applications*.; 1995.

20. Burch I., Underwood J. Crack Arrest Fracture Toughness Measurement of a Quenched and Tempered Ship Plate Steel. *MRL Tech Rep*. Published online 1992. http://www.dtic.mil/dtic/tr/fulltext/u2/a264037.pdf

21. Une ED, En M, La VUEDE, et al. Collection de notes internes de la Direction des Etudes et Recherches i. *Practice*.

22. Bonenberger RJ, Dally JW. On improvements in measuring crack arrest toughness. *Int J Solids Struct*. 1995;32(6-7):897-909. doi:10.1016/0020-7683(94)00167-U

23. Mayer U, Mutz A, Ag G, Nicak T. Compact crack arrest tests for the validation of a finite element material model of the reactor pressure vessel steel of the nuclear power plant kkg. *Proc ASME 2018 Press Vessel Pip Conf PVP2018*. Published online 2018:PVP2018-84068.

24. Ship Structures Committee. *Crack Arrest Toughness of Steel Weldments*.; 2000.

25. Bass BR, Williams PT, Pugh CE. An updated correlation for crack-arrest fracture toughness for nuclear reactor pressure vessel steels. *Int J Press Vessel Pip*. 2005;82(6):489-495. doi:10.1016/j.ijpvp.2004.12.006

26. Taylor J, Mehmanparast A, Kulka R, Moore P, Xu L, Hossein Farrahi G. Experimental study of the relationship between fracture initiation toughness and brittle crack arrest toughness predicted from small-scale testing. *Theor Appl Fract Mech*. 2020;110(October):102799. doi:10.1016/j.tafmec.2020.102799

27. An GB, Ryu KM, Park JS, et al. Increase of Brittle Crack Arrestability Using Arrest Welding of Thick Steel Plate in Large Container Ship. 2011;8:2006-2009.

28. Moniz BJ, Miller RT. *Welding Skills. American Technical Publishers*.; 2010.

29. Wallin K. Application of the Master Curve method to crack initiation and crack arrest. In: *American Society of Mechanical Engineers, Pressure Vessels and Piping Division (Publication) PVP*. Vol 393. ; 1999.

30. Wallin K, Karjalainen-roikonen P. Crack Arrest Toughness Estimation for High Strength Steels from Sub-Sized Instrumented Charpy-V Tests. *Proc Twenty-sixth Int Ocean Polar Eng Conf*. Published online 2016:85-91.

31. Kirk MT, Natishan ME, Wagenhofer M, et al. A Summary of Wallin ' s Empirical Findings. Published online 2002:729-740.

32. Pugh CE, Corwin WR, S RHBRYANBRBAS. C.e. pugh, w.r. corwin, r.h. *Nucl Eng Des*. 1986;96:297-312.

33. ASTM. E208 Standard Test Method for Conducting Drop-Weight Test to Determine Nil-Ductility Transition Temperature of Ferritic Steels 1. *Test*. 2000;06(Reapproved):1-13. doi:10.1520/E0208-06R12.2

34. Ishihara K, Hamada T, Kikuya N, Meshii T. Applicability Of Modified Ritchie-Knott-Rice Failure Criterion To Predict The Onset Of Cleavage Fracture For The Test Specimen With Residual Stress Introduced To The Crack Tip. *Procedia Struct Integr*. 2016;2:728-735. doi:10.1016/j.prostr.2016.06.094

35. Prabel B, Marie S, Combescure A. Using the X-FEM method to model the dynamic propagation and arrest of cleavage cracks in ferritic steel. 2008;75:2984-3009. doi:10.1016/j.engfracmech.2008.01.008

36. Link RE, Joyce JA, Roe C. Crack arrest testing of high strength structural steels for naval applications q. *Eng Fract Mech*. 2009;76(3):402-418. doi:10.1016/j.engfracmech.2008.11.006

37. Bousquet A, Marie S, Bompard P. Propagation and arrest of cleavage cracks in a nuclear pressure vessel steel. *Comput Mater Sci*. 2012;64:17-21. doi:10.1016/j.commatsci.2012.04.026

38. Berdin C, Hajjaj M, Bompard P, Bugat S. Local approach to fracture for cleavage crack arrest prediction. *Eng Fract Mech*. 2008;75:3264-3275.

39. Dahl A, Berdin C, Moinereau D. Dynamic modeling of cleavage crack propagation and arrest with a local approach. *Procedia Eng*. 2011;10:1853-1858. doi:10.1016/j.proeng.2011.04.308

40. Berdin C. 3D modeling of cleavage crack arrest with a stress criterion. *Eng Fract Mech*. 2012;90:161-171. doi:10.1016/j.engfracmech.2012.05.002

41. Nishioka Y, Shibanuma K, Nishioka Y, Yanagimoto F. Finite element model to

simulate crack propagation based on local fracture stress criterion. Published online 2016.

42. Yanagimoto F, Shibanuma K, Suzuki K, Matsumoto T, Aihara S. Local stress in the vicinity of the propagating cleavage crack tip in ferritic steel. *Mater Des*. 2018;144:361-373.

43. Yanagimoto F, Shibanuma K, Suzuki K, Matsumoto T. A physics based model to simulate brittle crack arrest in steel plates incorporating experimental and numerical evidences. *Eng Fract Mech*. 2019;221(January):106660. doi:10.1016/j.engfracmech.2019.106660

44. Shibanuma K, Yanagimoto F, Namegawa T, Suzuki K. Brittle crack propagation / arrest behavior in steel plate – Part Ⅰ: Model formulation. *Eng Fract Mech*. 2016;162:324-340. doi:10.1016/j.engfracmech.2016.02.054

45. Link R. Analysis of Dynamic Fracture and Crack Arrest of an HSLA Steel in an SE (T) Specimen. 2006;3(1):1-26.

46. Ritchie RO, Knott JF, Rice JR. On the relationship between critical tensile stress and fracture toughness in mild steel. *J Mech Phys Solids*. 1973;21(6):395-410. doi:10.1016/0022-5096(73)90008-2

47. International Association of Classification Societies. *W31 YP47 Steels and Brittle Crack Arrest Steels*.; 2019.

48. An GB, Ryu KM, Park JS, et al. Increase of Fracture Toughness using Crack Arrest Design of Thick Steel Plate Welds in Large Container Ship. 2010;7:119-121.

6 Overall Discussion and Future Work

The results presented from this project provide a comprehensive characterisation of the fracture properties of EH47 shipbuilding steel which is not currently available in the public domain. This is presented alongside the properties of four other steel grades for comparison to determine which characteristics of a steel provide enhanced brittle crack arrest properties. This research will be taken forward by Lloyd's Register to the International Association of Classification Societies (IACS) and inform the development of new standards which allow the certification of a shipbuilding steel's brittle crack arrest toughness based on small-scale testing.

The main focus of this research was on EH47 shipbuilding steel, as requested by the project sponsor. Regardless, the six steels presented in this study were used to correlate the different steels' properties against each other to determine if trends could be found i.e. relationships between certain material properties. In this way, it was attempted to determine why a particular material had improved toughness compared to another – is it due to the grain size, chemical composition, texture, or other metallurgical property of the material. Some of the correlations between material properties confirmed those which are well known e.g. small grain size correlated with high initiation toughness. This indicates that the other correlations determined in this research have some weight behind them.

6.1 Discussion of Results

The results confirm concerns that have been raised at TWI Ltd. about some modern steels having high toughness measured from Charpy impact testing, but are nonetheless susceptible to brittle failure at a temperature on the upper shelf. This can be explained by the fact that the nil-ductility transition temperature (NDTT), which is not usually reported by steel manufacturers, was located on the upper shelf in 4 out of 6 of the steels examined in this study. i.e., Charpy testing alone is not enough to ensure brittle fracture is prevented and the NDTT is a more suitable and conservative parameter to use in this case. One of the most interesting findings was that the smaller the grain size, the higher the NDTT – i.e. the worse the brittle crack arrest properties. It had been expected that grain refinement would improve the crack arrest toughness but this is evidently not the case for these steels.

This result was recently confirmed by another researcher who carried out experimental and numerical work confirming that this is due to larger grains having a higher critical threshold of local stress ahead of the crack tip which aids in arresting a brittle crack (see section 2.7). The high Charpy toughness can be attributed to grain refinement, but this has the opposite effect on crack arrest toughness. This important result shows that brittle crack arrest properties must be considered independently from initiation properties when selecting, designing, and manufacturing materials. Therefore, it is not recommended to use any upper-shelf properties to indicate crack arrestibility, which is dominated by the lower-shelf transition region. If Charpy testing is to be used to predict brittle crack arrest behaviour, T_{27J} should be used. T_{27J} is preferable over T_{4kN} because it is simpler and easier to calculate – it avoids analysis of the instrumented Charpy force-time trace and potential extrapolation to find the T_{4kN} value. T_{27J} can be calculated simply from the Charpy transition curve and is often provided as part of a material specification. T_{27J} can be used to predict NDTT with high accuracy. Preferably, NDTT should be directly measured from the materials although it is appreciated that these facilities may not be as readily available as the very common Charpy testing equipment.

Where large scale testing is concerned, very few test centres have the facilities to carry out wide-plate crack arrest testing. Indeed most test centres certified to carry out wide-plate crack arrest testing according to IACS standards are in Asia. This research is based in the UK, and it can be appreciated that there is a need for test methods which can be carried out more locally. Since wide-plate testing has already been carried out on EH47 shipbuilding steel, it was decided to undertake Compact Crack Arrest (CCA) testing in this work. Although the CCA method is standardised by ASTM, it is not included in IACS standards and is not a popular test method for shipbuilding steels. This may be because it was developed with pressure vessel steels in mind and there is no tensile loading component during the test which is a more realistic in-service condition for shipbuilding steels. Nonetheless, this method was very successful at measuring the brittle crack arrest toughness and showed good agreement with the master curve predictions from small-scale testing. Other benefits of this method over wide-plate testing are the greatly reduced cost of CCA testing. Quotations for carrying out the testing at TWI Ltd. revealed that CCA testing was 5 times cheaper than double tension testing, which would be the cheapest option of the wide-plate testing. Of course, there were some drawbacks of the

CCA testing, namely that the toughness results were far lower than expected for this material. However, the results showed the expected relationship between temperature and CCA toughness which indicates that the CCA method could be adapted to include a factor which adjusts the results so that this method can be used in place of expensive wide-plate testing.

6.2 Impact of this Research

Going forward, these results will be taken into consideration by Lloyd's Register to the International Association of Classification Societies (IACS) to inform the development of new standards which will allow the certification of a shipbuilding steel's brittle crack arrest toughness based on small-scale testing. This will make it more accessible for a steel's brittle crack arrest toughness to be quantified and make it more likely that the methodology will be considered in other industries. Once the use of small-scale testing is approved for the shipbuilding industry, it can be carried out by steelmakers on each batch of steel to ensure that the quality is adequate for the requirements. Additionally, it will ensure that appropriate crack arrest testing is always carried out since it will no longer be prohibitively expensive. This will help to ensure that maritime disasters such as the break-in-two failures of the MSC Napoli and the MOL Comfort never happen again and ensure that fewer lives are lost at sea.

Any structures which are at risk of brittle fracture would benefit from assurance that a brittle crack will not result in catastrophic failure. With the huge cost reduction of brittle crack arrest testing associated with using small-scale test methods, it would be feasible to incorporate the crack arrest toughness into defect tolerance assessments. In such a way, the lifetime of an asset could be extended once it is confirmed that the materials used have a sufficient crack arrest toughness to arrest a brittle crack. For example: if this methodology was implemented for offshore wind turbine foundation structures, it would enable further reductions to the levelised cost of energy through reduced operational costs and increased operational lifetime. This would further promote the take-up of offshore wind, which relies heavily on cost reduction in order to compete with other energy sources, and help with reduction of global carbon emissions.

6.3 Suggestions of Future Work

One of the main limitations of this work, and the key area for future work, is finite element modelling (FEM). It was not possible for the crack speed during the CCA tests to be measured because the standard technique of using crack propagation monitoring wires was unsuccessful. This technique did not work because there was extensive crack tunnelling which meant that the crack propagation monitoring wires, which were attached to the surface of the specimen, did not break. It may be possible to use other non-visual methods to determine the crack speed (e.g. ultrasonics). This should be investigated in future work as large-scale testing is very expensive and it is important to capture as much data as possible from each test. The crack speed is an essential input into FEM, which would allow the experiments to be modelled and predictive models to be developed. This has successfully been carried out by other researchers, but never for the CCA specimens – see Section 2.7 for further details. Future work should focus on developing a predictive model for crack arrest in CCA specimens. This would allow CCA testing to become more widely used for brittle crack arrest toughness measurement.

In future work, it would be recommended to take further measurements of the texture from multiple specimens and throughout the thickness of the material. This will help to see the full picture more clearly, understand the in-service properties of the steels, and investigate how the texture variation affects the resistance to fracture propagation. This was not possible in this piece of work due to the high demand for neutron imaging facilities and the high cost of EBSD – instead it was chosen to focus on large scale crack arrest testing which was supplemented by comprehensive material characterisation on the small scale.

It is recommended to carry out CCA testing and wide-plate testing on the same batch of steel in future work to have confidence in the agreement between the results of these two test methods. This would enable determination of a correction factor which can directly relate CCA results to wide-plate test results. Additionally, it is recommended to carry out CCA testing on the other materials used in this study which will give more confidence in the relationships between small-scale mechanical properties and crack arrest toughness that have been presented in this research.

7 Overall Conclusions

It is vital to prevent brittle fracture of welded offshore structures. This is particularly important for a number of industry sectors including offshore wind, oil & gas, and shipbuilding where structural failure risks loss of human life and loss of expensive assets. By ensuring that a material has resistance to a propagating brittle crack, i.e. high brittle crack arrest toughness, catastrophic failure can be avoided even in the case that a brittle fracture initiates. Wide-plate test methods allow for direct measurement of the crack arrest toughness but this kind of testing is incredibly expensive. Therefore, there is a need for cheaper and simpler test methods which are able to measure a material's brittle crack arrest toughness and ensure the asset and human life is protected from accidental damage.

Small-scale testing was carried out on five different steels, which include S355 structural steel (with two different thicknesses), X65 pipeline steel, two high strength reactor pressure vessel steels and EH47 shipbuilding steel. The small-scale testing included a full microstructural analysis of the materials, and mechanical testing such as: tensile, drop weight Pellini, instrumented Charpy and SEN(B) fracture toughness testing. Furthermore, compact crack arrest testing was successfully carried out on 80mm thick EH47 shipbuilding steel to measure its crack arrest toughness. This research will be taken forward by Lloyd's Register to the International Association of Classification Societies (IACS) and inform the development of new standards which allow the certification of a material's brittle crack arrest toughness based on small-scale testing. The key conclusions from this research are:

- There was a low correlation between microstructural measures of texture and macroscopic fracture parameters of the steels, indicating that the texture does not play a large role in fracture initiation and arrest.
- Although grain refinement contributes to increased initiation toughness for a steel, it has the opposite effect on crack arrest toughness. i.e. steels with smaller grain size have a lower brittle crack arrest toughness.
- For modern steels, the criteria that result in good crack arrest properties are not the same as those which result in a high upper shelf fracture initiation toughness. Therefore, it is suggested to avoid using upper shelf fracture toughness parameters

such as CTOD δ_m and Charpy energy to indicate crack arrestibility of modern steels due to poor correlation.

- The present study has proved the possibility of achieving valid results from CCA testing on thick (i.e. 80 mm) steel plates. The wide-plate test results available in the literature on the EH47 steel indicate that more conservative values of brittle crack arrest toughness may be achieved from CCA testing.
- The crack arrestibility of a material is most strongly correlated with reference temperatures based on the onset of brittle behaviour (such as T_{27J} and T_{4kN} from Charpy tests or NDTT from drop weight Pellini tests) – even for a steel where the NDTT is located at a temperature on the upper shelf of the Charpy transition curve.
- There is good agreement between crack arrest toughness predictions based on a master curve approach and the toughness measured through CCA testing.
- It is recommended to characterise the brittle crack arrest properties of steels using lower shelf parameters. The recommended method is to use the NDTT determined from Pellini testing.
- The cost reduction associated with using small-scale testing to quantify brittle crack arrestibility of a steel will enable other industries such as offshore wind to make use of the brittle crack arrest methodology. This can be incorporated into the defect assessment tolerance procedure and allow for asset life extension under certain circumstances.
- This research will be taken forward by Lloyd's Register to the International Association of Classification Societies (IACS) and inform the development of new standards which allow the certification of a material's brittle crack arrest toughness based on small-scale testing.